Review

Review of computational studies on boiling and condensation

CrossMark

Chirag R. Kharangate, Issam Mudawar *

Boiling and Two-Phase Flow Laboratory (BTPFL), School of Mechanical Engineering, Purdue University, 585 Purdue Mall, West Lafayette, IN 47907, USA

ARTICLE INFO	ABSTRACT
	Developments in many modern applications are encountering rapid escalation in heat dissipation, coupled with a need to decrease the size of thermal management hardware. These developments have spurred unprecedented interest in replacing single-phase hardware with boiling and condensation counterparts. While computational methods have shown tremendous success in modeling single-phase systems, their effectiveness with phase change systems is limited mostly to simple configurations. But, given the complexity of phase change phenomena important to many modern applications, there is an urgent need to greatly enhance the capability of computational tools to tackle such phenomena. This article will review the large pool of published papers on computational simulation of boiling and condensation. In the first part of the article, popular two-phase computational schemes will be discussed and contrasted, which will be followed by discussion of the different methods adopted for implementation of interfacial mass, momentum and energy transfer across the liquid-vapor interface. This article will then review papers addressing computational modeling of bubble nucleation, growth and departure, film boiling, flow boiling, and flow condensation, as well as discuss validation of predictions against experimental data. This review will be concluded with identification of future research needs to improve predictive computational capabilities, as well as crucial phase change phenomena found in modern thermal devices and systems that demand extensive computational modeling. © 2016 Elsevier Ltd. All rights reserved.

Contents

* Corresponding author.
  E-mail address: mudawar@ecn.purdue.edu (I. Mudawar).
  URL: https://engineering.purdue.edu/BTPFL (I. Mudawar).

Nomenclature

A_i	interfacial area
C	color function
c	parameter in Eq. (18a); wave speed
c_p	specific heat at constant pressure
C_{PF}	phase-field parameter
D	diameter of circular channel; bubble diameter
d	distance of liquid-vapor interface from wall
D_d	departure diameter during nucleate boiling
E	specific internal energy (J/kg)
F	force
Fo_{bi}	Fourier number based on initial bubble diameter
G	mass velocity (kg/m^2 s)
g	gravitational acceleration
g_e	earth gravity
H	heaviside function
h	cell width or grid spacing; heat transfer coefficient
$\bar{h}$	average heat transfer coefficient
h_{fg}	latent heat of vaporization
h_i	interfacial heat transfer coefficient
I	indicator function
Ja	Jacob number
k	effective thermal conductivity
M	molecular weight
$\dot{m}$	mass transfer rate (kg/m^2 s)
Mo	Morton number
$\vec{n}$	unit vector normal to interface
Nu	Nusselt number
p	pressure
Pr	Prandtl number
Q	energy source term for energy equation (W/m^3); volume flow rate
q''	heat flux
q_i''	heat flux across interface
$\bar{q}_w''$	average wall heat flux
R	universal gas constant (8.314 J/mol K)
r	radial coordinate
Re	Reynolds number
R_{gas}	gas constant
r_i	mass transfer intensity factor (s^{-1})
$r_{i,m}$	modified mass transfer intensity factor (K^{-1} s^{-1})
R_0	radius of dry region below bubble in micro-region
R_1	radial location of interface at $y = h/2$
S	volumetric mass source in continuity equation (kg/m^3 s)
T	temperature
t	time
t_d	bubble growth time period during nucleate boiling
T_{sat}	saturation temperature
ΔT_{sub}	inlet subcooling, $\Delta T_{sub} = T_{sat} - T_{in}$
ΔT_w	wall superheat, $\Delta T_w = T_w - T_{sat}$
U	velocity

$\vec{u}$	velocity vector
$\vec{u}_{front}$	velocity of front
V	volume
$\vec{v}_f$	liquid velocity normal to liquid-vapor interface
x	x-coordinate; dimensionless parameter in Fig. 2
x_e	thermodynamic equilibrium quality
$\vec{x}_{front}$	position of front
y	y-coordinate; distance from wall; dimensionless parameter in Fig. 2
z	z-coordinate

Greek symbols

α	volume fraction
γ	accommodation coefficient
δ	liquid film thickness; thickness of liquid micro-layer
δ_s	Dirac delta function
δ_0	liquid film thickness at R_0
ε_m	eddy momentum diffusivity
λ	interfacial wavelength
κ	curvature given by Eq. (18b)
κ_m	diffusion parameter
μ	dynamic viscosity
ν	kinematic viscosity
ρ	density
σ	surface tension
τ	shear stress
φ	chemical potential
ϕ	contact angle
ψ	level set function

Superscripts

$\rightarrow$	vector
$*$	dimensionless

Subscripts

b	bubble
c	condensation
e	evaporation
f	liquid
g	vapor
i	interfacial
in	inlet
k	$k = f$ for liquid, $k = g$ for vapor
s	surface
sat	saturated
T	turbulent
$unsat$	unsaturated
w	wall

1. Introduction

1.1. Addressing the myriad of important boiling and condensation configurations

For many decades, thermal management systems in many applications have employed single-phase methods to meet specific cooling requirements. These systems include both natural convection and forced convection configurations. However, the recent rapid rise in rate of heat dissipation in many applications, coupled with the need to decrease the size of cooling hardware, has rendered single-phase systems incapable of meeting cooling requirements. This trend includes applications such as computer electronics and data centers, medical X-ray equipment, hybrid vehicle power electronics and heat exchangers for hydrogen storage in automobiles, fusion reactor blankets, particle accelerator targets, magnetohydrodynamic generator electrode walls, defense radars, rocket engine nozzles, and both laser and microwave directed-energy weapons [1–3]. Lack of effectiveness of single-phase methods has spurred a transition to two-phase systems to capitalize upon the high heat transfer coefficients associated with both boiling and condensation. The cooling advantages of two-phase systems are derived from their reliance on both sensible and latent heat of the working fluid compared to sensible heat alone for single-phase systems.

Early implementation of phase change cooling was focused on passive heat pipes that rely on capillary forces in a wicking structure to circulate coolant between evaporating (heat acquisition) and condensing (heat rejection) terminals of a closed tubular structure. But several fundamental limitations of heat pipes, especially small coolant flow rate, place stringent upper performance limits that fall short of cooling requirements in many emerging technologies [1]. This shortcoming shifted interest to other passive, unwicked cooling schemes, especially pool-boiling thermosyphons, which rely on buoyancy to circulate coolant between a lower boiling (heat acquisition) and upper condensing (heat rejection) sections of a closed vessel [4–6]. Here too, limited cooling performance spurred new innovations in passive cooling, such as the use of a pumpless loop consisting of two vertical tubes connected atop to a liquid reservoir fitted with a condenser [7,8]. In this system, the boiler is connected to one of the vertical tubes, and large vapor void reduces fluid density in the boiler tube compared to the other liquid tube, causing static pressure imbalance and triggering fluid circulation within the loop. The added benefits of coolant motion in the pumpless loop are also realized in semi-passive falling film cooling systems [9,10], where liquid from a small reservoir falls by gravity as a thin film along the heat dissipating surface, and vapor is lifted by buoyancy to the upper condensation section; the liquid is recollected in the reservoir passively by vapor condensation, assisted by a small pump to maintain constant liquid level in the reservoir. Further improvements in cooling performance involve the use of mechanically driven pumped loops to enhance cooling performance by increasing coolant velocity along the boiling surface. The simplest pumped loop configuration relies on flow boiling along a flow channel [11]. This configuration evolved in recent years to loops utilizing mini- or micro-channels, which offer the advantages of increased heat transfer coefficient, compact and lightweight cooling hardware, and small coolant inventory [12–14]. Two pumped-loop competitors to mini/micro-channel cooling are jet-impingement cooling [15–17] and spray cooling [18,19]. In jet impingement, the coolant exiting the jet nozzle is supplied to the heat-dissipating surface in bulk liquid form. In spray cooling, exiting the spray nozzle, the liquid breaks up into multiple droplets and, thus, provides high heat transfer effectiveness as well as increased surface area for cooling. The main difference between the two is that coolant in jet impingement is supplied to the heat-dissipating surface in liquid form, but broken into small liquid droplets prior to impact in spray cooling. Yet, additional enhancement in cooling performance of pumped loops is achieved with "hybrid" cooling configurations that combine the merits of micro-channel and jet-impingement cooling [20].

In a closed system, enhanced boiling performance often requires commensurate improvements in heat rejection by condensation using a variety of configurations, such as drop-wise condensation [21], falling film condensation on tubes [22] and vertical surfaces [23], and flow condensation in tubes [24]. Often cited as complicating factors in modeling film condensation (also film evaporation), both external and internal, are interfacial waves and suppression of turbulence along the liquid-vapor interface [9,10,23].

One important conclusion that can be drawn from trends in the development of thermal management systems is the existence of a myriad of possible boiling and condensation configurations, which greatly complicate efforts to develop universal predictive tools for system design and optimization.

1.2. Predictive methods for two-phase flow and heat transfer

Undoubtedly, the most popular approach to predicting boiling and condensing flows is the use of empirical or semi-empirical correlations. A key drawback to this approach is most correlations are limited to one or a few fluids, and to narrow ranges of geometrical and flow parameters. Most thermal management system designers are compelled to extrapolate predictions to other fluids or conditions beyond the validity range of a given correlation, which often leads to highly erroneous design decisions. A more effective tool is the use of "universal correlations" that are derived from large databases encompassing many coolants and very broad ranges of both geometrical and flow parameters [25–27]. These correlations utilize the World's most comprehensive databases, which include geometrical parameters that span a large range of scales to achieve unprecedented predictive capability.

Another approach to predicting two-phase behavior is the use of theoretical models. Unfortunately, only a few such models are available, which are limited to very basic flow configurations such as falling films [23], annular flow condensation [28], and annular flow boiling [29].

Because of limitations of both empirical correlations and theoretical models, there is now a great deal of interest in the use of computational fluid dynamics (CFD) simulations to predict phase-change processes. The main advantages of this technique are the ability to predict transient fluid flow and heat transfer behavior, and provide detailed spatial and temporal distributions

of phase velocities and temperatures, and void fraction. However, while CFD simulations have shown great success and versatility in predicting single-phase flows, their effectiveness for two-phase flows has not been fully realized. Presently, despite some recent promising results, two-phase simulations are quite expensive, very time consuming, and limited to only simple flow configurations.

1.3. Review objectives

The main goal of this paper is to review the large pool of articles addressing CFD simulations of boiling and condensation. This includes (1) popular two-phase computational schemes and key differences between schemes, (2) surface tension modeling in conjunction with different schemes, (3) different approaches to predicting interfacial mass, momentum and energy transfer, and (4) boiling and condensation articles involving comparison of predictions of CFD schemes with experiments and correlations. This review will be concluded with key recommendations for improving predictive capabilities of computational schemes.

2. Two-phase computational schemes

2.1. Solution of continuum two-phase conservation equations

Modeling two-phase flow and heat transfer requires accurate prediction of the behavior of each phase and interactions along the interface between phases. Several numerical methods are available for this purpose. Most popular CFD methods involve solving conservation equations using macroscopic depiction of the fluids, where fluid matter is described as consisting of a sufficiently large number of molecules that continuum hypothesis for fluid properties is valid. The mass, momentum and energy equations are expressed, respectively, as

$$\frac{\partial}{\partial t}(\rho) + \nabla \cdot (\rho \, \vec{u}) = 0, \tag{1}$$

$$\frac{\partial}{\partial t}(\rho \, \vec{u}) + \nabla \cdot (\rho \, \vec{u} \, \vec{u}) = -\nabla p + \nabla \cdot \left[\mu \left(\nabla \vec{u} + \nabla \vec{u}^T \right) \right] + \rho \, \vec{g} + \vec{F}_s, \tag{2}$$

and

$$\frac{\partial}{\partial t}(\rho E) + \nabla \cdot \left[\vec{u}(\rho E + p) \right] = \nabla \cdot (k \nabla T) + Q. \tag{3}$$

While most popular methods are based on this macroscopic depiction, there is now increasing interest in computational methods at the mesoscale, where fluid matter is considered a collection of atoms, which is much smaller than macroscale but larger than single atom ("atomistic" scale). This section will discuss the different methods used in two-phase simulations with focus on those employing conservations equations at the macroscale.

2.2. Moving mesh and Lagrangian methods

Early approaches to simulating two-phase flows included use of separate, boundary-fitted grids for each phase. Using this *Lagrangian* scheme, Ryskin and Leal [30] simulated the rise of a buoyancy-driven deformable bubble in quiescent liquid. Governing equations were solved separately for each phase and boundary conditions along the interface matched iteratively. While Ryskin and Leal employed a 2-D axisymmetric domain, Takagi and Matsumoto [31] simulated unsteady bubble rise in 3-D domain. Methods using boundary-fitted grids provide the highest accuracy in predictive capability among the different computational methods.

An alternative *moving-mesh Lagrangian* method allows the grid to follow boundaries of phases during interface deformation as illustrated in Fig. 1(a). Studies using this method include deformation of a buoyant bubble by Shopov et al. [32], and droplet impacting a solid wall by Fukai et al. [33]. Overall, Lagrangian and moving-mesh methods involve very complex formulations that are computationally intensive due to the nature of the solvers used, and hence have only been applied to very simple two-phase flow configurations.

2.3. Interface-capturing methods

Common Eulerian schemes used to simulate two-phase flows are termed interface-capturing methods. Most popular among these are the *volume of fluid* (VOF) method [34] and the *level-set* (LS) method [35].

2.3.1. Volume of fluid (VOF) method

The VOF method captures the interface using a color function C representing volume fraction with a value between 0 and 1, where 0 implies the cell is completely occupied by one phase, and 1 by the other, and the interface is identified by cells having values between 0 and 1. For flows without phase change, the color function is advected by velocity field according to the equation

$$\frac{\partial}{\partial t}(C) + \vec{u} \cdot \nabla(C) = 0. \tag{4}$$

The velocity field is obtained by solving the momentum (Navier-Stokes) equation. Because the interface is tracked by 0 to 1 color value, VOF methods are inherently conservative, which is a major advantage when solving conservation equations. However, they suffer inability to capture the interface accurately.

VOF methods can be divided into two categories: those that do not use interface reconstruction and others that do. Methods not requiring interface reconstruction include *donor-acceptor* scheme by Hirt and Nicholas [34], *flux corrected transport* (FCT) scheme by Rudman [36], and *compressive interface capturing scheme for arbitrary meshes* (CICSAM) by Ubbink and Issa [37]. These schemes use a color value of 0 to indicate one phase and 1 the other phase, with the interface identified by a value of 0.5. The transition from 0 to 1 occurs across a finite thickness interface encompassing multiple cells. In these schemes, Eq. (4) is modified for incompressible fluids as

$$\frac{\partial}{\partial t}(C) + \nabla \cdot (\vec{u} \, C) = 0, \tag{5}$$

which can be solved by different combinations of upwind and/or downwind schemes. After solving Eq. (5), the interface appears smeared across multiple cells and set to a finite thickness.

The second and more popular category of VOF methods involves interface reconstruction, where interface shape is solved using *piecewise constant* or *piecewise linear* schemes. Unlike the first category of VOF methods, these schemes capture the interface with zero thickness. They include *simple line interface calculation* (SLIC) [38], which is a piecewise constant scheme, and *piecewise linear interface calculation* (PLIC) [39], a piecewise linear scheme. As shown in Fig. 1(b), the interface in SLIC is oriented with x- or y-axis of domain (sidewalls of rectangular mesh cell). On the other hand, as shown in Fig. 1(c), the interface in PLIC is set by a straight line/plane whose direction is dictated by vector normal to the interface. Orientation of the normal vector for a specific cell containing the interface is obtained by interrogating volume fractions of all neighboring cells. Once the direction of the interface is computed, this vector is oriented in such a manner that the volume fraction of the cell is maintained. Although the original PLIC scheme by Youngs [39] is still widely used, alternative PLIC
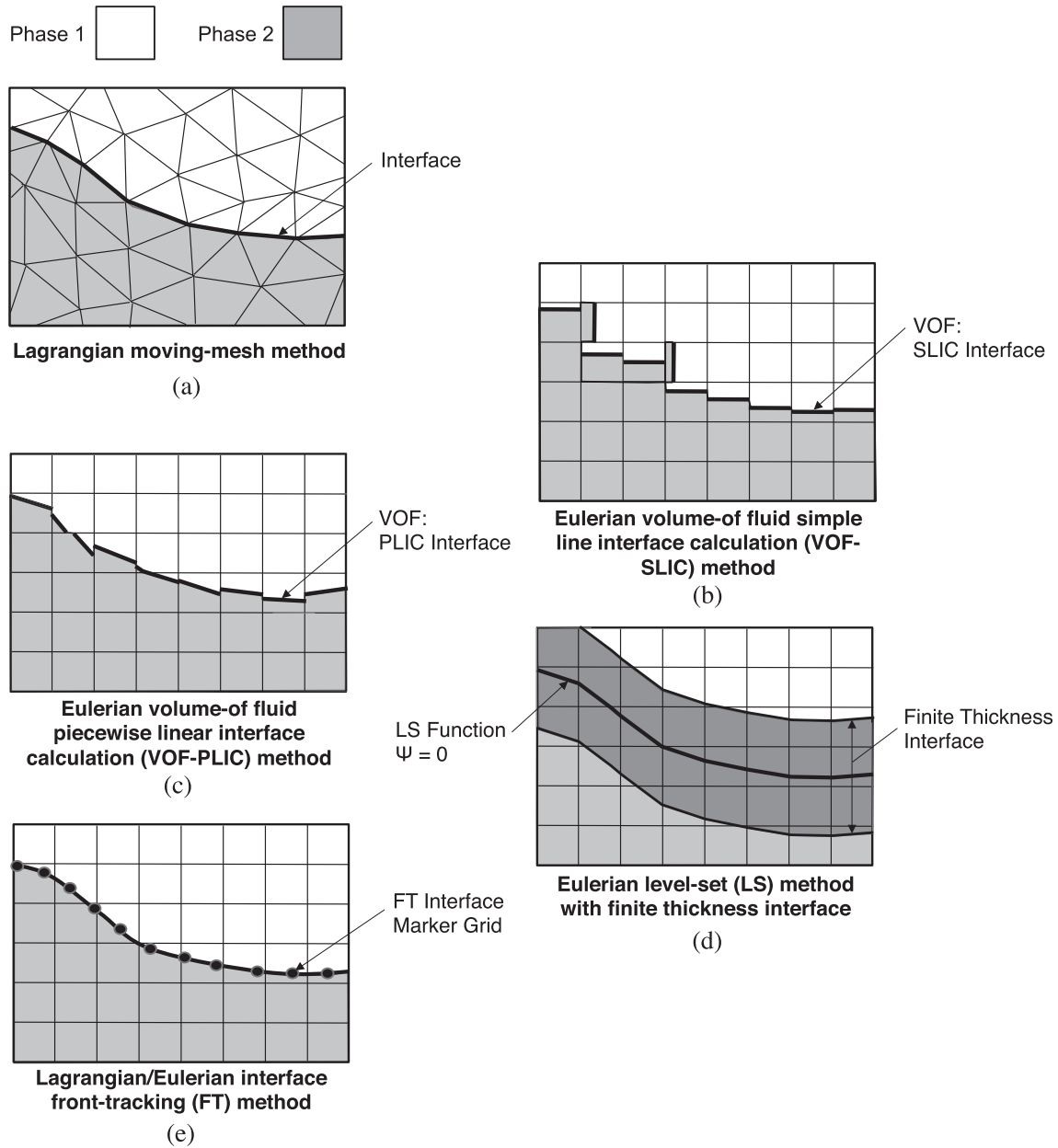
Fig. 1. Interfacial computational grids for (a) Lagrangian moving-mesh method, (b) Eulerian volume-of-fluid simple line interface calculation (VOF-SLIC) method, (c) Eulerian volume-of-fluid piecewise linear interface calculation (VOF-PLIC) method, (d) Eulerian level-set (LS) method with finite thickness interface, and (e) Lagrangian/Eulerian interface front-tracking (FT) method.

schemes have also been recommended [40,41]. A key concern with PLIC schemes is interface discontinuity (jump) between cells as depicted in Fig. 1(c). Some improvements to the PLIC scheme have been proposed that depart from piecewise linear formulation [42,43]. In all interface reconstruction schemes, once interface reconstruction is completed, the advection step given by Eq. (4) is performed to proceed with the numerical solution.

In VOF methods, the density, viscosity and thermal conductivity of the fluid are determined, respectively, as

$$\rho = \alpha_g \rho_g + (1 - \alpha_g)\rho_f, \tag{6a}$$

$$\mu = \alpha_g \mu_g + (1 - \alpha_g)\mu_f, \tag{6b}$$

and

$$k = \alpha_g k_g + (1 - \alpha_g)k_f, \tag{6c}$$

where α_g is the volume fraction, which is related to the color function, C, by the relation

$$\alpha = \frac{1}{V}\iiint_v C\,dv. \tag{7}$$

2.3.2. Level-set (LS) method

The second type of interface-capturing methods is the Level-set (LS) method. This method uses a function, ψ, to define distance from the interface as shown in Fig. 1(d). This function has a value of $\psi = 0$ at the interface (called zero level set), and is positive in one phase and negative in the other. In the absence of phase change, this function is advected by velocity field according to the equation

$$\frac{\partial}{\partial t}(\psi) + \vec{u}\cdot\nabla(\psi) = 0. \tag{8}$$

With the LS method, interface location is known only implicitly by the given values of ψ, therefore its location is captured by interpolating ψ values on the grid. This method is able to capture complicated interface topologies quite well, but with time evolution, ψ cannot maintain the property of a signed distance function and therefore might not remain a smooth function. This leads to error in interface curvature calculations, as well as causes serious mass conservation errors. To correct this problem, ψ needs to be re-initialized every few time steps, and is transformed into a scalar field that satisfies the property of the signed function with the same zero level set. This is commonly achieved by a technique recommended by Sussman et al. [35] involving iterative solution of the following relations

$$\frac{\partial \psi}{\partial t} = \frac{\psi_0}{\sqrt{\psi_0^2 + h^2}}[1 - |\nabla \psi|] \tag{9}$$

and

$$\psi(x, 0) = \psi_0, \tag{10}$$

where h is cell width, which is used to preclude zero denominator in Eq. (9). Russo and Smereka [44] showed the re-initialization step could cause errors in the solution, and suggested improvements to the method of Sussman et al. to correct the problem. Overall, the mass conservation errors are compounded for relatively long time durations. To correct this problem, investigators resort to employing explicit methods to force mass conservation [45,46].

Son and Dhir [47] used the following relations to determine fluid properties in their LS scheme:

$$\rho = \rho_g + (\rho_f - \rho_g)H, \tag{11a}$$

$$\mu^{-1} = \mu_g^{-1} + (\mu_f^{-1} - \mu_g^{-1})H, \tag{11b}$$

and

$$k^{-1} = k_g^{-1} + (k_f^{-1} - k_g^{-1})H, \tag{11c}$$

where k_g is assumed to be zero, and H is the smoothed *Heaviside function* proposed earlier by Sussman et al., who suggested that smoothing the Heaviside function in the LS method serves to remove numerical instabilities that arise from discontinuities in fluid properties. Use of harmonic mean, Eqs. (11b) and (11c), instead of arithmetic mean, Eqs. (6a)–(6c), is not uncommon even for VOF methods. Adapting from Sussman et al., Son and Dhir used the following relations in their study for smoothed *Heaviside function*:

$$H = 1 \quad \text{for } \psi \geqslant 1.5h, \tag{12a}$$

$$H = 0 \quad \text{for } \psi \leqslant -1.5h, \tag{12b}$$

and

$$H = 0.5 + \frac{\psi}{3h} + \frac{1}{2\pi}\sin\left(2\pi\frac{\psi}{3h}\right) \quad \text{for} |\psi| \leqslant 1.5h. \tag{12c}$$

This technique sets interface thickness equal to 3h, or three cell widths, as shown in Fig. 1(d).

Notice that properties are smeared out across multiple cells when using the Heaviside function. A key concern with this smearing effect is that phase change occurs only at the interface. To help resolve this issue, Fedkiw et al. [48] introduced the *ghost fluid* (GF) method, which involves including an additional artificial fluid cell implicitly representing the Rankine-Hugoniot jump condition at the interface. Kang et al. [49] used this GF method in conjunction with the LS scheme to study incompressible multiphase flows.

To tackle both mass conservation errors of the LS method and inaccurate interface capture of the VOF method, an improved *Coupled Level-set/Volume of Fluid* (CLSVOF) method [50,51] has been proposed. This method combines the merits of both earlier methods, while minimizing their errors. With the CLSVOF method, the distance function advection equation is solved first, followed by interface reconstruction using the LS method, which corrects the inaccuracies in interface capture of the VOF method. The VOF method is used to re-initialize ψ, thus tackling the mass conservation issues of the LS method. Another similar yet simpler approach is the *Coupled Volume of Fluid and Level-set* (VOSET) method [52]. This method only solves for *C* advection, Eq. (4), in the VOF method, but calculates LS function ψ using a simple iterative geometric operation, which is then used to calculate only geometric parameters and fluid properties at the interface.

2.4. Interface front-tracking methods

Interface *front-tracking* (FT) methods combine the advantages of both the Lagrangian and Eulerian perspectives by using fixed and moving grids. Using the FT scheme, Grimm et al. [53] treated both phases separately, but Unverdi and Tryggvason [54] and Tryggvason et al. [55] used one set of equations for both phases. Unverdi and Tryggvason's FT method, which is illustrated in Fig. 1(e), employs a regular structured grid to track the flow in both phases, and a finer marker cell grid to track the interface. Location of the finer grid is advected by velocity field according to the following equation:

$$\frac{d}{dt}(\vec{x}_{front}) = \vec{u}_{front}, \tag{13}$$

where $\vec{x}_{front}$ is the position of the front, and $\vec{u}_{front}$ the velocity of the front at that position, interpolated from the fixed grid. While FT methods do a good job calculating interface curvatures and handling multiple interfaces, they require explicit treatment for interface breakup and coalescence [56]. Property variations in Unverdi and Tryggvason's FT method are given by

$$\rho = \rho_g + (\rho_f - \rho_f)I \tag{14a}$$

and

$$\mu = \mu_g + (\mu_f - \mu_g)I, \tag{14b}$$

where *I* is the *indicator function*, which, like the Heaviside function discussed earlier, is used to smooth properties across the interface.

2.5. Other methods

Other methods that have been developed for fixed grids include the *constrained interpolation profile* (CIP) method [57] and *phase-field* (PF) method [58]. Yabe et al. [57] developed the CIP method for multiphase flows to tackle loss of information inside the computational grid resulting from the discretization process, and conserves mass accurately at the interface. This method transforms the color function into a smooth function by using a Lagrangian invariant solution scheme for advection. While most finite interface thickness schemes discussed earlier employ mathematical functions to smooth fluid properties across multiple cells, the PF method is based on the concept of diffuse interface with finite thickness [58]. The phases are defined by a phase-field parameter, C_{PF}, which, in contrast with the color function, *C*, is a physical parameter, and is constant within each phase and varies across the interface. Interface tracking is achieved by solving the following advection-diffusion equation:

$$\frac{\partial}{\partial t}(C_{PF}) + (\vec{u} \cdot \nabla)C_{PF} = \nabla \cdot (\kappa_m \nabla \varphi), \tag{15}$$

where κ_m is the diffusion parameter and φ the chemical potential defining the rate of change of free energy.

Yet another vastly different solution method, which is based on mesoscale formulation, is the Lattice-Boltzmann (LB) method [59,60]. Instead of solving the Navier–Stokes equation, the LB method involves solving discrete Boltzmann equation. To recover macroscopic fluid motion, the mesoscale physics is reduced to simplified microscopic models or mesoscopic kinetic equations. In contrast with methods requiring solution of the non-linear Navier–Stokes equation, the LB method solves semi-linear equations; it also does not require explicit tracking of the interface. This method is beyond the scope of the present study, and therefore its detailed formulation is excluded from review.

3. Surface tension modeling

Accurate capture of the interface requires a method for modeling surface tension force effects. The most popular method to addressing these effects is the *Continuum Surface Force* (CSF) model proposed by Brackbill et al. [61]. When solving the momentum equation

$$\frac{\partial}{\partial t}(\rho \vec{u}) + \nabla \cdot (\rho \vec{u} . \vec{u}) = -\nabla p + \nabla \cdot \left[\mu \left(\nabla \vec{u} + \nabla \vec{u}^T \right) \right] + \rho \vec{g} + \vec{F}_s \qquad (16)$$

with fixed grid methods, the surface tension force, $\vec{F}_s$, according to the CSF model for constant surface tension is defined as

$$\vec{F}_s = \sigma \kappa \delta_s \vec{n}, \qquad (17)$$

where δ_s is the Dirac delta function, which has finite value at the interface and zero values everywhere else away from the interface,

$$\vec{n} = \frac{\nabla c}{|\nabla c|}, \qquad (18a)$$

$$\kappa = \nabla \cdot \vec{n}, \qquad (18b)$$

and c is a parameter defined based on the method used. With the LS method, c is replaced by distance function, ψ. Because ψ is a continuous function, the interface normal vector according to Eq. (18a) can be calculated quite accurately. With the VOF method, on the other hand, c is replaced by volume fraction α. Because of surface discontinuities, this model precludes accurate determination of the normal vector. With the FT method, Eq. (17) uses interfacial curvature along the finer grid to calculate surface tension force. The force is then distributed over the fixed grid using Peskin's *immersed boundary method* [62] to conserve force when moving across grids.

Another promising method to calculating surface tension force effects is the *Continuum Surface Stress* (CSS) model by Lafaurie et al. [63], which has certain advantages compared to the CFS model. The CSS model features conservative formatting, and does not require explicit calculation of curvature, rendering it especially useful for sharp corners.

Even though surface tension models have been successfully used in numerical schemes, they are known to artificially induce *spurious currents* when capturing the interface. These are non-physical vortex currents induced close to the interface, resulting in unrealistic deformations and therefore compromising interface curvature calculations. These currents are caused mostly by inability to balance pressure gradient with surface tension force. Recently, investigators have recommended methods to suppress these spurious currents [64,65]

While finite thickness schemes are solved using surface tension force, the PF method uses fluid free energy. An example of this

approach is a study by Jacqmin et al. [58], where surface tension force is calculated according to

$$\vec{F}_s = -C_{PF} \nabla \varphi, \qquad (19)$$

φ being the chemical potential defining the rate of change of free energy.

4. Implementing mass transfer in two-phase schemes

4.1. Different approaches to solving conservation equations and accounting for interfacial mass, momentum and energy transfer

Phase change methods add multiple complications to two-phase schemes developed to track or capture the interface. In the presence of interfacial mass transfer, interface topology tends to be less stable, and numerical schemes must be able to tackle this issue. Phase change methods also require accurate estimation and implementation of mass, momentum, and heat transfer across the interface. With phase change, mass transfer rate, $\dot{m}$, normal to the interface, which is positive for evaporation and negative for condensation, is given by

$$\dot{m} = \rho_g (\vec{u}_g - \vec{u}_i) . \vec{n} = \rho_f (\vec{u}_f - \vec{u}_i) . \vec{n} . \qquad (20)$$

The jump conditions for velocity, momentum transfer rate, and energy transfer rate across the interface are given, respectively, by

$$(\vec{u}_g - \vec{u}_f) \cdot \vec{n} = \dot{m} \left(\frac{1}{\rho_g} - \frac{1}{\rho_f} \right), \qquad (21)$$

$$\dot{m}(\vec{u}_g - \vec{u}_f) = (\tau_g - \tau_f) \cdot \vec{n} - (p_g - p_f) \mathbf{I} \cdot \vec{n} + \sigma \kappa \vec{n}, \qquad (22)$$

and

$$q_i'' = \dot{m} h_{fg}, \qquad (23)$$

where $\mathbf{I}$ is an Idemfactor, and the energy jump relation accounts only for latent heat transfer.

In a two-phase scheme with phase change, the above jump conditions are usually used at the interface, while the mass, momentum and energy conservation equations given by Eqs. (1)–(3), respectively, are solved for the interior of each phase. The VOF method employs separate conservation equations for liquid and vapor that account for mass transfer between phases using mass source and mass sink terms. The continuity equations in the VOF method are expressed as

$$\frac{\partial}{\partial t}(\alpha_k \rho_k) + \nabla \cdot (\alpha_k \rho_k \vec{u}_k) = S_k, \qquad (24)$$

where subscript k refers to either liquid, f, or vapor, g, and S_k (kg/m^3 s) is the mass source term for phase k associated with the phase change.

As will become evident from the large pool of studies to be reviewed below, there is no universal approach to formulating a numerical solution to a two-phase flow problem involving phase change. When working with a fixed grid and using separate continuity equations for the two phases, phase change is accounted for using mass source and mass sink terms, or mass jump conditions are applied to the two phases separately. If the momentum equations are solved in combined form for both phases, as given by Eq. (2), then only surface tension forces need to be included in the governing equation, and the other terms in Eq. (22) need not be used. This is because pressure, shear stress and momentum flux due to mass transfer are already accounted for. Like the continuity equation, when the energy equation is solved in combined form, energy transfer due to phase change can be accounted for with either source terms or jump conditions along the interface. Son

and Dhir [47] adopted a yet different approach is which mass source was used in the continuity equation, but not the energy equation. They solved the energy equation by setting the temperature of the saturated phase equal to saturation temperature to ensure that energy transfer at the interface due to phase change is correctly account for.

Therefore, it is important to identify differences between solution procedures adopted by different researchers and appreciate the physical basis behind these procedures.

4.2. Mass transfer models

4.2.1. Energy jump condition

One of the most popular tools to account for interfacial phase change is the Rankine-Hugoniot jump condition [66]. Here, mass transfer rate is based on net energy transfer across the interface, including heat transfer due to conduction in the two phases to or from the interface.

$$q_i'' = \vec{n} \cdot (k_f \nabla T_f - k_g \nabla T_g) = \dot{m} h_{fg}, \tag{25}$$

where $\dot{m}$ (kg/m^2 s) is the mass flux due to phase change at the interface. Eq. (25) neglects the small kinetic energy contributions affecting micro-scale mass transfer. A substitute version for Eq. (25) is [67]

$$q_i'' = \left(k_f \frac{\partial T}{\partial \vec{n}}\Big|_f - k_g \frac{\partial T}{\partial \vec{n}}\Big|_g \right) = \dot{m} h_{fg}. \tag{26}$$

The volumetric mass source term, S (kg/m^3 s), is determined according to the relation

$$S_g = -S_f = \dot{m} |\nabla \alpha_f|, \tag{27}$$

where $|\nabla \alpha_g|$ for a particular cell of the computational domain is obtained from

$$|\nabla \alpha_g| = \frac{1}{V} \int |\nabla \alpha_g| dV = \frac{A_{int}}{V}, \tag{28}$$

where A_i is the interfacial area in the cell and V the cell volume.

In simplified form, Nichita and Thome [68] determined the volumetric mass source term from gradients of temperature and void fraction of liquid in the interfacial cell,

$$S_g = -S_f = \frac{k(\nabla T \cdot \nabla \alpha_f)}{h_{fg}}, \tag{29}$$

where k is the effective thermal conductivity given by Eq. (6c). Ganapathy et al. [69] used a similar formulation for the source term. Eq. (29) is less accurate than Eq. (25) and (26) because of the simplifying assumptions used. For example, use of effective thermal conductivity is not physical for calculating phase change at the interface since mass transfer should not depend on conductivity of the saturated phase. During boiling, the liquid phase is saturated and vapor phase unsaturated, as it can be superheated. During condensation, the vapor phase is saturated and liquid phase unsaturated, as it can be subcooled. To correct this error for both condensation and boiling situations, where saturated and unsaturated phases are present, Sun et al. [70] recommended an alternative simplified form based on the assumptions of negligible heat conduction in the saturated vapor ($k_{sat} = 0$) due to constant vapor temperature, and linear temperature variation in the subcooled liquid near the interface,

$$S_{sat} = -S_{unsat} = \frac{2k_{unsat}(\nabla T \cdot \nabla \alpha_{unsat})}{h_{fg}}. \tag{30}$$

Use of simplified source term models is quite common because they simplify source term calculation and implementation in commercial software packages, since they rely only on volume fraction and temperature gradient information within the current cell. Because these models are based on specific assumptions, they should only be used after confirming suitability to the specific phase change problem being addressed. Suitability can be confirmed by utilizing the source terms in specific phase change scenarios over a range of parameters under investigation and see how results compare to experimental data.

While the phase change model based on the Rankine-Hugoniot jump condition is physically based and therefore free from empiricism, it does not account for kinetic energy contributions. Also, notice that $|\nabla \alpha_g|$ in Eq. (27) is non-zero only at the interface, which limits mass transfer at the interface. This condition cannot tackle subcooled inlet boiling and superheated inlet condensation situations with no preexisting interfaces. Use of this model has been seen in situations involving nucleate pool boiling, film boiling, flow boiling, and flow condensation.

4.2.2. Schrage model

Schrage [71] used kinetic theory of gases to propose a mass transfer model in the 1950s based on the Hertz-Knudsen equation [72]. He assumed vapor and liquid are in saturation states, but allowed for jump in temperature and pressure across the interface, i.e., $T_{sat}(p_f) = T_{f,sat} \neq T_{sat}(p_g) = T_{g,sat}$. Kinetic theory of gases was used to relate the flux of molecules crossing the interface during phase change to the temperature and pressure of the phases. A fraction γ is used to define the number of molecules changing phase and transferring across the interface, and $1 - \gamma$ the fraction reflected. Relations for γ_c and γ_e, corresponding to situations involving condensation and evaporation, where defined, respectively, as

$$\gamma_c = \frac{number\ of\ molecules\ absorbed\ by\ liquid\ phase}{number\ of\ molecules\ impinging\ on\ liquid\ phase} \tag{31a}$$

and

$$\gamma_e = \frac{number\ of\ molecules\ transferred\ to\ vapor\ phase}{number\ of\ molecules\ emitted\ from\ liquid\ phase}. \tag{31b}$$

According to the above definitions, $\gamma_c = 1$ corresponds to perfect condensation, where all impinging molecules are absorbed by the liquid phase. Conversely, $\gamma_e = 1$ represents perfect evaporation, where all emitted molecules are transferred to the vapor phase. The net mass flux across the interface, $\dot{m}$ (kg/m^2 s), is determined from the difference between liquid-to-vapor and vapor-to-liquid mass fluxes,

$$\dot{m} = \frac{2}{2 - \gamma_c} \sqrt{\frac{M}{2\pi R}} \left[\gamma_c \frac{p_g}{\sqrt{T_{g,sat}}} - \gamma_e \frac{p_f}{\sqrt{T_{f,sat}}} \right], \tag{32}$$

where R is the universal gas constant (8.314 J/mol K), M the molecular weight, p_g and $T_{g,sat}$ are the vapor's pressure and saturation temperature at the interface, and p_f and $T_{f,sat}$ the liquid's pressure and saturation temperature, also at the interface. Generally, the evaporation and condensation fractions are considered equal and represented by a single accommodation coefficient γ. This simplifies Eq. (32) to the following form:

$$\dot{m} = \frac{2\gamma}{2 - \gamma} \sqrt{\frac{M}{2\pi R}} \left[\frac{p_g}{\sqrt{T_{g,sat}}} - \frac{p_f}{\sqrt{T_{f,sat}}} \right]. \tag{33}$$

A major difficulty in using the above relation is that γ is an unknown quantity, and a few investigators have attempted to determine its value by comparing model predictions to experimental data. For example, using published data, Marek and Straub [73] concluded that γ is between 0.1 and 1 for jets and moving films, and below 0.1 for stagnant liquid surfaces. Also using information from published literature, Paul [74] recommended a value between

0.02 and 0.04 for water during evaporation. Rose [75] recommended a value close to unity for dropwise condensation based on a review of available experimental data. Wang et al. [76] suggested an experimentally determined value of $\gamma = 1$ for non-polar liquids. Hardt and Wondra [77] and Magnini et al. [78] also used $\gamma = 1$ for film boiling. For evaporating falling films, Kharangate et al. [79] recommended a value of $\gamma = 0.1$, but indicated that higher values in the range of $\gamma = 0.1$–1 do not compromise the model's predictive accuracy, but do influence numerical stability. Doro [80] used $\gamma = 0.5$ for evaporating falling films. Kartuzova and Kassemi [81] recommended a low value of $\gamma = 0.01$ for turbulent phase change in a cryogenic storage tank in microgravity. Huang et al. [82] used a value of $\gamma = 0.03$ for bubbly flow of R141b in a serpentine tube.

Tanasawa [83] further simplified the Schrage model by suggesting that, for small interfacial temperature jump, mass flux is linearly dependent on temperature jump between the interface and vapor phase. This simplifies the model to the form

$$\dot{m} = \frac{2\gamma}{2-\gamma} \sqrt{\frac{M}{2\pi R}} \left[\frac{\rho_g h_{fg}(T - T_{sat})}{T_{sat}^{3/2}} \right], \tag{34}$$

where T_{sat} is determined at local pressure. The volumetric mass source term for both the Schrage model, Eq. (32), and Tanasava model, Eq. (34), is given by $S_g = -S_f = \dot{m}|\nabla \alpha_g|$.

Tansawa's model is a good approximation of the original Schrage formulation for most phase change phenomena other than at micro and nano scales, where interfacial temperature jump cannot always be neglected. At those scales, interfacial curvature can cause appreciable Laplace pressure, and Vander Walls forces on solid-liquid interfaces can become sufficiently significant to cause non-equilibrium between the phases [84]. In their investigation of evaporation across a liquid-vapor interface, Hardt and Wondra [77] provided a simple method to assess deviation of interfacial temperature from T_{sat}. As shown in Fig. 2, they plotted the deviation of dimensionless interfacial temperature versus the dimensionless parameter $x = \eta_e d/k_f$, where η_e is the evaporation heat transfer coefficient given by

$$\eta_e = \frac{2\gamma}{2-\gamma} \frac{h_{fg}^2}{\sqrt{2\pi R_{gas}}} \frac{\rho_g}{T_{sat}^{3/2}}, \tag{35}$$
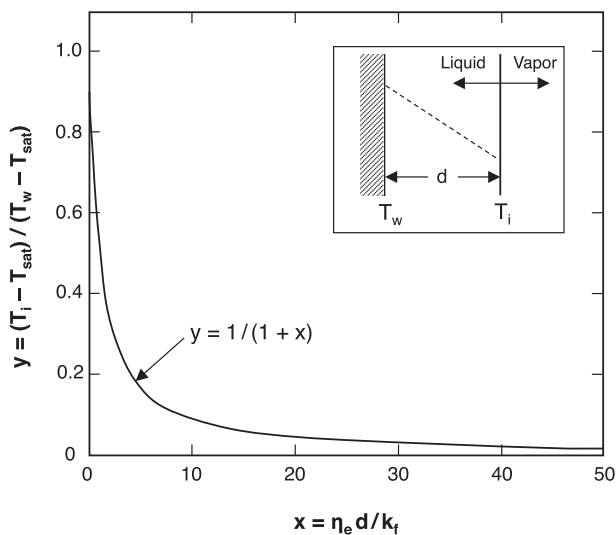

Fig. 2. Variation of deviation of dimensionless interface temperature with dimensionless distance from the wall to the interface. Adapted from Hardt and Wondra [77].

and d the distance of the liquid-vapor interface from the wall. Using the example of water evaporation at atmospheric conditions with an accommodation coefficient of $\gamma = 0.1$, they showed deviation of interfacial temperature increases with decreasing d. The dimensionless deviation is close to 0.01 at $d \approx 81 \mu m$, and increases to 0.1 at $d \approx 7 \mu m$. It is therefore important to assess such deviations in interfacial temperature before opting to use Tanasawa's simplified formulation to model micro- and nano-scale phenomena.

Overall, the Schrage model is both physically based and accounts for kinetic energy effects. As indicated earlier, a key challenge in using this model is deciding which value to use for the accommodation coefficient in the range of $0 < \gamma \leqslant 1$. The optimum value for this coefficient is obtained from experimental data. Kharangate et al. [79] recommended another procedure to setting the value of γ based on deviation of interfacial temperature from T_{sat}. This procedure is initiated by setting $\gamma = 0$, then gradually increasing γ until the deviation between interface temperature and T_{sat} is minimized to an acceptable level. Another challenge in using the Schrage model is the dependence of volumetric mass source term on $|\nabla \alpha_g|$, which has non-zero value only at the interface, allowing phase change to occur only along the two-phase interface. This model tends to maintain T_{sat} because deviation of interfacial temperature from T_{sat} increases the rate of mass transfer along the interface, which in turn reduces the temperature deviation. The Schrage model has been used to investigate nucleate pool boiling, flow boiling, film boiling, and evaporating falling films.

4.2.3. Lee model

Lee [85] developed a simplified saturation model for evaporation and condensation processes. The key premise of this model is that phase change is driven primarily by deviation of interfacial temperature from T_{sat}, and phase change rate is proportional to this deviation. Therefore, phase change occurs while maintaining temperatures of the saturated phase and interface equal to T_{sat}. The model assumes mass is transferred at constant pressure and quasi-thermo-equilibrium state according to the following relations:

$$S_g = -S_f = r_i \alpha_g \rho_g \frac{(T - T_{sat})}{T_{sat}} \quad \text{for condensation } (T < T_{sat}) \tag{36a}$$

and

$$S_g = -S_f = r_i \alpha_f \rho_f \frac{(T - T_{sat})}{T_{sat}} \quad \text{for evaporation } (T > T_{sat}), \tag{36b}$$

where r_i is an empirical coefficient called *mass transfer intensity factor* and has the units of s^{-1}. While the Lee model consistently aims to decrease the deviation from T_{sat}, there is great variability in the choice of r_i value. Researchers have used a very wide range of values, ranging from 0.1 to $1 \times 10^7 s^{-1}$, in attempts to achieve least deviation. Overall, optimum value of r_i depends on many factors, including, but not limited to, specific phase-change phenomenon, flow rate, mesh size, and computational time step. A key challenge in using the Lee model is that different r_i values have been recommended by different researchers for similar experimental configurations, depending on specific setup of numerical model used. Chen et al. [86] suggested a substitute version to the Lee model, given by

$$S_g = -S_f = r_{i,m} \alpha_g \rho_g (T - T_{sat}) \quad \text{for condensation } (T < T_{sat}), \tag{37a}$$

and

$$S_g = -S_f = r_{i,m} \alpha_f \rho_f (T - T_{sat}) \quad \text{for evaporation } (T > T_{sat}), \tag{37b}$$

eliminating T_{sat} from numerators of the source terms, and employing a modified mass transfer intensity factor, $r_{i,m}$.

While many researchers have used the Lee model in their simulations, some [87–89] have shown that this model is essentially a derivative of the Schrage model. Overall, the Lee model is a simplified saturation model that does not set limits on the value of mass transfer intensity factor r_i. While this lack of specificity is advantageous in that it allows investigators to assign their own optimum value, it also points to a lack of strong physical basis for the model. The model's tendency to maintain saturation temperature in both the saturated phase and along the interface serves as a good starting point to investigating rather complicated phase change phenomena without delving into the complex physics of the configuration in question. Unlike the Schrage model, which allows phase change only along the interface, the Lee model allows for phase change both along the interface and within the saturated phase. This is evidenced by the use of void fraction multipliers in the source terms, rendering the Lee model capable of accommodating phase change both within the vapor phase and along the interface for condensation, Eq. (36a), and within the liquid phase and along the interface for evaporation, Eq. (36b). This feature allows the model to simulate full scale flow boiling and flow condensation processes with relative ease, albeit with rather reduced accuracy.

A summary of the three popular mass transfer models discussed in Sections 4.2.1–4.2.3, along with their important assumptions and applications, is provided in Table 1.

4.2.4. Other techniques for simulating mass transfer

Other methods have also been used to simulate phase change, which rely on experimental data or heat transfer correlations. Zhuan and Wang [90] used a Marangoni heat flux correlation [91,92] to calculate mass transfer rate during the initial phase of nucleate boiling, and a bubble growth rate correlation [93,94] to estimate mass transfer during the subsequent phase. Jeon et al. [95] used an experimental heat transfer correlation developed by Kim and Park [96] for condensation to estimate source terms in their investigation of subcooled boiling. Krepper et al. [97] used

the following simple relations for mass transfer flux to model subcooled flow boiling:

$$\dot{m}_f = \max\left\{\frac{h_i(T_{sat}-T)}{h_{fg}}, 0\right\} \quad \text{for subcooled liquid at the interface } (T < T_{sat}),$$
(38a)

and

$$\dot{m}_g = \max\left\{\frac{h_i(T-T_{sat})}{h_{fg}}, 0\right\} \quad \text{for superheated liquid at the interface } (T > T_{sat}),$$
(38b)

where h_i is the heat transfer coefficient given by Ranz and Marshall [98]. But, as suggested earlier in this article, because these methods are correlation based, they should only be applied to the range of, and with fluids for which these correlations were developed. Zu et al. [99] adopted a different empirical approach to model "pseudo-nucleate boiling," where vapor was artificially injected through an inlet located on the heated wall to simulate a nucleation site, followed by vapor generation at the bubble and superheated wall contact area based on experimental observations [100]. Using the VOF model to capture the interface during flow condensation, Zhang et al. [101] incorporated a large artificial source term to force interface temperature to T_{sat}, then calculated energy and mass source terms using the updated temperature field.

Overall, while empirical models do simplify numerical solutions, they are often derived for specific fluids and valid over specific ranges of flow parameters. They are also based on specific assumptions that may not be valid for phase change configurations different from the ones they are based upon.

4.3. Incorporating source terms at two-phase interface

There are multiple ways in which source terms are incorporated in the computational grid. A common method is to include them in cells crossing the interface. This method was used in conjunction with the VOF scheme by Welch and Wilson [102], who calculated

Table 1
Popular mass transfer models used in phase change simulations.

Mass transfer model	Energy jump condition [66]	Schrage model [71]	Lee model [85]
General form	$\dot{m}_g = -\dot{m}_f = \frac{\vec{n}\cdot(k_f\nabla T_f - k_g\nabla T_g)}{h_{fg}}$	$\dot{m}_g = -\dot{m}_f = \frac{2}{2-\gamma_c}\sqrt{\frac{M}{2\pi R}}\left[\gamma_c\frac{p_g}{\sqrt{T_{g,sat}}} - \gamma_e\frac{p_f}{\sqrt{T_{f,sat}}}\right]$	$S_g = -S_f = r_i\,\alpha_g\,\rho_g\frac{(T-T_{sat})}{T_{sat}}$ for condensation $(T < T_{sat})$ $S_g = -S_f = r_i\,\alpha_f\,\rho_f\frac{(T-T_{sat})}{T_{sat}}$ for evaporation $(T > T_{sat})$
Simplified form	$S_g = -S_f = \frac{k(\nabla T\cdot\nabla\alpha_f)}{h_{fg}}$ [68]	$\dot{m}_g = -\dot{m}_f = \frac{2\gamma}{1-\gamma}\sqrt{\frac{M}{2\pi R}}\left[\frac{\rho_g h_{fg}(T-T_{sat})}{T_{sat}^{3/2}}\right]$ [83]	
Basis	– Physics-based model relying on energy jump across vapor-liquid interface	– Physics-based model based on kinetic theory of gases	– Simplified model with phase change defined such that saturating conditions at the interface can be achieved
Kinetic energy contribution	– Does not account for kinetic energy contribution	– Accounts for kinetic energy contribution	– Does not account for kinetic energy contribution
Interfacial temperature	– Different methods/assumptions in numerical scheme used to maintain interfacial temperature at T_{sat}	– Aims to maintain interfacial temperature at T_{sat} with the aid of empirical coefficient	– Aims to maintain interfacial temperature at T_{sat} with the aid of empirical coefficient r_i
Source term implementation	– Implemented at vapor-liquid interface – Requires identifiable interface for model to predict phase change	– Implemented at vapor-liquid interface – Requires identifiable interface for model to predict phase change	– Implemented at vapor-liquid interface and in saturated phase – Can perform bulk phase change calculations – Does not require preexisting interface
Empirical coefficients		– Empirical coefficient needs to be assigned – Value of is usually based on experimental data	– Empirical coefficient r_i needs to be assigned – Value of r_i is based on minimizing deviation of interface temperature from T_{sat}
Phase change configurations addressed in literature	– Nucleate pool boiling – Film boiling – Flow boiling – Condensation	– Nucleate pool boiling – Film boiling – Flow boiling – Evaporating falling films	– Flow boiling – Condensation

the mass source term by combining interfacial relations for heat transfer and continuity across the interface as

$$(\vec{u}_g - \vec{u}_i) \cdot \vec{n} - (\vec{u}_f - \vec{u}_i) \cdot \vec{n} = \left(\frac{1}{\rho_g} - \frac{1}{\rho_f}\right)\frac{q_i''}{h_{fg}}, \tag{39}$$

where the mass flux source term is given by q_i''/h_{fg}.

Another common method is to smear the source term across a finite thickness of the interface including multiple cells. This is the method that was adopted by Son and Dhir [47] in their LS scheme. The mass flux source term, $\dot{m}$, appears in the following continuity equation:

$$\nabla \cdot \vec{u} = \left(\frac{1}{\rho_g} - \frac{1}{\rho_f}\right)\dot{\vec{m}} \cdot \nabla H, \tag{40}$$

where H is the Heaviside function described earlier. Because H in their study varies across three cells, the mass term is smeared across the same three cells. Another approach to smearing the source term was recently recommended by Hardt and Wondra [77]. They first mathematically smeared source and sink terms across multiple cells on the grid around the interface. They then artificially shifted the source and sink terms towards the individual phases. Fig. 3(a) shows how Kunkelmann [103] smeared the source and sink terms using the Hardt and Wondra technique. The smearing process is initiated with a sharp interface, with the source and sink terms concentrated at the interface. After the smearing process is completed, the source (positive) terms and sink (negative) terms are shifted away from the interface. Fig. 3(b) provides a 1-D depiction of cells around the interface, with source and sink terms after the smearing. Fig. 3(c) and (d) shows volume fraction and corresponding mass source and sink terms across multiple cells, respectively. During evaporation, for example, the generated mass of vapor is concentrated on the vapor side of the grid, and the lost mass of liquid on the liquid side. While this method correctly conserves mass, it is not physically correct, since it artificially shifts the mass generation or loss that occur at the interface towards the respective phases. Nonetheless, this method does appear to improve stability of numerical schemes. This method can also be applied to condensation configurations by shifting the generated mass of liquid to the liquid side, and lost mass of vapor to the vapor side.

A third approach to implementing mass transfer was adopted by Juric and Tryggvason [104], who solved iteratively for velocity of the interface markers. This method can accurately capture interfacial topologies in simple two-phase situations, but less so in complicated scenarios like flow boiling.

4.4. Early implementation of phase change across numerical schemes

The past few decades have witnessed widespread implementation of phase change models into a variety of computational schemes. A variety of test cases have been investigated to assess the validity of the phase change models used. They include 1-D Stephan problem [47,66,77,102,105], 1-D sucking interface problem [102,105,106], 2-D horizontal film boiling [47,102,104], 2-D and/or 3-D growth of spherical vapor bubble in superheated liquid [105,106], 2-D and/or 3-D bubble growth due to gravity [105], and 2-D and/or 3-D bubble growth and departure from heated wall [105–107].

Welch and Wilson [102] used the VOF method with Youngs' enhancement [39] for interface advection and phase change based on energy jump condition to solve the 1-D Stephan problem, 1-D sucking interface problem, and 2-D film boiling problem. Son and Dhir [47] used the LS method developed by Sussman et al. [35] and phase change based on energy jump condition to investigate

interface evolution during film boiling. While use of Continuum Surface Force (CSF) model in the VOF and LS methods works well in flows without phase change, it is less accurate with phase change. To solve problems with CSF, Nguyen et al. [108] and Gibou et al. [66] used the ghost-fluid (GF) model in conjunction with the LS scheme and phase change based on energy jump condition. As indicated earlier, the GF model involves implicit representation of the Rankine-Hugoniot jump condition at the interface by adding an artificial fluid cell. For Lagrangian schemes, Welch [109] and Son and Dhir [110] implemented phase change using triangular grid and moving coordinate scheme, respectively. Welch used a phase change model based on energy jump condition. Tomar et al. [111] implemented phase change in the CLSVOF scheme to investigate film boiling and bubble formation. Juric and Tryggvason [104] extended the FT scheme to film boiling with phase change based on Tanasawa's model. Shin and Juric [67] used the FT scheme with level contour reconstruction in 3-D domain with phase change based on energy jump condition to investigate film boiling. Sato and Niceno [105] implemented phase change using the mass-conservative CIP method to simulate bubble growth and nucleate boiling with phase change based on energy jump condition. Jamet et al. [112] constructed a phase-field model for liquid-vapor flows with phase change. Dong et al. [113] implemented phase change in the phase-field LB method by calculating heat and mass transfer using the thermal LB method by Inamuro et al. [114] combined with a multiphase model by Zheng et al. [115]. Zhang and Chen [116] implemented phase change in a pseudopotential LB approach to model nucleate boiling.

5. Applications in boiling and condensation

5.1. Boiling

5.1.1. Bubble nucleation, growth and departure

The nucleate boiling process is characterized by liquid-to-vapor phase change from nucleation sites on a heated wall. A finite degree of wall superheat is necessary for nucleation to commence at the onset of nucleate boiling (ONB). Nucleate boiling at low heat fluxes is characterized by discrete bubbles growing and departing from the nucleation sites. High heat fluxes increase active nucleation site density, with bubbles showing tendency to merge laterally. Important considerations necessary to simulate these flows include nucleation site density and heated wall thermal response, in addition of course to bubble dynamics and heat and mass transfer.

In their numerical study of bubble growth, Lee and Nydahl [117] used simplified depiction where the bubble was assumed to acquire hemispherical shape, trapping a wedge-shaped liquid micro-layer at the wall, whose thickness was based on a model by Cooper and Lloyd [118]. Welch [119] used a finite-volume method and a moving unstructured mesh in conjunction with an interface tracking scheme to predict bubble growth, but did not simulate micro-layer formation. In most studies, the thin liquid micro-layer is considered a region of extremely high heat transfer coefficient [120].

Dhir and co-workers published a series of very successful simulations of bubble growth and departure in pool boiling, including the first complete simulation of saturated nucleate pool boiling by Son et al. [107]. They used the LS scheme and implemented phase change based on energy jump condition in 2-D axisymmetric domain that was subdivided into micro and macro regions as shown in Fig. 4(a). This is a form of multiscale modeling, where a separate model is used to solve the high-resolution portion of the domain, avoiding the need for finer mesh in this region. Lubrication theory [121,122] was used to model radial variation of the
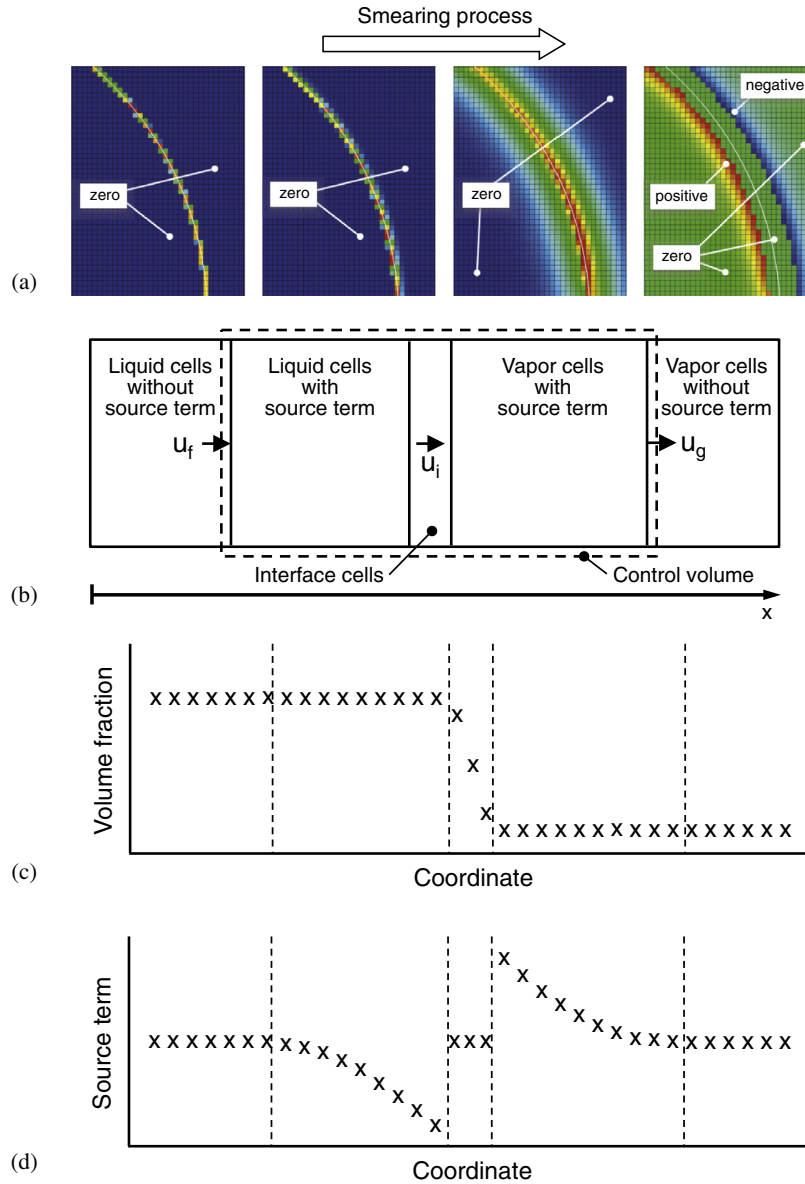
Fig. 3. (a) Illustration of smearing process around two-phase interface. (b) 1-D control volume of smeared interface. (c) Variation of volume fraction in control volume depicted in part (b). (d). Source term distribution in control volume depicted in part (b). Adapted from Kunkelmann [103].

micro-layer thickness. Conservation of mass, momentum and energy in the micro-layer were presented, respectively, as

$$\frac{\partial \delta}{\partial t} = \vec{v}_f - \frac{q''}{\rho_f h_{fg}}, \tag{41}$$

$$\frac{\partial p_f}{\partial r} = \mu_f \frac{\partial^2 \vec{u}_f}{\partial y^2}, \tag{42}$$

and

$$q'' = k_f \frac{(T_w - T_i)}{\delta}. \tag{43}$$

In the macro region, they used the LS scheme for interface tracking. The vapor temperature was set equal to T_{sat}, and effective conductivity was dependent on conductivity of liquid alone and given by

$$k^{-1} = k_f^{-1} H. \tag{44}$$

Son et al. used this approach to investigate bubble shape during growth and departure from a single nucleation site. For a wall superheat of 8.5 °C, simulation results of bubble growth compare well with experimental data, as shown in Fig. 4(b), though slight differences are evident in the neck region. They were also successful in predicting the effects of superheat on bubble growth rate and departure diameter as shown in Fig. 4(c). Singh and Dhir [123] extended the model to subcooled nucleate pool boiling and showed that increased subcooling decreases bubble growth rate and departure diameter and increases growth period. Abarajith and Dhir [124] extended this model to investigate the influence of fluid properties, surface wettability, and contact angle. They showed that dielectric fluid PF-5060, whose surface tension is much smaller than that for water, produces smaller growth rate and smaller departure diameter than water. Nam et al. [125] studied bubble dynamics of water on a superhydrophilic surface and, once again, showed good agreement with experiments. By adding the species conservation equation to earlier formulations of conti-
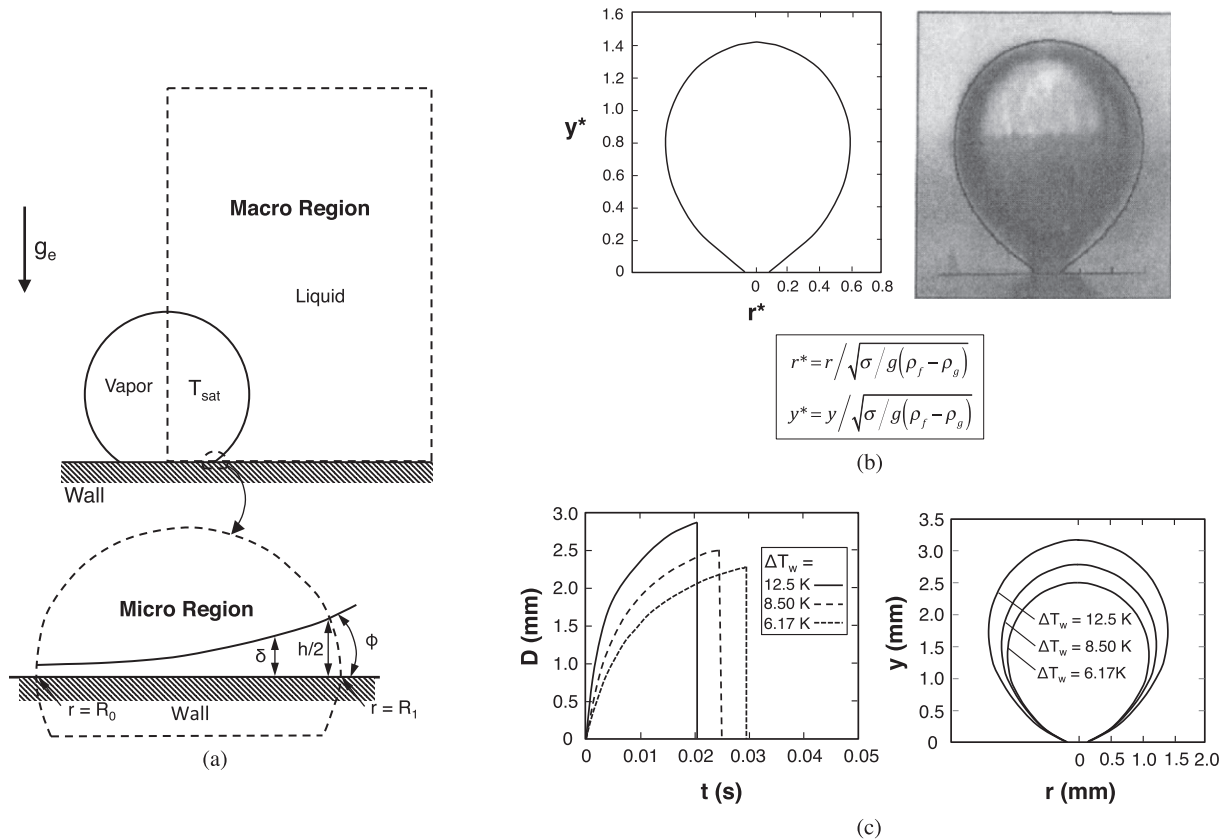
Fig. 4. (a) Computational domain used for simulation of bubble nucleation in pool boiling with micro and macro regions. (b) Bubble shape predictions using 2-D axisymmetric model with LS scheme and energy jump condition, compared to captured image for water with ΔT_w = 8.5 °C and φ = 50°. (c) Effects of wall superheat on bubble growth, and bubble shape at departure for water with φ = 38°. Adapted from Son et al. [107].

nuity, momentum and energy of Son et al., Wu and Dhir [126] investigated the effects of noncondensables on subcooled pool boiling using the coupled level set and moving mesh method developed by Wu et al. [127]. They found that noncondensables have minimal influence on heat transfer. Aparajith et al. [128] extended the 2-D model of Son et al. [107] to 3-D, and numerically simulated bubble growth for water and PF-5060 in reduced gravity, concluding that departure diameter and bubble growth time vary with gravity according to $D_d \sim g^{-0.5}$ and $t_d \sim g^{-0.9}$, respectively. Dhir et al. [129] then studied bubble growth of perfluoro-n-hexane for $g/g_e = 1 \times 10^{-7}$ and showed excellent agreement with experimental data. Studies by a different group showed that decreasing gravity increases growth time and departure diameter [130]. Son et al. [131] and Mukherjee and Dhir [132] simulated vertical bubble merger from a single nucleation site in 2-D domain, and lateral bubble merger from separate nucleation sites in 3-D domain, respectively, and, in both cases, achieved good agreement with experimental data. All earlier studies by Dhir and co-workers described in this paragraph employed constant wall temperature, thereby neglecting thermal response of the wall. Aktinol and Dhir [133] incorporated wall response in their simulations and concluded that wall heat flux varies by up to four orders of magnitude during bubble growth. They also found that wall thickness and material have a significant impact on waiting time between successive nucleations.

More recently, Dhir and co-workers also addressed the influence of slow fluid motion on bubble growth and departure. Li and Dhir [134] simulated single bubble nucleation in horizontal flow and vertical upflow for liquid flow velocities from 0.076 to 0.23 m/s in 3-D domain, using experimental contact angle data

as input to the model. Fig. 5(a) and (b) compares experimental results and numerical predictions of volume fraction for a liquid velocity of 0.076 m/s and 5.3 °C wall superheat for horizontal flow and vertical upflow, respectively. They achieved good agreement for horizontal flow, with the bubble initially assuming spherical shape and then getting tilted in the flow direction and growing asymmetrically. For vertical upflow, reasonable agreement was achieved in terms of bubble location and shape, sliding motion, and eventual lift-off from the wall. More recently, Son and Dhir [135] revisited the problem of nucleate pool boiling, by addressing high wall heat fluxes. By implementing the GF method and LS scheme, they used 2-D and 3-D simulations to demonstrate a significant increase in bubble merger in both vertical and lateral directions at high heat fluxes.

Using a simulation approach similar to that of Dhir and co-workers but with a simplified micro-layer model from [106], Lee et al. [136] investigated bubble growth on a microcavity. By testing various shapes of microcavities on which bubbles nucleate, they found out that truncated conical cavities show better nucleation in comparison to cylindrical and conical cavities. Lee and Son [137] and Lee et al. [138] continued pursuing this approach to study boiling heat transfer enhancement on microstructured and microfinned surfaces, respectively, and confirmed their benefits.

Kunkelmann and Stephan [106] simulated bubble growth using the VOF scheme in the CFD software OpenFOAM in 2-D axisymmetric domain, with phase change based on Tanasawa's model. Unlike the approach used by Dhir and co-workers, Kunkelmann and Stephan used a micro-layer model developed by Stephan and Busse [139] to study bubble growth and departure on a heated wall. They complemented this study with simulations of nucleate
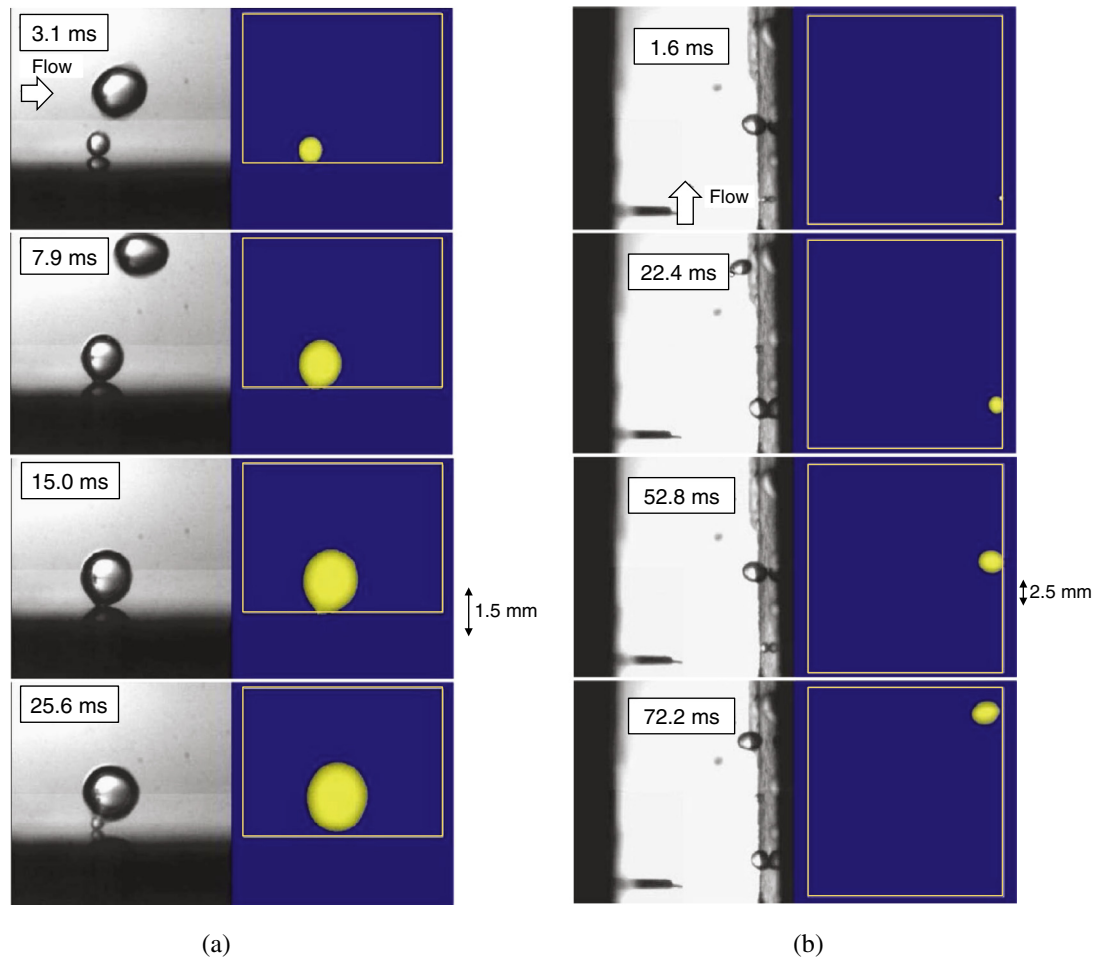
Fig. 5. Predictions of bubble shape for single bubble during flow boiling of water at 0.076 m/s and ΔT_w = 5.3 °C using LS scheme in 3-D domain and energy jump condition, and corresponding experimental images for (a) horizontal orientation, and (b) vertical upflow orientation. Adapted from Li and Dhir [134].

boiling of HFE-7100 using a coupled VOF and LS model in Open-FOAM, but with phase change based on energy jump condition [140,141]. This approach greatly reduced mesh refinement requirements at the interface. They examined single bubble growth and departure, and lateral bubble merger, while also including micro-layer effects at the three-phase contact line. In a separate study, Kunkelmann et al. [142] investigated both experimentally and numerically the effects of three-phase contact line on evaporative heat transfer. Sielaff et al. [143] used a VOF scheme similar to [106], with phase change based on energy jump condition, to study lateral bubble coalescence; their simulations were able to capture residual droplets in merged bubbles. Chen and Utaka [144] solved micro-layer evaporation separately using experimentally measured micro-layer thickness, and implemented computed mass, momentum and energy source terms in the VOF scheme. Jia et al. [145] used the micro-layer formulation by Stephan and Busse [139] in their VOF scheme.

Sato and Niceno [105] studied nucleate boiling using the mass conservative constrained interpolation profile (CIP) scheme in 3-D domain, including a micro-layer treatment similar to that of Kunkelmann and Stephan [106], with phase change based on energy jump condition. Fig. 6(a) shows a sample of Sato and Niceno's bubble growth sequence during nucleate boiling in water, along with the temperature and velocity fields. Bubbles are depicted growing and departing, followed by emergence of a new bubble at the nucleation site. Fig. 6(b) shows corresponding temporal variations of integrated wall heat flux and bubble radius,

which also shows minimum heat flux coinciding with bubble departure from the wall. Fig. 6(c) shows predictions agree quite well with experimental results in terms of bubble shape and bubble departure period. Sato et al. [146] later extended the model to vertical and horizontal flow boiling by incorporating in the phase change model turbulent thermal conductivity according to

$$q_i'' = \vec{n} \cdot \{(k_f + k_T)\nabla T_f - (k_g + k_T)\nabla T_g\}, \tag{45}$$

and demonstrated reasonable agreement with experiments. Lal et al. [147] investigated near-saturated flow boiling using Sato and Niceno's [105] model, but used a very fine grid, and were therefore able to account for turbulence without using Eq. (45). They achieved good overall agreement of bubble shape and diameters with experimental data. It should be mentioned that this CIP method conserves mass, while the FT and LS methods do not.

In another study, Ling et al. [148] studied nucleate boiling of a single bubble, two-bubbles, and bubble mergers using the VOSET scheme in 2-D domain with the micro-layer model of Ma et al. [149]. There have also been a number of studies of bubble nucleation, growth and departure that do not account for micro-layer evaporation effects. Among those, Aus der Wiesche [150] simulated nucleate pool boiling with the VOF scheme. Kunugi et al. [151] used a different method for interface reconstruction called *Multi-Interface Advection and Reconstruction Solver* (MARS) developed in [152] in the VOF scheme to study bubble nucleation in pool boiling and flow boiling. Tryggvason and Lu [153] used the FT
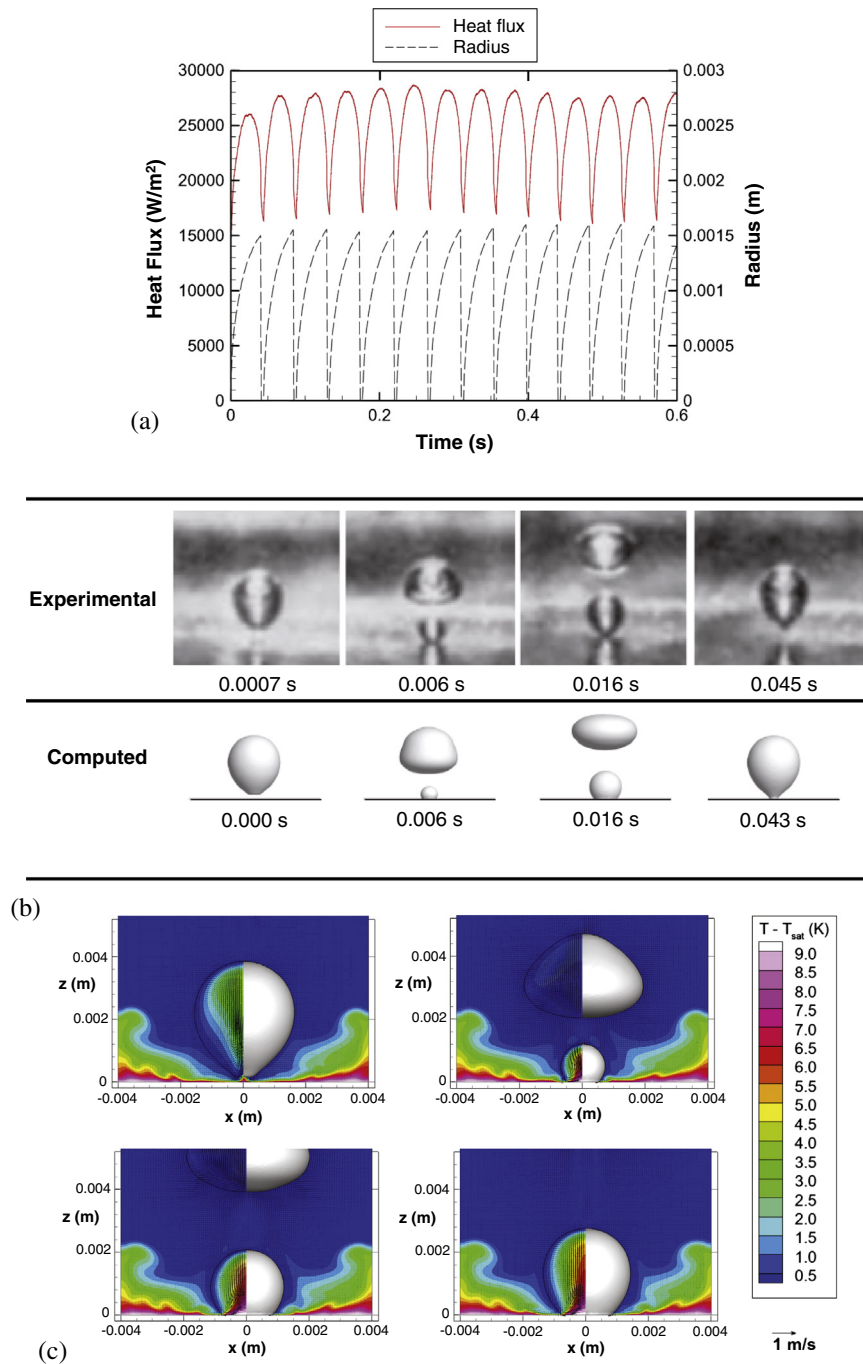
(a)

(b)

(c)

Fig. 6. Predictions of bubble growth in saturated nucleate pool boiling of water computed using mass conservative CIP scheme in 3-D domain and energy jump condition. (a) Temporal variations of area averaged wall heat flux and bubble radius. (b) Comparison of computed and experimental bubble shape. (c) Bubble growth predictions, with right half of bubble showing bubble shape and left half temperature field; total duration of sequence is approximately 0.027 s. Adapted from Sato and Niceno [105].

scheme to simulate nucleate boiling in 3-D domain. Shin et al. [154] extended the LCRM method also to simulate nucleate boiling in 3-D domain. Yoon et al. [155] used the mesh free technique (MPS-MAFL) developed by Koshizuka et al. [156] to simulate bubble growth, departure and rise in nucleate pool boiling. LB methods have also been used by researchers to study bubble growth and departure on a horizontal surface [157,158] and in slow moving flow [159].

5.1.2. Film boiling

Film boiling involves formation of a continuous vapor film on the heated wall, blocking any wetting of the wall by liquid. There-

fore, the wall heat transfer coefficient is considerably poorer than in nucleate boiling. Here, vapor bubbles are released with rather uniform frequency from the wavy liquid-vapor interface, rather than from the wall, which is why film boiling is easier to model than nucleate boiling. This relative simplicity has spurred a large number of studies aiming to simulate film boiling as a precursor to more complex phase change phenomena.

Early film boiling simulations were performed by Son and Dhir [110], who adopted a moving body-fitted coordinate system. They used 2-D axisymmetric domain and modeled surface tension using the continuum surface force (CSF) model by Brackbill et al. [61]. Son and Dhir's model showed good predictions of bubble size

and breakoff diameter, while Nusselt number predictions were lower than experimental data. However, this model is applicable only as long as a single interface is present. Therefore, once the bubble detaches, and multiple interfaces are formed, the computation is brought to an end. Also using a moving body-fitted coordinate system, Banerjee and Dhir [160,161] investigated subcooled film boiling on a horizontal disc in 2-D axisymmetric domain. They achieved good agreement with experiments in terms of interface shape, temporal position of interface, interface growth rate, and wall heat flux.

Juric and Tryggvason [104] simulated film boiling using the FT scheme in 2-D domain, with phase change based on Tanasawa's model [83], but did not encounter the disjointed interface problem. By inputting wall heat flux as boundary condition instead of wall temperature (as was used in many other studies), they studied growth of initial instability of the film along with bubble departure. Fig. 7(a) shows predictions for a Morton number of $Mo = 1 \times 10^{-3}$ with a relatively low value of dimensionless heat flux of $q''^* = 10$ at different dimensionless times t^*. Shown is the liquid-vapor interface undergoing a Rayleigh-Taylor instability, and the vapor bubble subsequently pinching-off and rising. For a lower $Mo = 1 \times 10^{-6}$ and higher $q''^* = 20$, Fig. 7(b) shows the vapor being converted into a mushroom shaped bubble, preventing

pinch-off of its stem. While the predicted bubble shape did not exactly match experiments, both heat transfer rate and wall temperature showed good agreement with correlations. Shin and Juric [67] simulated film boiling on a horizontal surface in 3-D domain using the level contour reconstruction method assuming interface is maintained at T_{sat}, with phase change based on energy jump condition. Their approach eliminated the iterative procedure used by Juric and Tryggvason to match interface velocity. Esmaeeli and Tryggvason [162,163] also eliminated the iterative procedure in simulations of film boiling on a horizontal surface using 3-D domain, with phase change based on energy jump condition. Later, they used the same scheme to investigate film boiling on a single horizontal cylinder and multiple cylinders [164], by incorporating an immersed boundary method [165] to tackle uneven surfaces. Fig. 8 shows their predictions for a bubble pinching off from the cylinder in 3-D domain. Notice how, as vapor is generated and bubble grows, the upper half portion becomes tighter and lower half thinner. Eventually, the bubble is pinched off and surface tension pulls the interface back, re-initiating the process is a repeatable manner.

Son and Dhir [47] investigated film boiling using the LS method in 2-D axisymmetric domain with phase change based on energy jump condition, but unlike their earlier work [110], the newer
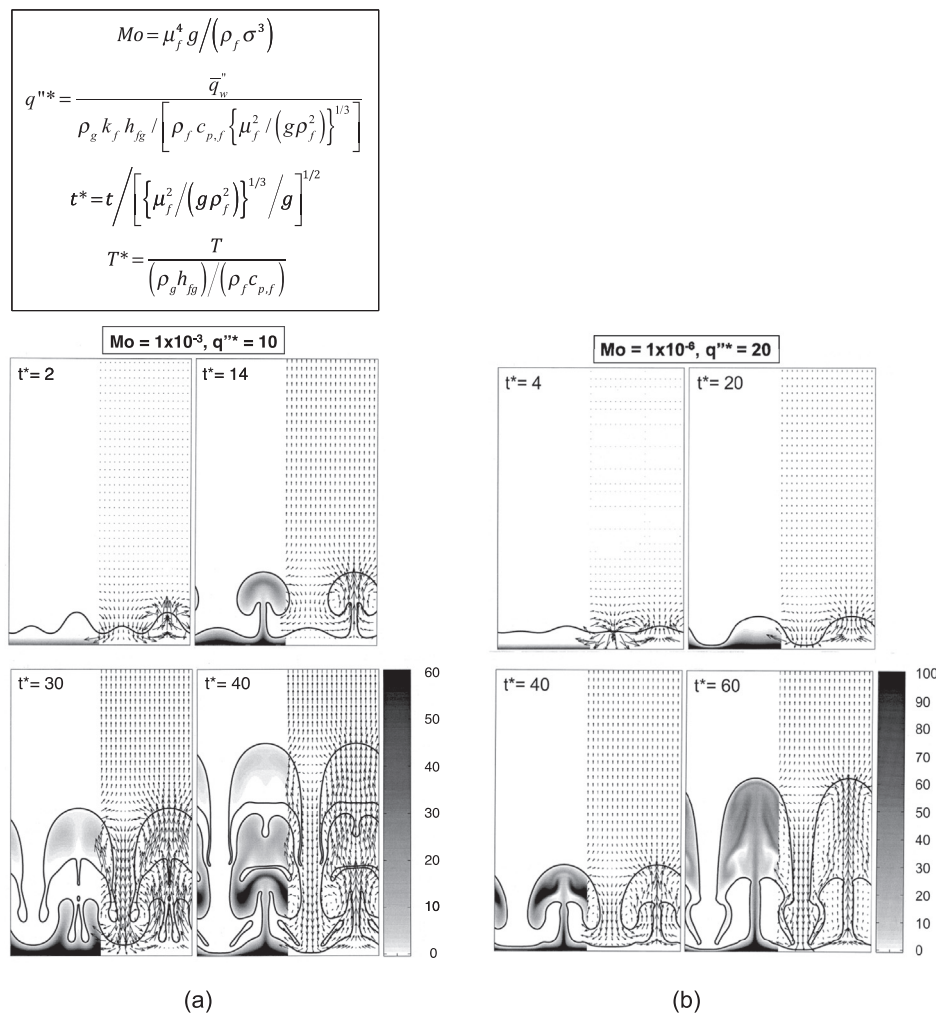

$$Mo = \mu_f^4 \, g \Big/ \left(\rho_f \, \sigma^3 \right)$$

$$q''^* = \frac{\overline{q}_w''}{\rho_g \, k_f \, h_{fg} \Big/ \left[\rho_f \, c_{p,f} \left\{ \mu_f^2 \Big/ \left(g \rho_f^2 \right) \right\}^{1/3} \right]}$$

$$t^* = t \Big/ \left[\left\{ \mu_f^2 \Big/ \left(g \rho_f^2 \right) \right\}^{1/3} \Big/ g \right]^{1/2}$$

$$T^* = \frac{T}{\left(\rho_g h_{fg} \right) \Big/ \left(\rho_f \, c_{p,f} \right)}$$

Fig. 7. Simulations of hydrogen film boiling using FT scheme in 2-D domain with Tanasawa phase change model for different times: (a) $Mo = 1 \times 10^{-3}$ and $q''^* = 10$. (b) $Mo = 1 \times 10^{-6}$ and $q''^* = 20$. The vapor-liquid interface is shown as solid black line, with temperature field plotted to the left and velocity vectors to the right of domain. Adapted from Juric and Tryggvason [104].
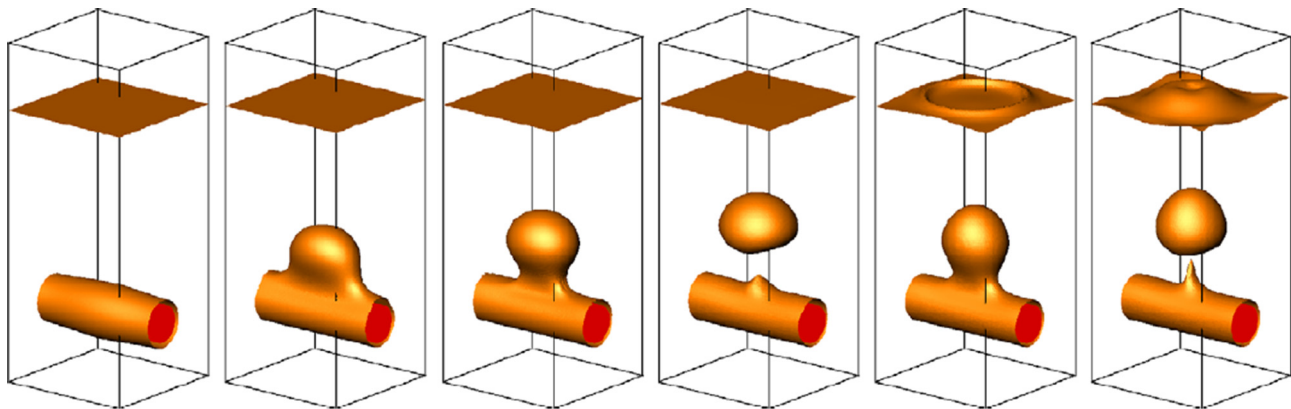
Fig. 8. Simulations of film boiling on a horizontal cylinder using the FT method in 3-D domain with energy jump condition. Domain size is 0.06 m × 0.06 m × 0.15 m, and simulation parameters are ΔT_w=10 °C, ρ_f/ρ_g = 40, μ_f/μ_g = 10, k_f/k_g = 40, $c_{p,f}/c_{p,g}$=10, h_{fg}=10 kJ/kg. Adapted from Esmaeeli and Tryggvason [164].

model was capable of tackling multiple interfaces. They assumed constant liquid temperature equal to T_{sat}, and an effective conductivity dependent on conductivity of vapor alone,

$$k^{-1} = k_g^{-1}(1 - H). \tag{46}$$

Fig. 9(a) shows evolution of the interface in water for three wall superheats of ΔT_w = 10, 22, and 30 °C. Notice, for all superheats, how discrete bubbles are released at interfacial nodes and antinodes. At the higher superheat, long vapor jets form simultaneously below the bubbles at the nodes and antinodes. The numerical simulations predict average wall heat flux values of $\bar{q}''_w$ = 9.28, 21.60 and 29.90 W/cm² for ΔT_w = 10, 22, and 30 °C, respectively. The computed modes bear reasonable similarity with experimental results by Reimann and Grigull [166] corresponding to $\bar{q}''_w$ = 16.21, 21.49, and 27.10 W/cm², as shown in Fig. 9(b). In addition, Nusselt number predictions are within those based on the Berenson [167] and Klimenko [168] correlations. Bazdidi-Tehrani and Zaman [169] extended the LS method to saturated film boiling on a vertical wall. Son and Dhir [170] used the ghost fluid (GF) method in conjunction with their LS scheme to investigate film boiling on a horizontal cylinder in 2-D and 3-D domains, also accounting for the cylinder wall. Son and Dhir [171] explored the effects of decreasing cylinder diameter on film boiling in 3-D domain, and the simulated trends were consistent with prior experimental data. Gibou et al. [66] also implemented the GF method in conjunction with the LS scheme to study film boiling in 2-D domain and obtained good qualitative results. Kim and Son [172] investigated film boiling in a simple jet impingement configuration.

Welch and Wilson [102] were the first to implement the VOF method in boiling situations, with phase change based on energy jump condition, and tested their approach with film boiling in 2-D domain. Their simulation results compare well with those of Son and Dhir [47] and Juric and Tryggvason [104], who used different numerical schemes. Fig. 10(a) and (b) shows simulation results for bubbles pinching off the vapor–liquid interface, and corresponding temporal variations of Nusselt number, respectively. Fig. 10(b) shows the time-averaged Nusselt number agrees with predictions based on the Berenson correlation [167]. Simulations at higher heat flux predicted mushroom shaped behavior similar to that from [104]. Welch and Rachidi [173] extended the Welch and Wilson model by incorporating the solid wall in the computational domain, therefore incorporating all three phases: liquid, vapor, and solid. Agarwal et al. [174] also used the VOF scheme to investigate bubble growth and heat transfer in film boiling in 2-D domain, but Nusselt number was under-predicted compared

to predictions based on the Berenson [167] and Klimenko's [168] correlations. Hardt and Wondra [77] used the VOF scheme with Tanasawa's phase change model to study film boiling in 2-D domain. They developed a different mass source term smearing scheme at the interface to decrease numerical instabilities as discussed earlier. Their simulations produced mushroom shaped bubbles with long jets connecting the bubbles to the vapor film at the wall. Yuan et al. [175] used the VOF scheme to investigate both natural convection and forced convection film boiling on a sphere in non-orthogonal body-fitted coordinates. Sun et al. [70] studied 2-D film boiling using the VOF scheme along with their simplified conductivity formulation. Another example of VOF-based simulations is an investigation of film boiling on a spherical surface by Arevalo et al. [176].

Several other methods have also been used to simulate film boiling. Using the CLSVOF scheme, Tomar et al. [111] showed bubbles generating alternatively at nodes and anti-nodes and, above certain superheat values, captured long vapor jets below the bubbles, similar to simulation results of Son and Dhir [47]. They studied film boiling of both R134a and water, and found that bubble frequency is higher for R134a. Welch and Biswas [177] and Tomar et al. [178] explored the effects of applying an electric field on film boiling by coupling electrohydrodynamics with the CLSVOF method. Guo et al. [179] simulated film boiling on a horizontal wall using the VOSET method. Tsui et al. [180] used a modified VOF method to simulate horizontal film boiling. Li et al. [181] used a hybrid LB scheme, where the LB method was used to simulate fluid flow, but the energy equation was solved using a traditional finite difference scheme. They were able to simulate, not only film boiling, but the entire boiling curve, including nucleate, transition, and film boiling, and demonstrated quantitative agreement with experimental results.

5.1.3. Flow boiling

In the studies discussed above, it is quite obvious that investigators have focused most two-phase computational efforts on relatively simple and elemental nucleate pool boiling (and very slow flow boiling) and film boiling phenomena. However, these phenomena do serve as important test cases for validation of numerical schemes and phase change models, and constitute an important foundation for addressing more complicated two-phase phenomena. As discussed in the Introduction, most modern heat transfer applications involve far more complicated phase change phenomena, which include high flow velocities, turbulence, and many discrete moving interfaces.

Flow boiling is characterized by liquid-to-vapor phase change along a heated wall where flow velocity plays a crucial role in
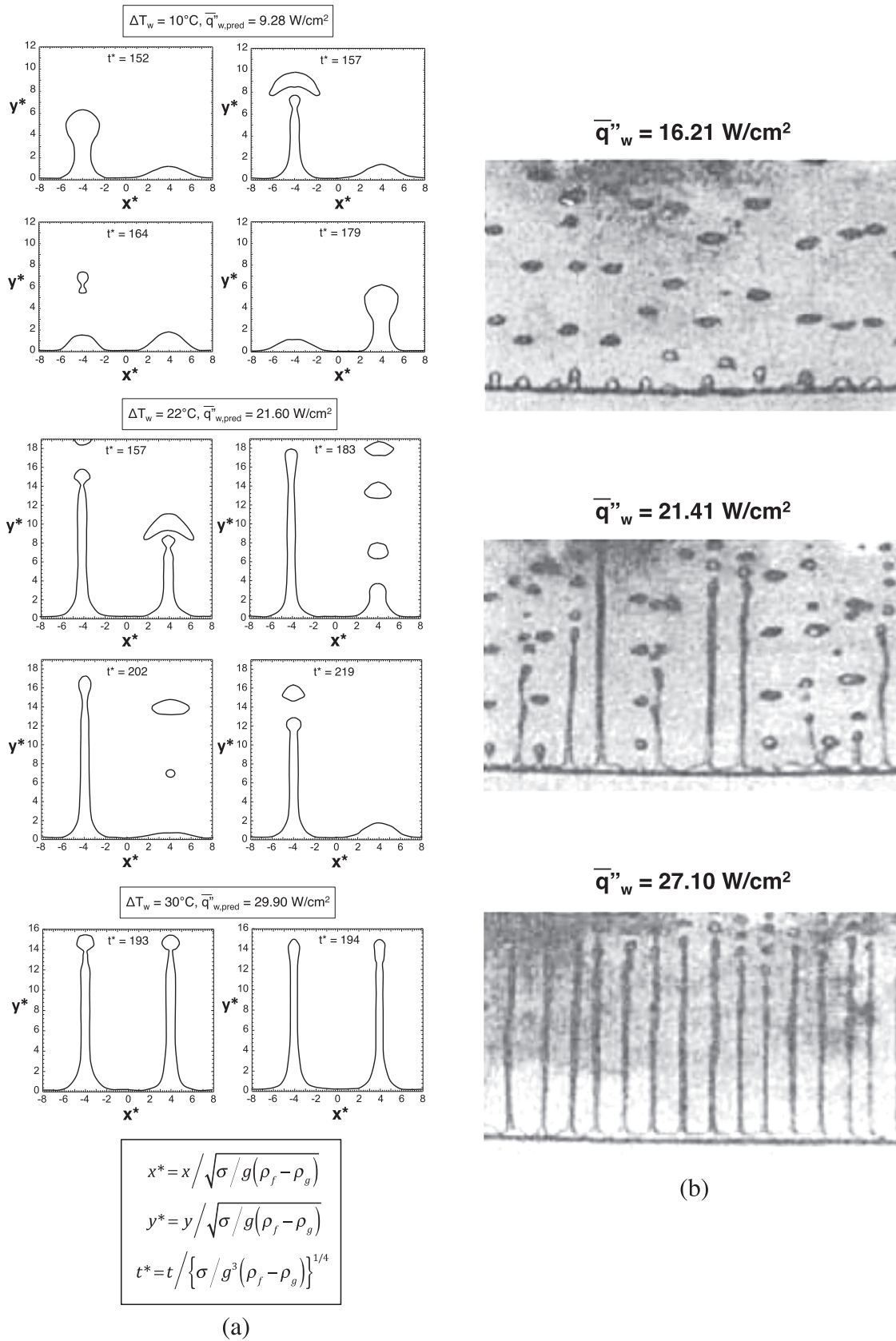
$$x* = x \Big/ \sqrt{\sigma \big/ g(\rho_f - \rho_g)}$$

$$y* = y \Big/ \sqrt{\sigma \big/ g(\rho_f - \rho_g)}$$

$$t* = t \Big/ \left\{ \sigma \big/ g^3(\rho_f - \rho_g) \right\}^{1/4}$$

(a)

(b)

Fig. 9. (a) Simulation results for film boiling of water using LS scheme in 2-D domain with energy jump condition for ΔT_w = 10, 22, and 30 °C. (b) Experimental results for film boiling of water for different heat fluxes. Adapted from Son and Dhir [47]
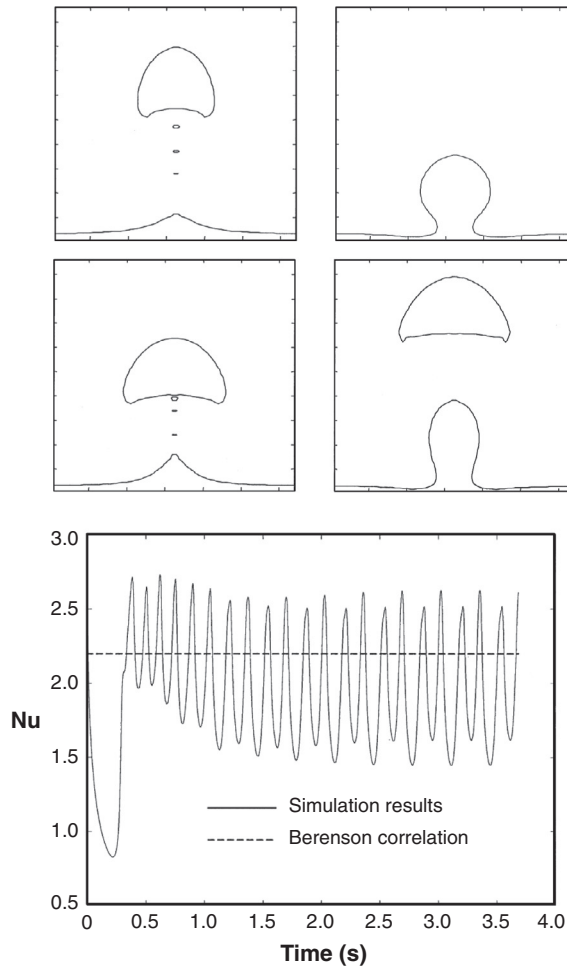
Fig. 10. (a) Simulation results of film boiling using VOF scheme in 2-D domain with energy jump condition. (b) Comparison of simulation results of Nusselt number and prediction of prior correlation. Operating conditions for simulations are: T_{sat}=500 K, p_{sat} = 1.013 × 10^5 Pa, σ = 0.1 N/m, h_{fg}=10 kJ/kg, ΔT_w = 10 °C, ρ_f = 200 kg/m³, ρ_g = 5 - kg/m³, $c_{p,f}$ = 400 J/kg K, $c_{p,g}$ = 200 J/kg K, k_f = 40 W/m K, k_g = 1 W/m K, μ_f = 0.1 Pa s, and μ_g = 0.005 Pa s. Adapted from Welch and Wilson [102].

vapor bubble was initiated at the center of a square 200-μm micro-channel with superheated liquid flowing around it. Using a constant contact angle, they found that bubble growth rate increases with increasing superheat and decreases with increasing flow rate. Fig. 11 depicts bubble growth for T_{in} = 102 °C and wall superheat of ΔT_w = 7 °C. The initial bubble maintains spherical shape while growing until it reaches the size of the channel's cross-section, following which it begins to grow axially into oblong shape, a behavior that is qualitatively consistent with experimental observations. Mukherjee [183] extended this model to bubble growth in flow boiling along the wall of a micro-channel. His simulations suggest the effect of contact angle on a moving meniscus in flow boiling is far less significant than in nucleate pool boiling. Mukherjee and Kandlikar [184] extended this model further to flow boiling in a micro-channel with inlet flow constriction, and showed that the restriction decreases bubble growth and increases flow reversal. Mukherjee et al. [185] also examined wall heat flux during vapor bubble growth along a micro-channel. Their simula-
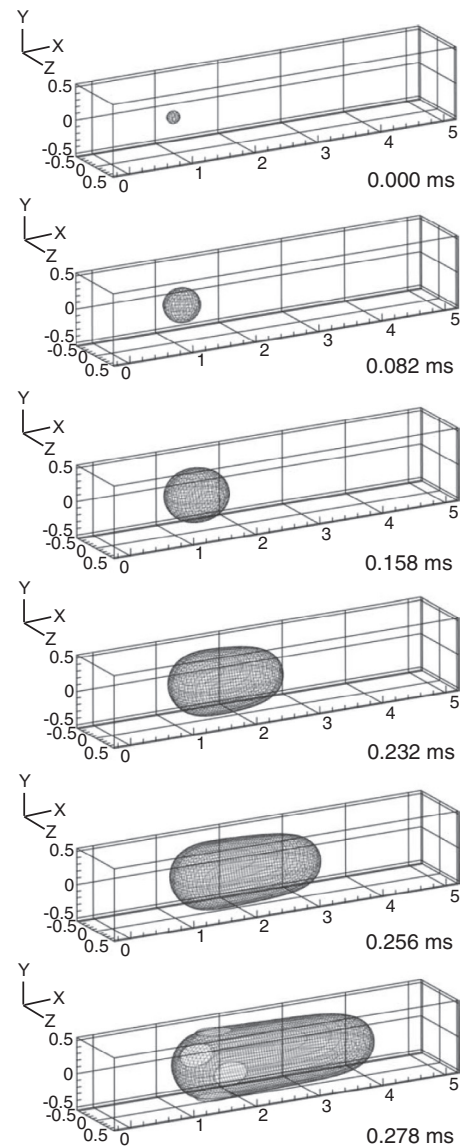
maintaining heat flux above incipient boiling, but safely below CHF. There is also a gradual axial increase in vapor production, which increases void fraction and results in several transitions between two-phase flow patterns. For example, vertical upflow in a long heated circular tube with subcooled inlet produces a succession of flow patterns, including pure liquid, bubbly, slug, annular, mist, and pure vapor. However, changes in any of the system parameters, such as inlet pressure, inlet quality, mass velocity, heat flux, tube diameter, or orientation relative to gravity, can have a drastic influence on transport behavior within each flow pattern, as well as transitions between patterns, hence on pressure drop, heat transfer coefficient, and CHF.

By examining the progress made with direct numerical simulations of nucleate boiling and film boiling, it is evident that their adaptability to flow boiling scenarios of practical interest requires extremely high grid resolution, rendering computations practically impossible. This is why investigators attempting full-scale simulation of flow boiling, such as in micro-channels, usually rely on simple models with coarser grid. Reviewed below are these flow boiling simulation efforts.

Mukherjee and Kandlikar [182] studied vapor bubble growth in water along a micro-channel using the LS method in 3-D domain, with phase change based on energy jump condition. A spherical

Fig. 11. Simulation results for vapor bubble growth in water flow boiling along a 200-μm micro-channel using LS scheme in 3-D domain with energy jump condition for T_{in} = 102 °C, ΔT_w=7 °C, Re = 100, and g = 0. Adapted from Mukherjee and Kandlikar [182].

tions yielded good agreement of bubble growth rate with experiments, and wall heat flux was shown to increase with increasing superheat, unaffected by changes in flow rate.

Magnini et al. [78] incorporated the height function interface reconstruction method in the VOF scheme, with phase change according to Tanasawa's model, to simulate growth of a Taylor bubble during flow boiling in micro-channel. The model was solved in Fluent using 2-D domain for three different fluids, R113, R134a, and R245fa. Fig. 12(a) shows axial growth of an R113 bubble for $G = 600\ kg/m^2\ s$ and $q''_w = 9\ kW/m^2$. Figs. 12(b) shows velocity contours along with variations of axial and radial velocities, and Fig. 12(c) temperature contours and corresponding heat transfer coefficient variations as compared to single-phase flow. Magnini et al. performed single-phase computations separately in the single-phase liquid domain. Based on the computed flow and temperature field variations around the bubble, they identified four separate heat transfer regions: wake region downstream from the bubble ($z/D = 8$–10), wake region near the bubble ($z/D = 10$–12.5), liquid film region ($z/D = 12.5$–19), and liquid region upstream of the bubble ($z/D > 19$). Magnini et al. [186] extended this work to two elongated Taylor bubbles, and showed how bubble overlap improves heat transfer compared to a single bubble. In another study, Magnini and Thome [187] investigated back-to-back vapor bubbles that are generated at fixed frequency.

Lee and Son [188] studied flow boiling of water in a micro-channel using the LS method in 3-D domain, with phase change based on energy jump condition, by incorporating a simplified model for micro-layer evaporation as in [106], and achieved good agreement of predicted bubble growth rate with experiments. They showed that both bubble growth rate and wall heat transfer rate increase when channel size is smaller than bubble departure diameter. Suh et al. [189] extended the same model to parallel micro-channels, accounting also for the solid wall. They captured the backward bubble expansion responsible for flow reversal that occurs when bubbles do not form concurrently in the separate channels. They also showed that the backward bubble growth reduces wall heat transfer rate in multiple micro-channels compared to a single micro-channel.

Zu et al. [99] studied flow boiling of water in a micro-channel using the VOF method in 3-D domain by approximating phase change using a method they termed "pseudo-boiling". They injected vapor artificially through a small hole on the wall to simulate nucleation. Then bubble growth was defined by a fixed rate of vapor generation at the contact area between the bubble and the superheated wall; the vapor injection and generation rate were based on experimental observations [100]. This method was shown to reproduce experimental observations of bubble distortion and trajectory. Zhuan and Wang [90] studied nucleate boiling of water in a micro-channel using the VOF method in 3-D domain, along with correlations to define interfacial mass and energy transfer for different stages of boiling, and achieved qualitative agreement with prior experiments. Zhuan and Wang [190] extended this model to flow boiling of R134a and R22 in a micro-channel with mass velocities ranging from 350 to 2000 kg/m² s, and demonstrated good agreement of predicted flow patterns and flow pattern transitions with experimental data.
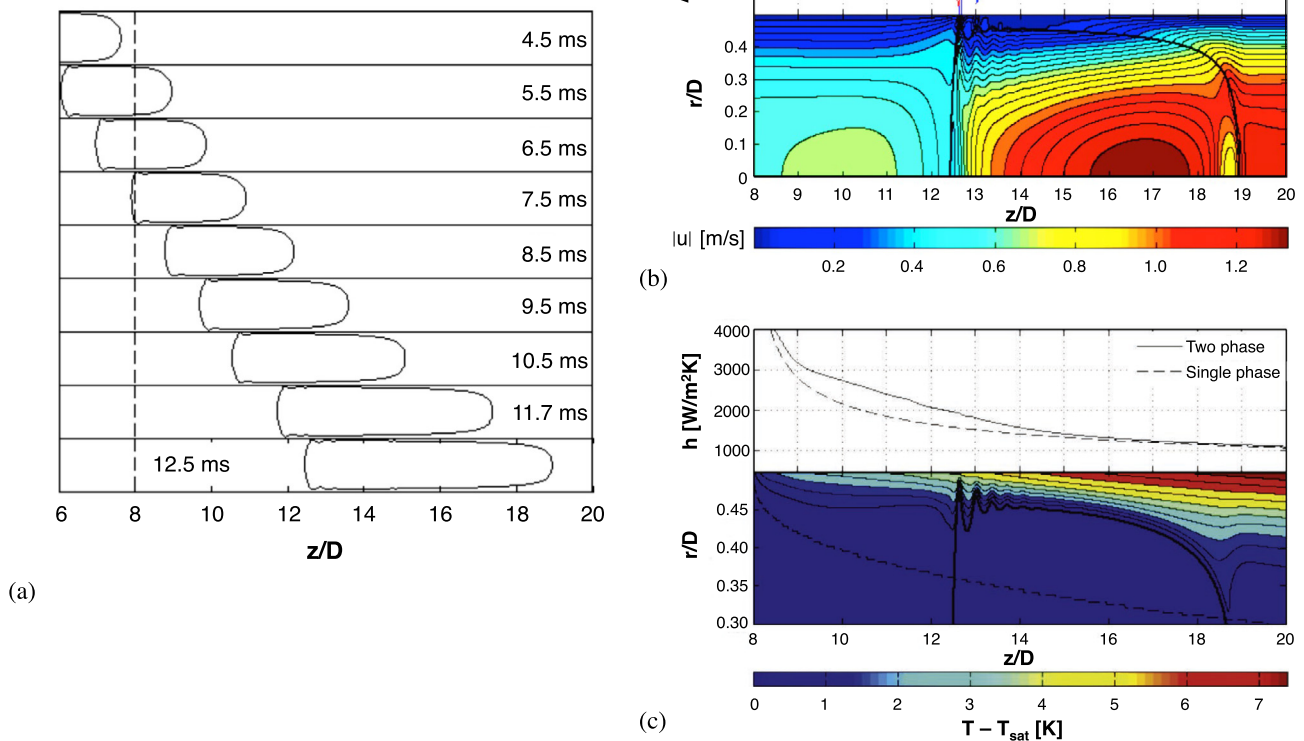

Fig. 12. (a) Simulation results for bubble growth in flow boiling of R113 along a 0.5-mm channel at $G = 600\ kg/m^2\ s$ using VOF scheme in 2-D axisymmetric domain with Tanasawa phase change model (dashed line marks entrance to heated region). (b) Average liquid axial and radial velocities (above) and velocity contours (below); the thick solid black line indicates bubble interface. (c) Heat transfer coefficient (above) and temperature contours (below). Adapted from Magnini et al. [78].

Bubble growth in subcooled flow boiling is undoubtedly more complicated that in saturated flow boiling. Here, superheated liquid is present close to the heated wall, and subcooled liquid in the central core, causing bubbles departing from the wall to incur condensation in the core. Zhuan and Wang [191] studied the effects of subcooled boiling of water on bubble growth, condensation and collapse using the VOF model with bubble condensation rate based on a heat transfer coefficient correlation by Warrier et al. [192]. The predicted flow patterns corresponded well with experimental observations, but heat transfer coefficient predictions were less accurate. Jeon et al. [95] investigated condensation of a bubble in subcooled water in a channel with rectangular cross section in vertical upflow using the VOF method in 3-D domain, with phase change based on an interfacial heat transfer correlation from [96]. Fig. 13(a) compares predicted temporal variations of bubble shape alongside actual bubble images. Since initial conditions affect bubble shape, they were not able to compare exact bubble shape with experiments. However, as shown in Fig. 13(b), bubble volume agrees well with experimental data, an indication of the effectiveness of the model in capturing mass transfer rate. Pan et al. [193] also studied condensation of water bubbles in a vertical channel using the VOF scheme in 3-D domain, and formu-lated phase change based on heat transfer coefficient $h_i = k_f Nu_b/D$, where $Nu_b = f(Re_b, Pr_f, Ja, Fo_{bi})$, and Re_b, Pr_f, Ja, and Fo_{bi} are, respectively, the bubble Reynolds number, liquid Prandtl number, Jacob number, and Fourier number evaluated using initial bubble diameter. Their predictions of bubble size, deformation and lifetime compare well with prior experiments. Bahreini et al. [87] studied bubble condensation in subcooled water flow using the VOF scheme in 2-D domain with phase change based on the Lee model [85], and their predictions show consistency with prior experimental observations.

Several researcher teams [88,194–199] have relied on the Lee model [85] to simulate phase change during flow boiling using 3-D domain. Wu et al. [194] used the Eulerian multiphase phase model in Fluent. Unlike the VOF model, this model solves continuity and momentum equations separately for the two phases, and coupling at the interface is achieved through pressure and inter-phase exchange coefficients. Wu et al. studied flow boiling of R141b in a horizontal serpentine tube with heating along only the straight sections, where flow enters the tube 3 °C subcooled and exits saturated. They accounted for turbulence using Realiz-able k-ε model, and showed good agreement of predictions with experiments. Yang et al. [195] simulated flow boiling of R141b in
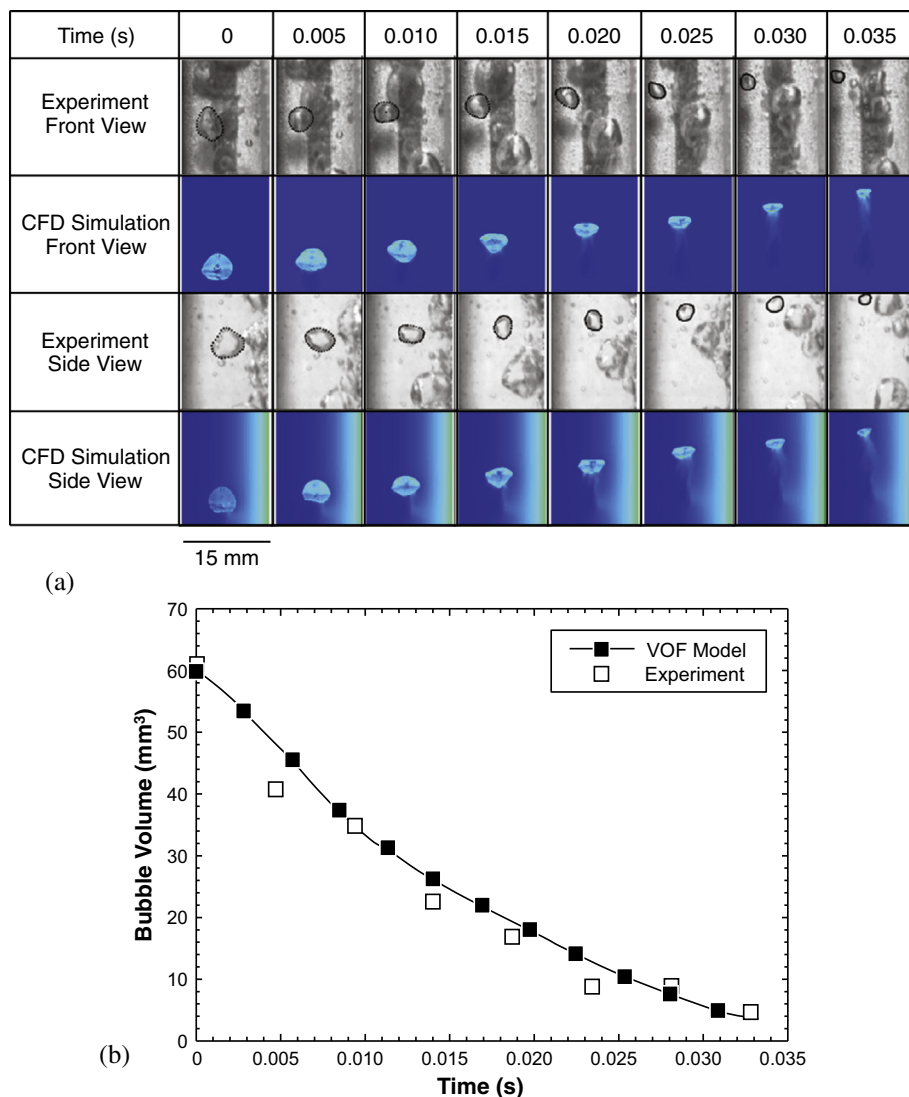

(a)

(b)

Fig. 13. (a) CFD simulations of void fraction for condensation in subcooled water flow using VOF scheme in 3-D domain with phase change based on heat transfer correlation, compared to experimentally captured images. (b) Comparison of temporal variations of predicted and experimental bubble volume. Adapted from Jeon et al. [95].

heated coiled tube with circular cross section, with the flow entering the tube 8.5–10.5 °C subcooled. They used the VOF scheme in Fluent using 3-D domain and, like Wu et al., used Realizable k-ε model for turbulence. They captured experimentally observed flow regimes, including bubbly, churn, slug, stratified, and wavy, in order of increasing flow quality. As shown in Fig. 14, both simulations and experiments show increasing flow rate for fixed heat flux delays transition to higher quality flow regimes, while increasing heat flux for fixed flow rate promotes earlier transition to high quality regimes. Fang et al. [196] simulated flow boiling of water in a vapor venting micro-channel with 3 °C inlet subcooling using VOF model in Fluent, and assumed laminar flow because of low Reynolds numbers. They showed that the vapor venting micro-channel produces lower pressure drop than a micro-channel without venting for the entire range of heat fluxes below critical value, which defines when vapor generation rate exceeds vapor venting capacity of the channel, but pressure drops are similar above this value. Wei et al. [197] simulated subcooled flow boiling of water in a vertical rectangular channel with single-sided heating using the VOF scheme, and achieved good agreement with correlations from literature. They also induced inertia by swing motion and, as expected, found pressure to increase in comparison to motionless conditions. De Schepper et al. [88] simulated hydrocarbon feedstock of the convection section of a steam cracker in 3-D domain using standard k-ε model for turbulence, and were able to capture flow regimes from the literature. Lee et al. [198] investigated void fraction patterns, temperature, and pressure in specially designed micro-channels for GaN-on-SiC semiconductor devices. Lorenzini and Joshi [199] studied the effects of non-uniform heating on high-flux micro-channel flow boiling.

Other noteworthy simulations of micro-channel boiling flow include a study by Nichita and Thome [68], who used CLSVOF with a simplified source term based on energy jump condition to study bubble growth and departure in a micro-channel. Using the Level Set Two-Phase Flow Mode available in Chemical Engineering Module in the commercial finite element analysis software COMSOL, Zhou et al. [200] performed both steady state and transient computations of flow boiling to explore both bubble flow patterns and flow transitions. They also showed how reentrant cavities increase dryout heat flux. Pan et al. [201] defined a new source term for phase change based on energy required for the cell containing the interface to achieve saturation conditions. They defined the energy and mass source terms as

$$Q = \frac{\alpha_g \rho_g c_{p.g}(T_{sat} - T) + \alpha_f \rho_f c_{p.f}(T_{sat} - T)}{\Delta t} \tag{47}$$

and

$$S_g = -S_f = -Q/h_{fg}. \tag{48}$$

They tested this method with saturated flow boiling in circular and square micro-channels using 2-D and 3-D domains, respectively. They used the non-iterative time advancement (NITA) scheme in Fluent and iteratively solved the energy equation to set interfacial temperature to T_{sat}, and showed good agreement with prior findings.

As an example of other simulation approaches, Krepper et al. [97] studied subcooled flow boiling in a channel of a nuclear fuel assembly in commercial software CFX using a two-fluid Eulerian approach. This approach requires validation and improvement in interfacial source/sink terms and results are very application specific. Krepper et al. adopted the wall boiling model by Kurul and Podowski [202] and compared predictions to experimental data by Bartolomej and Chanturiya [203] and Bartolomej et al. [204] for preliminary model validation. Krepper and Rzehak [205] and Krepper et al. [206] further improved this model for vertical upflow boiling of R12 in a heated circular pipe.
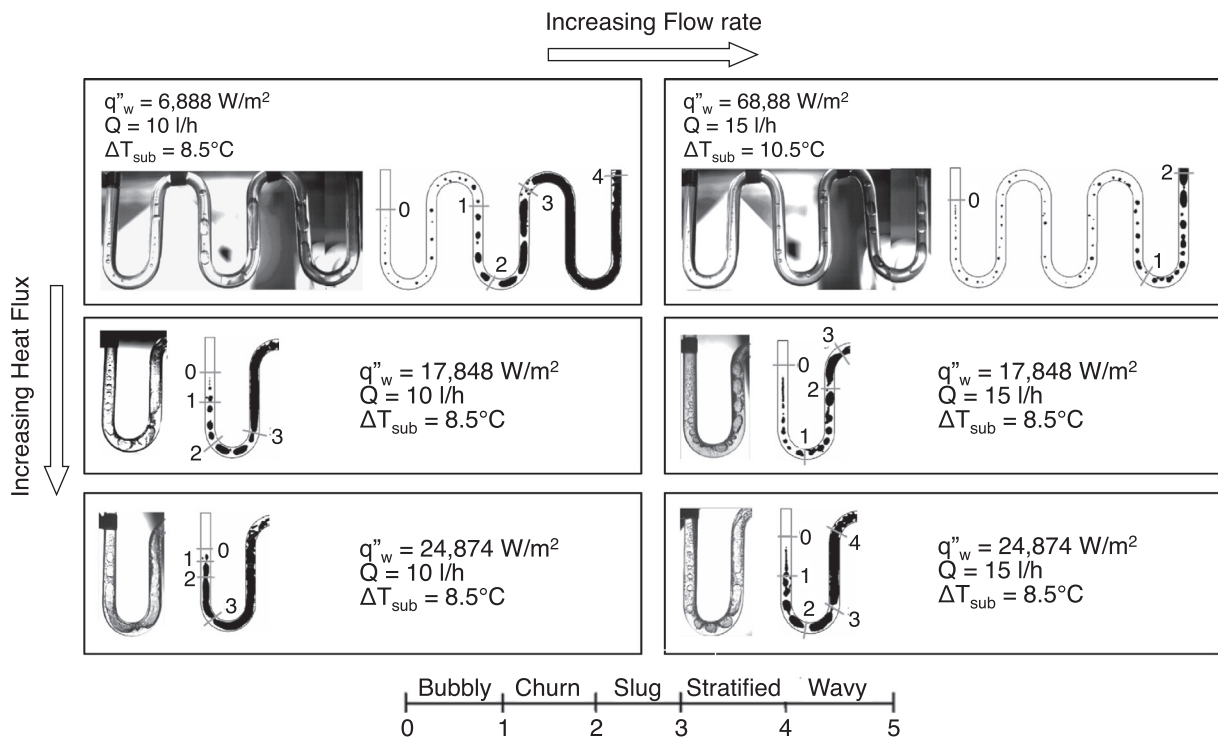

Fig. 14. Comparison of simulation predictions and experimental results for axial variations of flow regimes and void fraction for horizontal flow boiling of R141b along a 6-mm diameter serpentine tube. Simulations are based on VOF scheme in 3-D domain and Lee phase change model. The tube has a centerline length of 70 mm and 28 mm pitch. Dark color in simulation results represents vapor-liquid interface and not vapor phase. Adapted from Yang et al. [195].

5.2. Condensation

Condensation is commonly encountered in heat exchange devices tasked with rejecting heat from a closed two-phase loop, and is associated with conversion of vapor to liquid. Common condensation configurations include film condensation with and without flow, dropwise condensation, and internal flow condensation. Film condensation involves formation of a liquid on a wall whose temperature is below saturation, and the film increases in thickness and flow rate in the direction of gravity in the absence of vapor flow, or in the flow direction in the presence of high vapor shear. This form of condensation is encountered mostly on tubes or vertical walls. Dropwise condensation is characterized by droplets covering the wall, which range in thickness from a few micrometers to larger, more visible liquid masses. Flow condensation occurs within a tube and involves a succession of flow patterns including pure vapor, annular, slug, bubbly and pure liquid [207] in order of decreasing quality. In the literature, numerical simulations have been focused on film condensation and internal flow condensation. This is why the review below will be focused on these configurations.

Early simulations of flow condensation were performed by Zhang et al. [101] in an investigation of capillary blockage in mini-channel. Using the VOF scheme in 2-D domain, they applied an artificial source term to force the interface to T_{sat}, then calculated an energy source term and corresponding mass source term using the newly updated temperature field. Their results show that increasing flow velocity increases the length required to achieve full condensation, and higher flow rates increase interfacial waviness. Yuan et al. [208] studied film condensation between parallel plates in vertical downflow in 2-D domain using an approach to achieve T_{sat} at the interface similar to that of Zhang et al., along with the traditional VOF scheme, but defined fluid fraction in terms of total enthalpy. Liu et al. [89] also studied vertical downflow film condensation between parallel plates using the VOF method in 2-D domain, but with phase change based on the Lee model [85]. They showed the condensing film is initiated in smooth laminar state and becomes wavy laminar downstream due to increases in both Reynolds number and film thickness as depicted in Fig 15.

Da Riva and Del Col [209] used the VOF scheme with phase change based on the Lee model [85] to study flow condensation of R134a in a circular micro-channel at different orientations relative to gravity and in microgravity. Gravity dominance was observed at low mass velocity of $G = 100$ kg/m^2 s, with large differences in flow and heat transfer behaviors corresponding to different orientations. Differences were significantly reduced as mass velocity was increased to $G = 800$ kg/m^2 s, where inertia began to dominate gravity. Ganapathy et al. [69] studied flow condensation of R134a in a micro-channel using the VOF scheme with phase change based on a simplified form of energy jump condition, and achieved qualitative agreement with flow patterns captured in prior experiments as shown in Fig 16. They also achieved good agreement of two-phase frictional pressure drop and Nusselt number predictions with prior correlations from the literature. In another study, Chen et al. [86] used the VOF scheme to simulate flow condensation of FC-72 in a micro-channel, and their predictions of two-phase flow patterns agreed quite well with prior experiments. Yin et al. [210] and Zhang et al. [211] studied flow condensation in horizontal tubes. Yin et al. [210] studied the effect of non-condensable gases on flow condensation in horizontal micro-tubes using the VOF scheme and showed how heat transfer is significantly compromised in the presence of air. Zhang et al. [211] investigated flow condensation of R410a in horizontal tubes ranging in diameter from 0.25 to 4 mm. Using the VOF scheme,
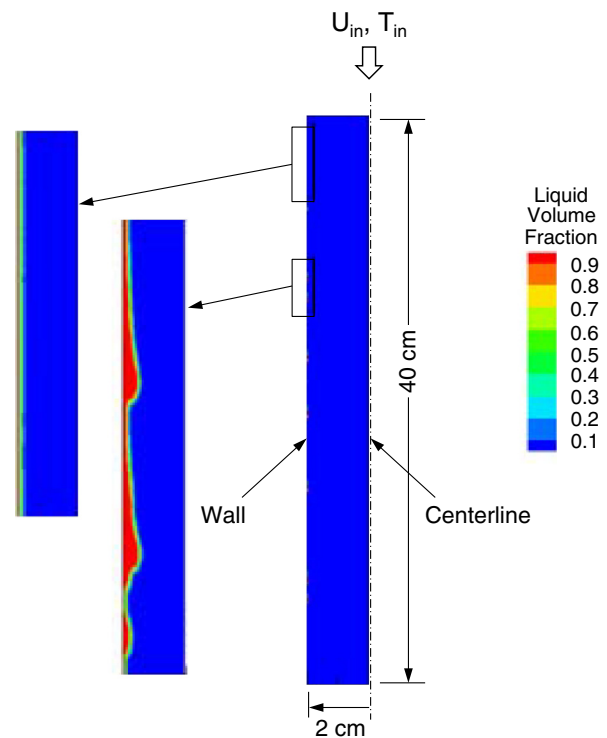

Fig. 15. Void fraction predictions for film condensation of water during vertical downflow between parallel plates using VOF scheme in 2-D domain and Lee phase change model. Adapted from Liu et al. [89].

they achieved good agreement of predicted heat transfer coefficients and pressure drops with empirical correlations.

Internal flow condensation studies at the macro scale include vertical downflow by Lee et al. [212] and vertical upflow by Qiu et al. [213] and Kharangate et al. [214]; all of whom used the VOF scheme with phase change based on the Lee model [85]. Kharangate et al. investigated high heat flux vertical upflow condensation of FC-72 by rejecting heat to water flowing in counter-flow through an outer annulus. They used the k-ω model with Shear Stress Transport (SST) and a turbulence dampening factor of 10 as defined in the ANSYS Guide [215] to account for turbulence across the annular liquid film and the vapor core. Their simulations yielded predictions of axial variations of void fraction, radial temperature profile, and heat transfer coefficient. Fig. 17(a) compares predicted and measured annular film flows corresponding to the climbing (upward moving) film regime. They both show interfacial ripples along the liquid film's interface, and liquid droplets entrained in the vapor core. Fig. 17(b) shows good agreement between predicted and measured average heat transfer coefficient for a broad range of mass velocities. Another important aspect of their study is the temperature distribution across the liquid film and influence of interfacial dampening of eddy diffusivity at the interface due to surface tension, as shown in Fig. 17(c). This important interfacial dampening phenomenon will be addressed in more detail later in this paper. In another study, Qiu et al. [216] used the VOF scheme to study flow condensation of propane in an upright spiral tube. Alizadehdakhel et al. [217] used the VOF scheme in 2-D domain, with phase change based on the Lee model, to investigate simultaneous evaporation and condensation of water in a thermosyphon. Fig. 18(a) shows predicted wall temperature along the evaporation, adiabatic, and condensation sections of the thermosyphon, alongside closely matched experimental data. Fig. 18

Fig. 16. Comparison of numerically predicted condensation flow regimes for R134a along a 100-μm wide micro-channel using VOF scheme in 2-D domain with simplified form of energy jump condition, and experimental images from the literature. Adapted from Ganapathy et al. [69].

(b) shows the computational domain and vapor void fraction contours captured in the three sections.

Other noteworthy investigations are two simulation studies by Liu and Cheng [218,219], who used the LB method to model both film and dropwise condensation.

The reader should refer to [220] for more comprehensive summaries of relevant computational studies on bubble nucleation, growth and departure, film boiling, flow boiling, and flow condensation discussed in this paper, including information on phase change configuration, test fluid, multiphase scheme, mesh, and mass source formulation.

6. Future needs and recommendation

6.1. Overriding needs

Clearly, investigators have achieved many noteworthy breakthroughs in simulating boiling and condensation systems. However, there is broad diversity in the methods used, and computations are presently limited to rather simple configurations, unlike the many diverse configurations found in systems of practical interest as discussed in the Introduction. Looking forward, it is universally acknowledged that computational tools will play a vital role in two-phase flow and heat transfer research, in departure from the present practice of relying on empirical correlations and costly experimental work. However, several important tasks must be undertaken before investigators can achieve the long-term objective of developing a *more unified, physically based, accurate, and computationally efficient methodology*. Key among these tasks are:

(1) New experiments designed specifically for validation of simulation models of boiling and condensation, and involving simultaneous use of state-of-the-art diagnostics tools.
(2) New or improved interface tracking schemes that conserve mass and accurately capture complex interface topologies.
(3) New or improved mass transfer models that capture the true physics of mass and energy transfer at the interface.

(4) New or improved turbulence models that accurately account for dampening of eddies across the liquid-vapor interface.
(5) More aggressive computational modeling of complicated phase-change configurations prevalent in modern applications.

6.2. Validation experiments and better diagnostics tools

Like experiments that have already been used to validate prior simulation work, future experiments must be carefully designed for the specific purpose of validating future simulations. Use of state-of-art diagnostic tools will play a vital role in these experiments. Aside from maximizing the use of conventional pressure, temperature, and flow rate measurement instrumentation, phase change experiments intended for validation of simulation models will require implementation of sophisticated diagnostic tools to measure volume fraction as well as both velocity and temperature contours. It is obvious from studies reviewed earlier that investigators have relied heavily on high-speed video imaging of the interface as a means of assessing the validity of two-phase schemes. This non-intrusive method of image capture and analysis has been used to determine interface shape and in many cases used to infer void fraction. But, while high-speed video will continue to play a vital role in most phase change experiments, investigators often face difficulty resolving accurate void fraction information in situations involving multiple overlapping interfaces or reflection from the heated wall. Some researchers [221,222] have employed a 'total reflection method' to mitigate reflection problems, by visualizing the boiling process from behind a completely transparent heated wall, with a silicon oil layer used beneath the wall. However, a key drawback of this approach is it precludes testing realistic metallic surfaces when performing boiling experiments, given that lateral conduction plays a key role in all boiling situations. Temperature measurements can be made with probes embedded directly in the heated wall and in the flow. But most temperature measurements suffer from spatial resolution issues and relatively slow response time. Temperature sensors with fast response and higher spatial resolution have been developed by Heng et al.
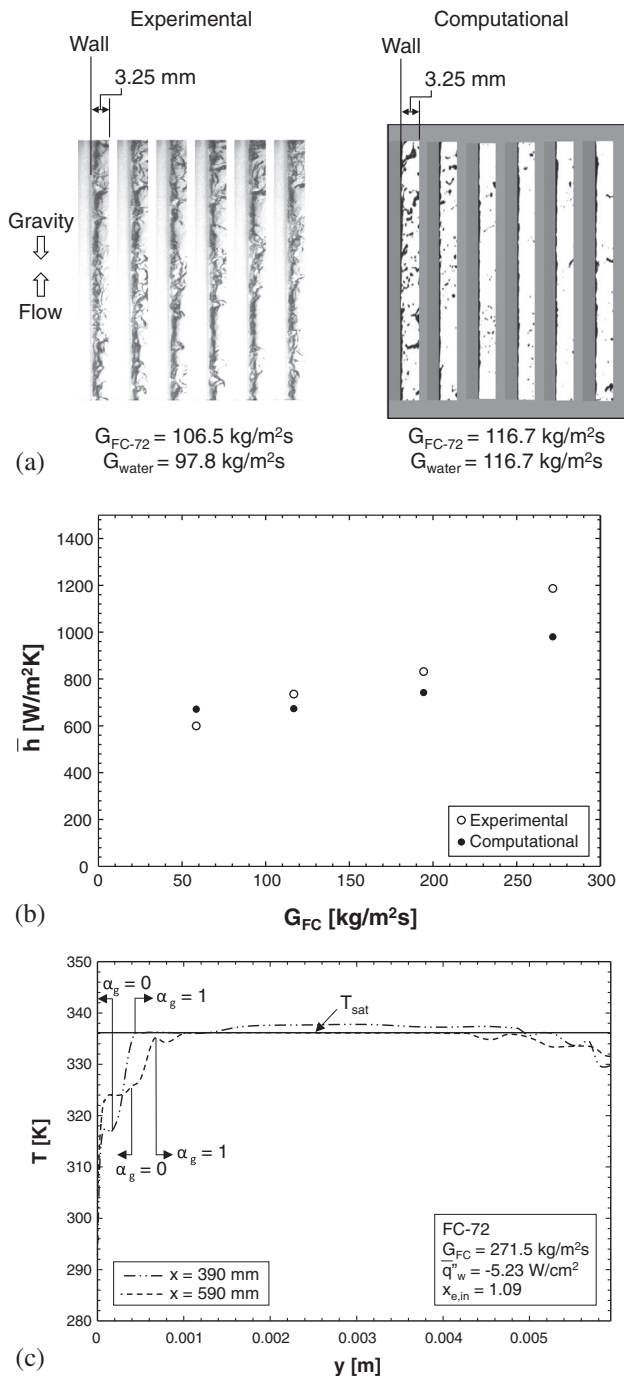
Fig. 17. (a) Void fraction predictions using VOF scheme in 2-D axisymmetric domain and Lee phase change model of climbing film regime during vertical upflow condensation of FC-72, and experimental images. (b) Comparison of experimental and computed spatially averaged condensation heat transfer coefficient versus mass velocity. (c) Variation of computed fluid temperature with radial distance from the wall at two axial locations for G_{FC} = 271.5 kg/m² s. Adapted from Kharangate et al. [214].

[223] and Moghaddam and Kiger [224], respectively. Multi-sensor conductivity and optical probes by Barrau et al. [225] and Kim et al. [226], and wire mesh probes by Prasser et al. [227] have been used to measure bubble diameter and velocity in pool boiling. Lyu and Mudawar [228–230] used a thin blade fitted with an array of micro-thermocouples to measure instantaneous temperature profile across a wavy, free-falling water film, simultaneously with measurements of film thickness and wave speed using thermal

conductance sensors. Mudawar and Houpt [231,232] used laser Doppler velocimetry (LDV) to measure velocity profile (including turbulent fluctuations) across a free-falling film simultaneously with film thickness, the latter using an electrical conductance probe. This technique facilitated detailed mapping of liquid velocity streamlines relative to interfacial waves. A key limitation of many of the instruments just mentioned is their intrusive nature. A very promising tool for velocity measurements is micro-particle image velocimetry (μ-PIV), which was used by Qu et al. [233] to measure liquid velocity profile in a micro-channel, and infrared (IR) thermography, used by Theofanous et al. [234,235] to capture thermal patterns on a heated wall. Khodaparast et al. [236] employed another type of μ-PIV called micro-particle shadow velocimetry (μ-PSV) to measure micro-channel flows. Further improvements in velocity measurements for boiling and condensing flows are possible with 3D PIV [237,238]. For micro-channel measurements, two noteworthy examples of studies involving simultaneous use of multiple diagnostic tools are experiments by Gerardi et al. [239] and Duan et al. [240]. These recent studies are good examples of the type of experiments and diagnostics tools that are needed for validation of future simulations of boiling and condensation.

6.3. Improving interface tracking methods

Reviewed earlier in this article were several methods of interface tracking along with their advantages and disadvantages. Overall, it is crucial for numerical schemes to accurately conserve mass as well as capture interface topologies accurately. Even though several advances have been made towards accomplishing these goals, further improvements are necessary to tackle complex phase change scenarios. One aspect of interface tracking is the treatment of interface thickness. Some models use zero thickness [102], but are numerically difficult to solve, while others use an artificial thickness to smooth properties across multiple cells [47,77].

While different methods are available to account for surface tension, spurious currents must be avoided. Phase-field methods [58] take into account physical interactions at the molecular level better than VOF, LS, and FT methods, hence improvements in those methods may be needed to better capture interfacial physics and surface tension effects.

Computing requirements are perhaps the biggest obstacle in computational modeling of phase change processes, and are the main impetus for preferring 2-D over 3-D simulations. However, two-phase flows are inherently highly three-dimensional and involve complex interface topologies that cannot be accurately resolved with 2-D simulations. Limitations of 2-D simulations have spurred the development of methods that combine multiscale (adaptive) meshes [47,241], where, to reduce computing requirements, analytical models are employed in certain regions of the grid where computations would have otherwise demanded very fine mesh. Overall, while researchers continue to develop new or improved methods for interface capturing, further validation of these methods is required using simulations of more complex phase change processes.

6.4. Improving mass transfer models

The different phase change models that have been developed and/or adopted thus far fall short in both accuracy and ability to capture the true physics of mass and energy transfer at the interface. Simplifying assumptions such as constant temperature in the entire saturated phase, interface maintaining saturation temperature, and zero conductivity of one of the phases, preclude model closure and jeopardize predictive accuracy. In the short term, new or improved adaptive phase change schemes are needed
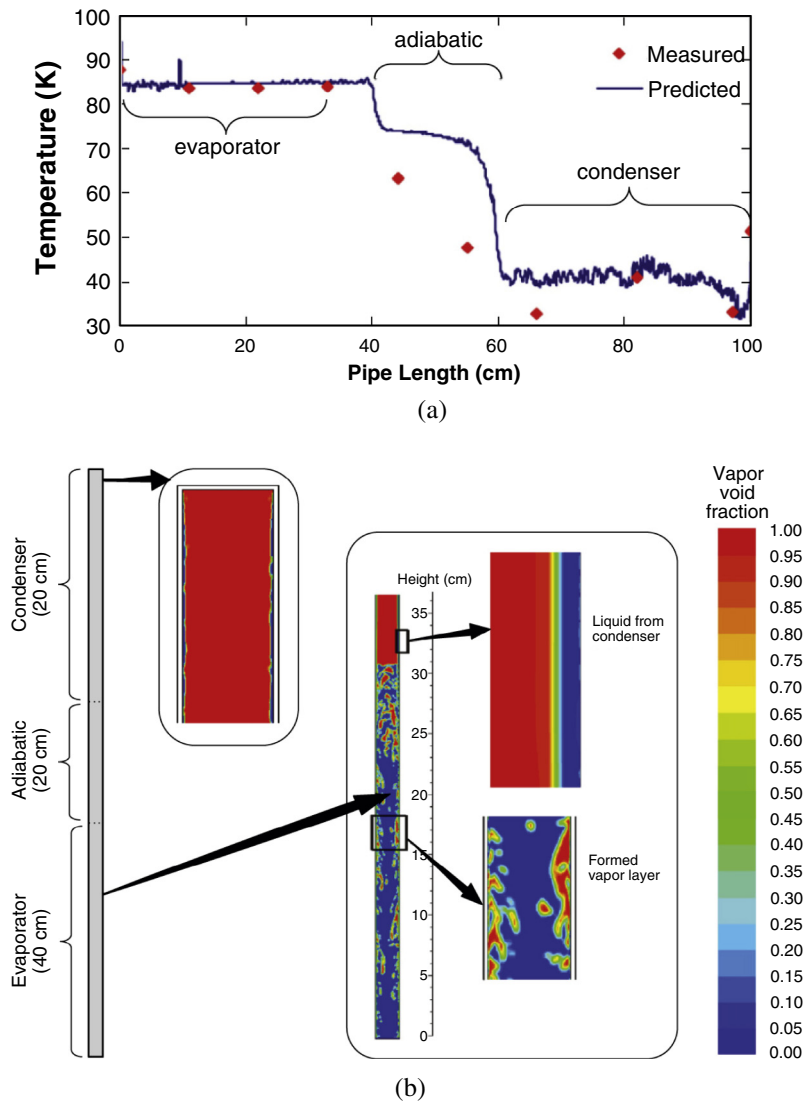
Fig. 18. Simulation results for water thermosyphon using VOF scheme in 2-D domain and Lee phase change model. (a) Comparison of predicted and measured wall temperatures. (b) Void fraction predictions. Adapted from Alizadehdakhel et al. [217].

that can accurately maintain interfacial temperature depending on local temperature deviation of the interface cell. The empirical coefficients in models like those of Tanasawa [83] and Lee [85] could be adjusted locally and not kept constant in simulations. In the long term, new or improved phase change models are needed that can more accurately estimate both mass and energy transfer at the interface, which is lacking is current models.

6.5. Better account of turbulence effects

Turbulence is prevalent in most practical two-phase flow and heat transfer processes. Moreover, two-phase flow generally promotes transition to turbulent flow at much lower Reynolds numbers than single-phase flow. Even though Direct Numerical Simulations (DNS) provide the highest accuracy, computing requirements are a major obstacle to implementing this method for full-scale phase change simulations. Many of the phase change studies involving turbulent modeling that were discussed earlier in this article employ Reynolds-averaged Navier-Stokes (RANS) models like the 2-equation, k-ε and k-ω models. While standard k-ε model is the most widely used turbulent model, it cannot accurately resolve momentum and thermal boundary layers in the

vicinity of the wall, which is why low Reynolds number k-ε model is used in those locations. The standard k-ω model and k-ω model with Shear Stress Transport (SST) are also good models for momentum and thermal boundary layers. Using either low Reynolds number k-ε model or k-ω models in simulations requires high resolution mesh in locations like the wall or near a liquid-vapor interface.

An important aspect of turbulence in two-phase flows is dampening of turbulent fluctuations at the liquid-vapor interface by surface tension force [79,212,214]. This phenomenon is illustrated in Fig. 19(a) for a thin, free-falling film undergoing interfacial evaporation. As discussed by Kharangate et al. [79], turbulence intensity is reflected in the magnitude of eddy momentum diffusivity, ε_m. Near the wall, $\varepsilon_m \to 0$, which, in the presence of a fairly constant heat flux across the thin film, produces large temperature gradient near the wall. A large increase in ε_m in the middle region of the film greatly decreases temperature gradient, resulting in fairly constant liquid temperature in the middle region. However, turbulent eddies are suppressed at the liquid-vapor interface by surface tension, and with $\varepsilon_m \to 0$ at the interface, a second large temperature gradient is produced near the interface. Fig. 19(b) shows temperature profiles across the film at different axial locations predicted
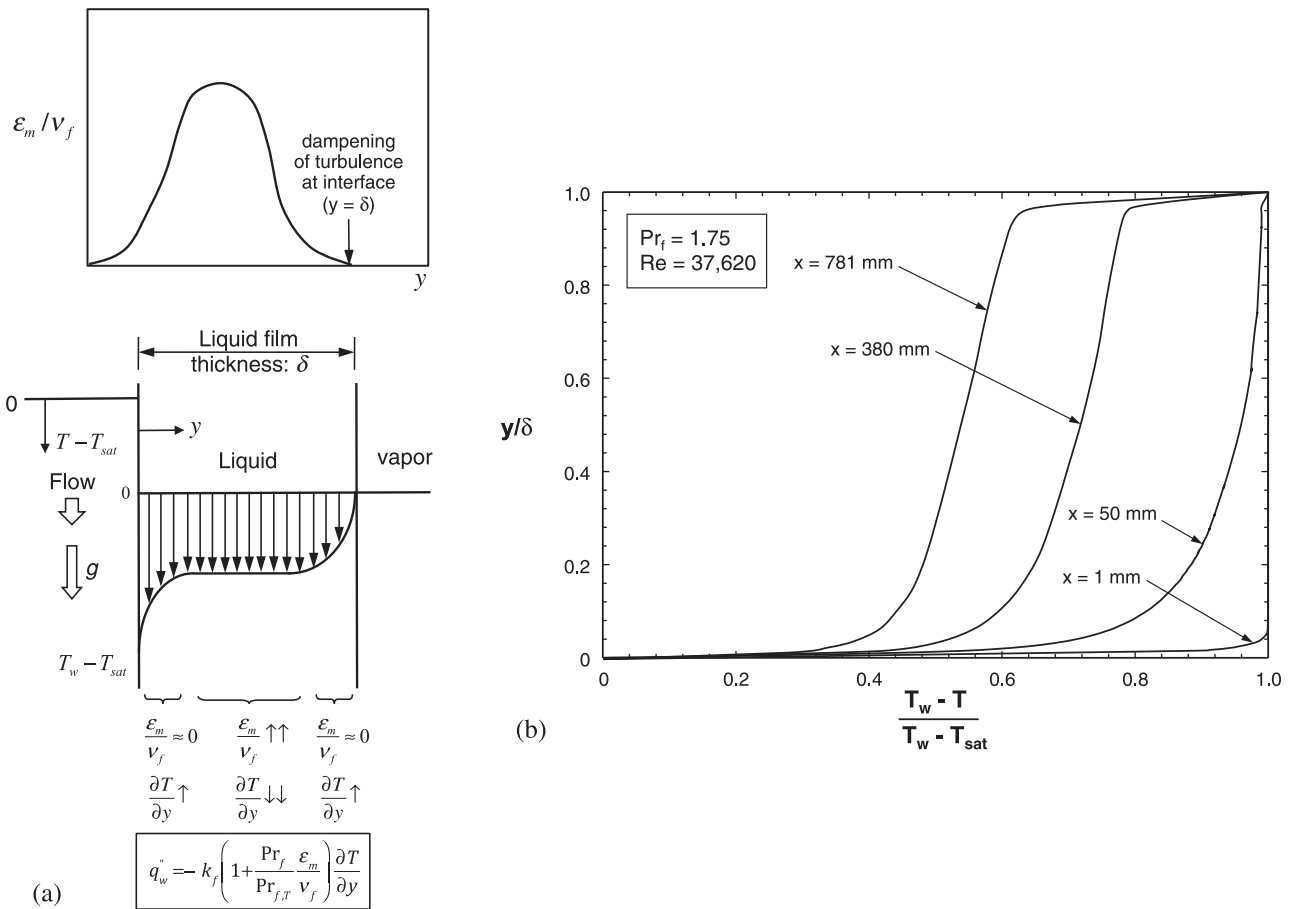
Fig. 19. (a) Schematic representations of eddy momentum diffusivity profile across free-falling evaporating water film, and influence of interfacial dampening of eddy momentum diffusivity on temperature profile. (b) Temperature profiles across evaporating film at different axial locations predicted using VOF scheme in 2-D axisymmetric domain with Tanasawa phase change model. Adapted from Kharangate et al. [79].

using VOF scheme in 2-D axisymmetric domain and Tanasawa's phase change model. To generate the temperature profiles in Fig. 19(b), Kharangate et al. used the k-ω model with Shear Stress Transport (SST), with a turbulence dampening factor of 10. The large interfacial temperature gradient is clearly captured for downstream locations. A similarly large interfacial temperature gradient is captured in annular condensing films [214] as was shown earlier in Fig. 17(c). As discussed by Kharangate et al. [79], the large interfacial gradient can in fact be used to assess the accuracy of phase change models used.

Moving forward, a shift to higher accuracy simulations like Large Eddy Simulations (LES) would constitute an important step towards improving predictive accuracy of computational models involving turbulent boiling and condensing flows.

6.6. Simulating more complex phase-change configurations prevalent in modern applications

It is obvious from the studies reviewed in this article that phase change simulation efforts have been focused on rather simple pool boiling, film boiling, flow boiling and flow condensation configurations. While some attempts have been made to address more complex phase change problems, including falling films [79,80], heat pipes [242], jet impingement [243] and cryogenics [81,244], there is now a need to undertake more aggressive steps to tackle several important phenomena that have received significant attention in

experimental studies and/or are crucial to design of modern phase change devices and systems. Following is a summary of such phenomena:

(1) As shown in Fig. 20(a), two distinct mechanisms have been proposed as dominating flow boiling heat transfer in micro-channel heat sinks: nucleate boiling and convective boiling. And recommendations have been made in numerous, mostly experimental studies regarding operating conditions that render dominant one mechanism versus the other [245,246]. Clearly, computational models might play a crucial role in capturing detailed interfacial behavior associated with each.

(2) Flow boiling CHF is one of the most important design parameters for heat-flux-controlled two-phase cooling systems. For the most common configuration of flow boiling in a tube, experimental evidence points to formation of a wavy insulating vapor layer prior to CHF, with cooling provided only in 'wetting fronts' correspond to the wave troughs, Fig. 20(b), with CHF triggered by lift-off of the troughs from the wall [247]. This depiction of interfacial behavior lends itself well to computational modeling.

(3) Two-phase micro-channel heat sinks are susceptible to different types of instabilities, including severe pressure drop oscillations and mild parallel channel oscillations, and these instabilities have been shown to trigger pre-mature CHF [2],
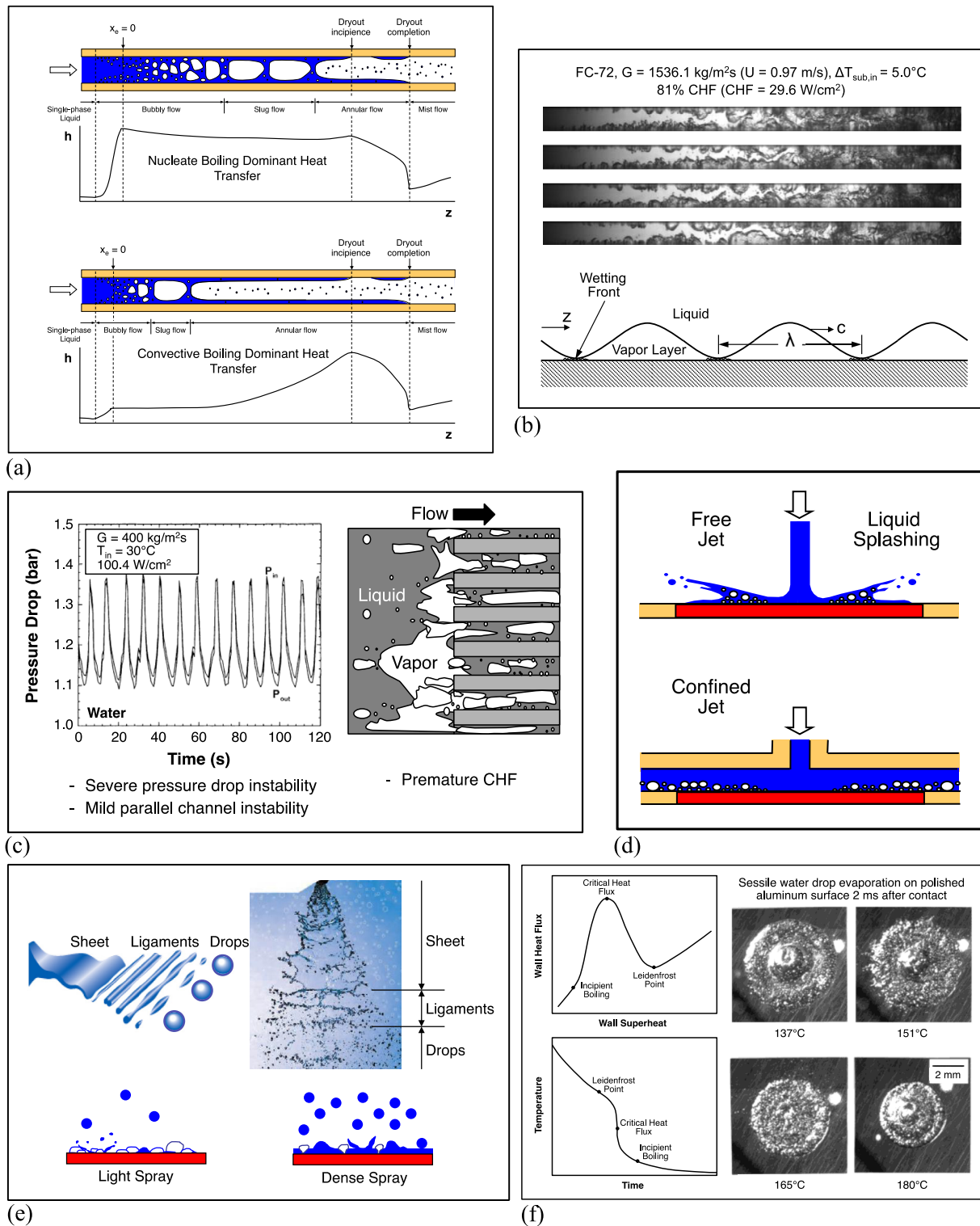
Fig. 20. Examples of phase change phenomena that are crucial to design of modern devices and systems, and which can benefit greatly from computational modeling. (a) Dominant flow boiling heat transfer mechanisms in micro-channels [245,246]. (b) Flow boiling CHF in tubes [247]. (c) Instabilities and premature CHF in micro-channels [2]. (d) Liquid splashing and dryout in free jet impingement [248]. (e) spray cooling and liquid film buildup [3,249]. (f) Leidenfrost phenomenon [250].

as shown in Fig. 20(c). While, as discussed earlier, some investigators have simulated the problem of bubble backflow in micro-channels, more aggressive computational efforts are needed to address these important phenomena.

(4) While jet impingement has been the target of a few computational efforts, important phenomena such as splashing of liquid away from the heated wall and ensuing wall dryout [248], Fig. 20(d), warrant more aggressive computational modeling efforts.

(5) Impact of individual droplets with dry or wet surfaces has been the subject of a substantial number of computational efforts. However, a very important application of droplet impact is spray cooling, where liquid supplied through a nozzle undergoes breakup into a large number of droplets with broad range of trajectories as shown in Fig. 20(e) [3,249]. Admittedly, computational modeling of spray cooling is a formidable task, given its flow complexity and large number of discrete interfaces. Nonetheless, computational efforts might shed light on crucial mechanisms associated with liquid film buildup on the heated wall, and its impact on spray cooling.

(6) The Leidenfrost point is one of the most important phenomena in the production of metal alloys, which is encountered during the quench phase of heat treating [250]. As the metal alloy part is cooled from very high temperature, this point marks a transition from slow cooling in the film boiling regime to fast cooling, as the surface enters the transition boiling regime. This behavior, which is depicted in Fig. 20(f), has a strong bearing on alloy microstructure and hence mechanical properties of the part produced. Accurate computational modeling of the Leidenfrost point will therefore have a profound practical impact on the entire heat treating industry.

7. Concluding remarks

This article reviewed published papers concerning computational fluid dynamics simulations of boiling and condensation. Two-phase schemes and surface tension models adopted by different research teams were discussed, followed by thorough discussion on implementation of mass transfer across the two-phase interface. Also included was a comprehensive review of articles covering a variety of boiling and condensation configurations, along with the computational methods used, examples of their predictions, and comparisons with experimental data. The article was concluded with identification of future research needs to improve predictive capabilities, as well as crucial phase change phenomena that warrant significant attention in future computational studies.

Acknowledgement

References

[1] I. Mudawar, Assessment of high-heat-flux thermal management schemes, IEEE Trans.-CPMT: Comp. Pack. Technol. 24 (2001) 122–141.
[2] I. Mudawar, Two-phase micro-channel heat sinks: theory, applications and limitations, J. Electron. Pack. - Trans. ASME 133 (2011) 041002.
[3] I. Mudawar, Recent advances in high-flux, two-phase thermal management, J. Therm. Sci. Eng. Appl. - Trans. ASME 5 (2013) 021012.
[4] P.J. Marto, V.J. Lepere, Pool boiling heat transfer from enhanced surfaces to dielectric fluids, J. Heat Transfer – Trans. ASME 104 (1982) 292–299.
[5] I. Mudawar, T.M. Anderson, Parametric investigation into the effects of pressure, subcooling, surface augmentation and choice of coolant on pool boiling in the design of cooling systems for high-power density chips, J. Electron. Pack. – Trans. ASME 112 (1990) 375–382.
[6] I. Mudawar, T.M. Anderson, Optimization of extended surfaces for high flux chip cooling by pool boiling, J. Electron. Pack. - Trans. ASME 115 (1993) 89–100.
[7] S. Mukherjee, I. Mudawar, Smart pumpless loop for micro-channel electronic cooling using flat and enhanced surfaces, IEEE Trans. - CPMT: Comp. Pack. Technol. 26 (2003) 99–109.
[8] S. Mukherjee, I. Mudawar, Pumpless loop for narrow channel and micro-channel boiling from vertical surfaces, J. Electron. Pack. – Trans. ASME 125 (2003) 431–441.
[9] J.A. Shmerler, I. Mudawar, Local heat transfer coefficient in wavy free-falling turbulent liquid films undergoing uniform sensible heating, Int. J. Heat Mass Transfer 31 (1988) 67–77.
[10] J.A. Shmerler, I. Mudawar, Local evaporative heat transfer coefficient in turbulent free-falling liquid films, Int. J. Heat Mass Transfer 31 (1988) 731–742.
[11] T.C. Willingham, I. Mudawar, Forced-convection boiling and critical heat flux from a linear array of discrete heat sources, Int. J. Heat Mass Transfer 35 (1992) 2879–2890.
[12] H.J. Lee, S.Y. Lee, Heat transfer correlation for boiling flows in small rectangular horizontal channels with low aspect ratios, Int. J. Multiphase Flow 27 (2001) 2043–2062.
[13] J. Lee, I. Mudawar, Low-temperature two-phase micro-channel cooling for high-heat-flux thermal management of defense electronics, IEEE Trans. - CPMT: Comp. Pack. Technol. 32 (2009) 453–465.
[14] J. Lee, I. Mudawar, Critical heat flux for subcooled flow boiling in micro-channel heat sinks, Int. J. Heat Mass Transfer 52 (2009) 3341–3352.
[15] M. Monde, T. Inoue, Critical heat flux in saturated forced convective boiling on a heated disk with multiple impinging jets, J. Heat Transfer – Trans. ASME 113 (1991) 722–727.
[16] D.C. Wadsworth, I. Mudawar, Enhancement of single-phase heat transfer and critical heat flux from an ultra-high-flux-source to a rectangular impinging jet of dielectric liquid, J. Heat Transfer – Trans. ASME 114 (1992) 764–768.
[17] M.E. Johns, I. Mudawar, An ultra-high power two-phase jet-impingement avionic clamshell module, J. Electron. Pack. – Trans. ASME 118 (1996) 264–270.
[18] D.D. Hall, I. Mudawar, Experimental and numerical study of quenching complex-shaped metallic alloys with multiple, overlapping sprays, Int. J. Heat Mass Transfer 38 (1995) 1201–1216.
[19] L. Lin, R. Ponnappan, Heat transfer characteristics of spray cooling in a closed loop, Int. J. Heat Mass Transfer 46 (2003) 3737–3746.
[20] M.K. Sung, I. Mudawar, Experimental and numerical investigation of single-phase heat transfer using a hybrid jet-impingement/micro-channel cooling scheme, Int. J. Heat Mass Transfer 49 (2006) 682–694.
[21] J.W. Rose, Dropwise condensation theory and experiment: a review, J. Power Energy 216 (2002) 115–128.
[22] K.A. Swensen, Further Studies in Filmwise Condensation of Steam on Horizontal Finned Tubes (Masters Thesis), Naval Postgraduate School, Monterey, CA, 1992.
[23] I. Mudawar, M.A. El-Masri, Momentum and heat transfer across freely-falling turbulent liquid films, Int. J. Multiphase Flow 12 (1986) 771–790.
[24] J.R. Thome, Condensation in plain horizontal tubes: recent advances in modelling of heat transfer to pure fluids and mixtures, J. Brazil. Soc. Mech. Sci. Eng. 27 (2005) 23–30.
[25] M.M. Shah, An improved and extended general correlation for heat transfer during condensation in plain tubes, HVAC&R Res. 15 (2009) 889–913.
[26] S.M. Kim, I. Mudawar, Universal approach to predicting two-phase frictional pressure drop for adiabatic and condensing mini/micro-channel flows, Int. J. Heat Mass Transfer 55 (2012) 3246–3261.
[27] S.M. Kim, I. Mudawar, Universal approach to predicting heat transfer coefficient for condensing mini/micro-channel flows, Int. J. Heat Mass Transfer 56 (2013) 238–250.
[28] S.M. Kim, I. Mudawar, Theoretical model for annular flow condensation in rectangular micro-channels, Int. J. Heat Mass Transfer 55 (2012) 958–970.
[29] S.M. Kim, I. Mudawar, Theoretical model for local heat transfer coefficient for annular flow boiling in circular mini/micro-channels, Int. J. Heat Mass Transfer 73 (2014) 731–742.
[30] G. Ryskin, L.G. Leal, Numerical solution of free-boundary problems in fluid mechanics. Part 2. Buoyancy-driven motion of a gas bubble through a quiescent liquid, J. Fluid Mech. 148 (1984) 19–35.
[31] S. Takagi, Y. Matsumoto, Three-dimensional deformation of a rising Bubble, in: Proceedings of the German-Japanese Symposium on Multi-Phase Flow, Karlsruhe, Germany, 1994, pp. 499–511.
[32] P.J. Shopov, P.D. Minev, I.B. Bazhekov, Z.D. Zapryanov, Interaction of a deformable bubble with a rigid wall at moderate Reynolds numbers, J. Fluid Mech. 219 (1990) 241–271.
[33] J. Fukai, Y. Shiiba, T. Yamamoto, O. Miyatake, D. Poulikakos, C.M. Megaridis, Z. Zhao, Wetting effects on the spreading of a liquid droplet colliding with a flat surface: experiment and modeling, Phys. Fluids 7 (1995) 236–247.
[34] C.W. Hirt, B.D. Nichols, Volume of fluid (VOF) method for the dynamics of free boundaries, J. Comput. Phys. 39 (1981) 201–225.
[35] M. Sussman, P. Smereka, S. Osher, A level set approach for computing solutions to incompressible two-phase flows, J. Comput. Phys. 114 (1994) 146–159.
[36] M. Rudman, Volume-tracking methods for interfacial flow calculations, Int. J. Numer. Meth. Fluids 24 (1997) 671–691.
[37] O. Ubbink, R.I. Issa, A method for capturing sharp fluid interfaces on arbitrary meshes, J. Comput. Phys. 153 (1999) 26–50.
[38] W.F. Noh, P. Woodward, SLIC (simple line interface calculation), in: Proceedings of the Fifth International Conference on Numerical Methods in Fluid Dynamics, Twente University, Enschede, 1976, pp. 330–340.
[39] D.L. Youngs, Time-dependent multi-material flow with large fluid distortion, in: K.W. Morton, M.J. Baines (Eds.), Numerical Methods for Fluid Dynamics, Academic Press, New York, 1982, pp. 273–285.
[40] W.J. Rider, D.B. Kothe, Reconstructing volume tracking, J. Comput. Phys. 141 (1998) 112–152.

[41] D.J. Benson, Volume of fluid interface reconstruction methods for multi-material problems, Appl. Mech. Rev. 55 (2002) 151–165.

[42] G.R. Price, G.T. Reader, R.D. Rowe, J.D. Bugg, A piecewise parabolic interface calculation for volume tracking, Proceedings of the Sixth Annual Conference of CFD Society of Canada, vol. 11, University of Victoria, Victoria, British Columbia, 1998, pp. 9–14.

[43] I. Ginzburg, G. Wittum, Two-phase flows on interface refined grids modeled with VOF, staggered finite volumes, and spline interpolants, J. Comput. Phys. 166 (2001) 302–335.

[44] G. Russo, P. Smereka, A remark on computing distance functions, J. Comput. Phys. 163 (2000) 51–67.

[45] Y.C. Chang, T.Y. Hou, B. Merriman, S. Osher, A level set formulation of Eulerian interface capturing methods for incompressible fluid flows, J. Comput. Phys. 124 (1996) 449–464.

[46] Y. Zhang, Q. Zou, D. Greaves, Numerical simulation of free-surface flow using the level-set method with global mass correction, Int. J. Numer. Meth. Fluids 63 (2010) 651–680.

[47] G. Son, V.K. Dhir, Numerical simulation of film boiling near critical pressures with a level-set method, J. Heat Transfer – Trans. ASME 120 (1998) 183–192.

[48] R.P. Fedkiw, T. Aslam, B. Merriman, S. Osher, A non-oscillatory Eulerian approach to interfaces in multimaterial flows (the ghost fluid method), J. Comput. Phys. 152 (1999) 457–492.

[49] M. Kang, R.P. Fedkiw, X.-D. Liu, A Boundary condition capturing method for multiphase incompressible flow, J. Scient. Comput. 15 (2000) 323–360.

[50] M. Sussman, E.G. Puckett, A coupled level set and volume-of-fluid method for computing 3D and axisymmetric incompressible two-phase flows, J. Comput. Phys. 162 (2000) 301–337.

[51] D. Enright, R. Fedkiw, J. Ferziger, I. Mitchell, A hybrid particle level set method for improved interface capturing, J. Comput. Phys. 183 (2002) 83–116.

[52] D.L. Sun, W.Q. Tao, A coupled volume-of-fluid and level set (VOSET) method for computing incompressible two-phase flows, Int. J. Heat Mass Transfer 53 (2010) 645–655.

[53] J. Glimm, J.W. Grove, X.L. Li, W. Oh, D.H. Sharp, A critical analysis of Rayleigh-Taylor growth rates, J. Comput. Phys. 169 (2001) 652–677.

[54] S.O. Unverdi, G. Tryggvason, A front-tracking method for viscous, incompressible, multi-fluid flows, J. Comput. Phys. 100 (1992) 25–37.

[55] G. Tryggvason, B. Bunner, A. Esmaeeli, N. Juric, N. Al-Rawahi, W. Tauber, J. Han, S. Nas, Y.-J. Jan, A front-tracking method for the computations of multiphase flow, J. Comput. Phys. 169 (2001) 708–759.

[56] M.R.H. Nobari, G. Tryggvason, Numerical simulations of three-dimensional drop collisions, AIAA J. 34 (1996) 750–755.

[57] T. Yabe, F. Xiao, T. Utsumi, The constrained interpolation profile (CIP) method for multiphase analysis, Comput. Phys. 169 (2001) 556–593.

[58] D. Jacqmin, Calculation of two-phase Navier-Stokes flows using phase-field modeling, J. Comput. Phys. 155 (1999) 96–127.

[59] Y.Y. Yan, Y.Q. Zu, A lattice Boltzmann method for incompressible two-phase flows on partial wetting surface with large density ratio, J. Comput. Phys. 227 (2007) 763–775.

[60] Y.Y. Yan, Y.Q. Zu, Numerical modelling based on lattice Boltzmann method of the behaviour of bubbles flow and coalescence in microchannels, in: Proceedings of the. 6th International Conference on Nanochannels, Microchannels, and Minichannels, Darmstadt, Germany, 2008, pp. 313–319.

[61] J.U. Brackbill, D.B. Kothe, C. Zemach, A continuum method for modeling surface tension, J. Comput. Phys. 100 (1992) 335–354.

[62] C.S. Peskin, Numerical analysis of blood flow in the heart, J. Comput. Phys. 25 (1977) 220–252.

[63] B. Lafaurie, C. Nardone, R. Scardovelli, S. Zaleski, G. Zanetti, Modelling merging and fragmentation in multiphase flows with SURFER, J. Comput. Phys. 113 (1994) 134–147.

[64] Y. Renardy, M. Renardy, PROST: A parabolic reconstruction of surface tension for the volume-of-fluid method, J. Comput. Phys. 183 (2002) 400–421.

[65] E. Aulisa, S. Manservisi, R. Scardovelli, A novel representation of the surface tension force for two-phase flow with reduced spurious currents, Comput. Meth. Appl. Mech. Eng. 195 (2006) 6239–6257.

[66] F. Gibou, L. Chen, D. Nguyen, S. Banerjee, A level set based sharp interface method for the multiphase incompressible Navier-Stokes equations with phase change, J. Comput. Phys. 222 (2007) 536–555.

[67] S. Shin, D. Juric, Modeling three-dimensional multiphase flow using a level contour reconstruction method for front tracking without connectivity, J. Comput. Phys. 180 (2002) 427–470.

[68] B.A. Nichita, J.R. Thome, A level set method and a heat transfer model implemented into FLUENT for modeling of microscale two phase flows, in: AVT-178 Specialists' Meeting on System Level Thermal Management for Enhanced Platform Efficiency, Bucharest, Romania, 2010.

[69] H. Ganapathy, A. Shooshtari, K. Choo, S. Dessiatoun, M. Alshehhi, M. Ohadi, Volume of fluid-based numerical modeling of condensation heat transfer and fluid flow characteristics in microchannels, Int. J. Heat Mass Transfer 65 (2013) 62–72.

[70] D. Sun, J. Xu, L. Wang, Development of a vapor–liquid phase change model for volume-of-fluid method in FLUENT, Int. Commun. Heat Mass Transfer 39 (2012) 1101–1106.

[71] R.W. Schrage, A Theoretical Study of Interphase Mass Transfer, Columbia University Press, New York, 1953.

[72] M. Knudsen, The Kinetic Theory of Gases: Some Modern Aspects, Methuen's Monographs Physical Subjects, Methuen and Co., London, 1934.

[73] R. Marek, J. Straub, Analysis of the evaporation coefficient and the condensation coefficient of water, Int. J. Heat Mass Transfer 44 (2001) 39–53.

[74] B. Paul, Complication of evaporation coefficient, Am. Rock. Soc. J. 32 (1962) 1321–1328.

[75] J.W. Rose, On interphase matter transfer, the condensation coefficient and dropwise condensation, Proc. R. Soc. Lond. A 411 (1987) 305–311.

[76] H. Wang, S.V. Garimella, J.Y. Murthy, Characteristics of evaporating thin film in a microchannel, Int. J. Heat Mass Transfer 50 (2007) 3933–3942.

[77] S. Hardt, F. Wondra, Evaporation model for interfacial flows based on a continuum-field representation of the source terms, J. Comput. Phys. 227 (2008) 5871–5895.

[78] M. Magnini, B. Pulvirenti, J.R. Thome, Numerical investigation of hydrodynamics and heat transfer of elongated bubbles during flow boiling in a microchannel, Int. J. Heat Mass Transfer 59 (2013) 451–471.

[79] C.R. Kharangate, H. Lee, I. Mudawar, Computational modeling of turbulent evaporating falling films, Int. J. Heat Mass Transfer 81 (2015) 52–62.

[80] E.O. Doro, Computational Modeling of Falling Liquid Film Free Surface Evaporation (Doctoral dissertation), Georgia Institute of Technology, Atlanta, GA, 2012.

[81] O. Kartuzova, M. Kassemi, Modeling interfacial turbulent heat transfer during ventless pressurization of a large scale cryogenic storage tank in microgravity, in: 47th AIAA/ASME/SAE/ASEE Joint Propulsion Conference & Exhibit, San Diego, California, 2011.

[82] M. Huang, Z. Yang, Y. Duan, D. Lee, Bubble growth for boiling bubbly flow for R141b in serpentine tube, J. Taiwan Inst. Chem. Eng. 42 (2011) 727–734.

[83] I. Tanasawa, Advances in condensation heat transfer, in: J.P. Hartnett, T.F. Irvine (Eds.), Advances in Heat Transfer, Academic Press, San Diego, 1991.

[84] P.C. Wayner Jr., Intermolecular forces in phase-change heat transfer: 1998 Kern award review, AIChE J. 45 (1999) 2055–2068.

[85] W.H. Lee, A pressure iteration scheme for two-phase flow modeling, in: T.N. Veziroglu (Ed.), Multiphase Transport Fundamentals, Reactor Safety, Applications, vol. 1, Hemisphere Publishing, Washington, DC, 1980.

[86] S. Chen, Z. Yang, Y. Duan, Y. Chen, D. Wu, Simulation of condensation flow in a rectangular microchannel, Chem. Eng. Process.: Process Intens. 76 (2014) 60–69.

[87] M. Bahreini, A. Ramiar, A.A. Ranjbar, Numerical simulation of bubble behavior in subcooled flow boiling under velocity and temperature gradient, Nucl. Eng. Des. 293 (2015) 238–248.

[88] S.C.K. De Schepper, G.J. Heynderichx, G.B. Marin, Modeling the evaporation of a hydrocarbon feedstock in the convection section of a steam cracker, Comp. Chem. Eng. 33 (2009) 122–132.

[89] Z. Liu, B. Sundén, J. Yuan, VOF modeling and analysis of film wise condensation between vertical parallel plates, Heat Transfer Res. 43 (2012) 47–68.

[90] R. Zhuan, W. Wang, Simulation on nucleate boiling in micro-channel, Int. J. Heat Mass Transfer 53 (2010) 502–512.

[91] S. Petrovic, T. Robinson, R.L. Judd, Marangoni heat transfer in subcooled nucleate pool boiling, Int. J. Heat Mass Transfer 47 (2004) 5115–5128.

[92] P. Arlabosse, L. Tadrist, H. Tadrist, J. Pantaloni, Experimental analysis of the heat transfer induced by thermocapillary convection around a bubble, J. Heat Transfer – Trans. ASME 122 (2000) 66–73.

[93] J.R. Thome, V. Dupont, A.M. Jacobi, Heat transfer model for evaporation in microchannels. Part I: presentation of the model, Int. J. Heat Mass Transfer 47 (2004) 3375–3385.

[94] N. Zhang, D.F. Chat, Models for enhanced boiling heat transfer by unusual Marangoni effects under microgravity conditions, Int. Commun. Heat Mass Transfer 26 (1999) 1081–1090.

[95] S. Jeon, S. Kim, G. Park, Numerical study of condensing bubble in subcooled boiling flow using volume of fluid model, Chem. Eng. Sci. 66 (2011) 5899–5909.

[96] S. Kim, G. Park, Interfacial heat transfer of condensing bubble in subcooled boiling flow at low pressure, Int. J. Heat Mass Transfer 54 (2011) 2962–2974.

[97] E. Krepper, B. Koncar, Y. Egorov, CFD modelling of subcooled boiling - concept, validation and application to fuel assembly design, Nuclear Engng Design 237 (2007) 716–731.

[98] W.E. Ranz, W.R. Marshall, Evaporation from drops - part I, Chem. Eng. Prog. 48 (1952) 141–146.

[99] Y.Q. Zu, Y.Y. Yan, S. Gedupudi, T.G. Karayiannis, D.B.R. Kenning, Confined bubble growth during flow boiling in a mini-/micro-channel of rectangular cross-section part II: approximate 3-D numerical simulation, Int. J. Therm. Sci. 50 (2011) 267–273.

[100] S. Gedupudi, Y.Q. Zu, T.G. Karayiannis, D.B.R. Kenning, Y.Y. Yan, Confined bubble growth during flow boiling in a mini/micro-channel of rectangular cross-section part I: experiments and 1-D modelling, Int. J. Therm. Sci. 50 (2011) 250–266.

[101] Y. Zhang, A. Faghri, M.B. Shafii, Capillary blocking in forced convection condensation in horizontal miniature channels, J. Heat Transfer – Trans. ASME 123 (2001) 501–511.

[102] S.W.J. Welch, J. Wilson, A volume of fluid based method for fluid flows with phase change, J. Comput. Phys. 160 (2000) 662–682.

[103] C. Kunkelmann, Numerical Modeling and Investigation of Boiling Phenomena (Ph.D. thesis), Technische Universität Darmstadt, Germany, 2011.

[104] D. Juric, G. Tryggvason, Computations of boiling flows, Int. J. Multiphase Flow 24 (1998) 387–410.

[105] Y. Sato, B. Niceno, A sharp-interface phase change model for a mass conservative interface tracking method, J. Comput. Phys. 249 (2013) 127–161.

[106] C. Kunkelmann, P. Stephan, CFD simulation of boiling flows using the volume-of-fluid method within OPENFOAM, Numer. Heat Transfer, Part A 56 (2009) 631–646.

[107] G. Son, V.K. Dhir, N. Ramanujapu, Dynamics and heat transfer associated with a single bubble during nucleate boiling on a horizontal surface, J. Heat Transfer – Trans. ASME 121 (1999) 623–632.

[108] D.Q. Nguyen, R.P. Fedkiw, M. Kang, A boundary condition capturing method for incompressible flame discontinuities, J. Comput. Phys. 172 (2001) 71–98.

[109] S.W.J. Welch, Local simulation of two-phase flows including interface tracking with mass transfer, J. Comput. Phys. 121 (1995) 42–54.

[110] G. Son, V.K. Dhir, Numerical simulation of saturated film boiling on a horizontal surface, J. Heat Transfer – Trans. ASME 119 (1997) 25–54.

[111] G. Tomar, G. Biswas, A. Sharma, A. Agrawal, Numerical simulation of bubble growth in film boiling using a coupled level-set and volume-of-fluid method, Phys. Fluids 17 (2005) 112103.

[112] D. Jamet, O. Lebaigue, N. Coutris, J. Delhaye, The second gradient method for the direct numerical simulation of liquid–vapor flows with phase change, J. Comput. Phys. 169 (2001) 624–651.

[113] Z. Dong, W. Li, Y. Song, A numerical investigation of bubble growth on and departure from a superheated wall by lattice Boltzmann method, Int. J. Heat Mass Transfer 53 (2010) 4908–4916.

[114] T. Inamuro, M. Yoshino, H. Inoue, R. Mizuno, F. Ogino, A lattice Boltzmann method for a binary miscible fluid mixture and its application to a heat-transfer problem, J. Comput. Phys. 179 (2002) 201–215.

[115] H.W. Zheng, C. Shu, Y.T. Chew, A lattice Boltzmann model for multiphase flows with large density ratio, J. Comput. Phys. 218 (2006) 353–371.

[116] R. Zhang, H. Chen, Lattice Boltzmann method for simulations of liquid-vapor thermal flows, Phys. Rev. E 67 (2003) 066711.

[117] R.C. Lee, J.E. Nydahl, Numerical calculation of bubble growth in nucleate boiling from inception to departure, J. Heat Transfer – Trans. ASME 111 (1989) 474–479.

[118] M.G. Cooper, A.J.P. Lloyd, The microlayer in nucleate boiling, Int. J. Heat Mass Transfer 12 (1969) 895–913.

[119] S.W.J. Welch, Direct simulation of vapor bubble growth, Int. J. Heat Mass Transfer 41 (1998) 1655–1666.

[120] R.L. Judd, K.S. Hwang, A comprehensive model for nucleate pool boiling heat transfer including microlayer evaporation, J. Heat Transfer – Trans. ASME 98 (1976) 623–629.

[121] P.C. Wayner Jr., Evaporation and stress in the contact line region, in: Proceedings of the Engineering Foundation Conference on Pool and External Flow Boiling, Santa Barbara, CA, 1992, pp. 251–256.

[122] J.H. Lay, V.K. Dhir, Shape of a vapor stem during nucleate boiling of saturated liquids, J. Heat Transfer – Trans. ASME 117 (1995) 394–401.

[123] S. Singh, V.K. Dhir, Effect of gravity, Effect of gravity, wall superheat and liquid subcooling on bubble dynamics during nucleate boiling, in: V.K. Dhir (Ed.), Microgravity Fluid Physics and Heat Transfer, Begell House, New York, 2000, pp. 106–113.

[124] H.S. Abarajith, V.K. Dhir, Effect of contact angle on the dynamics of a single bubble during pool boiling using numerical simulations, in: Proceedings of the ASME International Mechanical Engineering Congress & Exposition, New Orleans, LA, 2002.

[125] Y. Nam, E. Aktinol, V.K. Dhir, Y.S. Ju, Single bubble dynamics on a superhydrophilic surface with artificial sites, Int. J. Heat Mass Transfer 54 (2011) 1572–1577.

[126] J. Wu, V.K. Dhir, Numerical simulation of dynamics and heat transfer associated with a single bubble in subcooled boiling and in the presence of noncondesables, J. Heat Transfer – Trans. ASME 133 (2011) 041502.

[127] J. Wu, V.K. Dhir, J. Qian, Numerical simulation of subcooled nucleate boiling by coupling level set method with moving mesh method, Numer. Heat Transfer B 51 (2007) 535–563.

[128] H.S. Aparajith, V.K. Dhir, G. Son, Numerical simulation of the dynamics of multiple bubble merger during pool boiling under reduced gravity, Multiph. Sci. Technol. 18 (2006) 277–304.

[129] V.K. Dhir, G.R. Warrier, E. Aktinol, D. Chao, J. Eggers, W. Sheredy, W. Booth, Nucleate pool boiling experiments (NPBX) on the International Space Station, Microg. Sci. Technol. 24 (2011) 307–325.

[130] J.F. Zhao, Z.D. Li, L. Zhang, Numerical simulation of single bubble pool boiling in different gravity conditions, in: Proceedings of the American Institute of Physics (AIP) Conference, vol. 1376, 2011, pp. 565–568.

[131] G. Son, N. Ramanujapu, V.K. Dhir, Numerical simulation of bubble merger process on a single nucleation site during pool nucleate boiling, J. Heat Transfer – Trans. ASME 124 (2002) 51–62.

[132] A. Mukherjee, V.K. Dhir, Study of lateral merger of vapor bubbles during nucleate pool boiling, J. Heat Transfer - Trans. ASME 126 (2004) 1023–1039.

[133] E. Aktinol, V.K. Dhir, Numerical simulation of nucleate boiling phenomenon coupled with thermal response of the solid, Microg. Sci. Technol. 24 (2012) 255–265.

[134] D. Li, V.K. Dhir, Numerical study of single bubble dynamics during flow boiling, J. Heat Transfer – Trans. ASME 129 (2007) 864–876.

[135] G. Son, V.K. Dhir, Numerical simulation of nucleate boiling on a horizontal surface at high heat fluxes, Int. J. Heat Mass Transfer 51 (2008) 2566–2582.

[136] W. Lee, G. Son, J.J. Jeong, Numerical analysis of bubble growth and departure from a microcavity, Numer. Heat Transfer B 58 (2010) 323–342.

[137] W. Lee, G. Son, Numerical simulation of boiling enhancement on a microstructured surface, Int. Commun. Heat Mass Transfer 38 (2011) 168–173.

[138] W. Lee, G. Son, H.Y. Yoon, Numerical study of bubble growth and boiling heat transfer on a microfinned surface, Int. Commun. Heat Mass Transfer 39 (2012) 52–57.

[139] P.C. Stephan, C.A. Busse, Analysis of the heat transfer coefficient of grooved heat pipe evaporator walls, Int. J. Heat Mass Transfer 35 (1992) 383–391.

[140] C. Kunkelmann, P. Stephan, Numerical simulation of the transient heat transfer during nucleate boiling of refrigerant HFE-7100, Int. J. Refrig. 33 (2010) 1221–1228.

[141] C. Kunkelmann, P. Stephan, Modification and extension of a standard volume-of-fluid solver for simulating boiling heat transfer, in: Proceedings of the 5th European Conference on Computational Fluid Dynamics ECCOMAS CFD2010, Lisbon, Portugal, 2010.

[142] C. Kunkelmann, K. Ibrahem, N. Schweizer, S. Herbert, P. Stephan, T. Gambaryan-Roisman, The effect of three-phase contact line speed on local evaporative heat transfer: experimental and numerical investigations, Int. J. Heat Mass Transfer 55 (2012) 1896–1904.

[143] A. Sielaff, J. Dietl, S. Herbert, P. Stephan, The influence of system pressure on bubble coalescence in nucleate boiling, Heat Transfer Eng. 35 (2014) 420–429.

[144] Z.H. Chen, Y. Utaka, On heat transfer and evaporation characteristics in the growth process of a bubble with microlayer structure during nucleate boiling, Int. J. Heat Mass Transfer 81 (2015) 750–759.

[145] H.W. Jia, P. Zhang, X. Fu, S.C. Jiang, A numerical investigation of nucleate boiling at a constant surface temperature, Appl. Therm. Eng. 88 (2015) 248–257.

[146] Y. Sato, S. Lal, B. Niceno, Computational fluid dynamics simulation of single bubble dynamics in convective boiling flows, Multiph. Sci. Technol. 25 (2013) 287–309.

[147] S. Lal, Y. Sato, B. Niceno, Direct numerical simulation of bubble dynamics in subcooled and near-saturated convective nucleate boiling, Int. J. Heat Fluid Flow 51 (2015) 16–28.

[148] K. Ling, Z.Y. Li, W.Q. Tao, A direct numerical simulation for nucleate boiling by the VOSET method, Numer. Heat Transfer A 65 (2014) 949–971.

[149] H.B. Ma, P. Cheng, B. Borgmeyer, Y.X. Wang, Fluid flow and heat transfer in the evaporating thin film region, Microfluid Nanofluid 4 (2008) 237–243.

[150] S. aus der Wiesche, Bubble growth and departure during nucleate boiling: the occurrence of heat flux reversal, in: Proceedings of the 4th Interenational Conference on Computational Heat and Mass Transfer, Paris, France, vol. 2, Paper ICCHMT2005-107, 2005.

[151] T. Kunugi, N. Saito, Y. Fujita, A. Serizawa, Direct numerical simulations of pool and forced convection flow boiling phenomena, Proceedings of the 12th International Heat Transfer Conference, Grenoble, France, vol. 3, 2002, pp. 497–502.

[152] T. Kunugi, MARS for multiphase calculation, Comput. Fluid Dyn. J. 9 (2001) 563–561.

[153] G. Tryggvason, J.C. Lu, Direct numerical simulations of flows with phase change, Proc. IUTAM 15 (2015) 2–13.

[154] S. Shin, S.I. Abdel-Khalik, D. Juric, Direct three-dimensional numerical simulation of nucleate boiling using the level contour reconstruction method, Int. J. Multiphase Flow 31 (2005) 1231–1242.

[155] H.Y. Yoon, S. Koshizuka, Y. Oka, Direct calculation of bubble growth, departure, and rise in nucleate pool boiling, Int. J. Multiph. Flow 27 (2001) 277–298.

[156] S. Koshizuka, Y. Oka, Moving-particle semi-implicit method for fragmentation of incompressible fluid, Nucl. Sci. Eng. 123 (1996) 421–434.

[157] S. Ryu, S. Ko, Direct numerical simulation of nucleate pool boiling using a two-dimensional lattice Boltzmann method, Nucl. Eng. Des. 248 (2012) 248–262.

[158] S. Gong, P. Cheng, A lattice Boltzmann method for simulation of liquid–vapor phase-change heat transfer, Int. J. Heat Mass Transfer 55 (2012) 4923–4927.

[159] T. Sun, W. Li, S. Yang, Numerical simulation of bubble growth and departure during flow boiling period by lattice Boltzmann method, Int. J. Heat Fluid Flow 44 (2013) 120–129.

[160] D. Banerjee, V.K. Dhir, Study of subcooled film boiling on a horizontal disc: Part I—Analysis, J. Heat Transfer – Trans. ASME 123 (2001) 271–284.

[161] D. Banerjee, V.K. Dhir, Study of subcooled film boiling on a horizontal disc: Part 2—Experiments, J. Heat Transfer – Trans. ASME 123 (2001) 285–293.

[162] A. Esmaeeli, G. Tryggvason, Computations of film boiling. Part I: numerical method, Int. J. Heat Mass Transfer 47 (2004) 5451–5461.

[163] A. Esmaeeli, G. Tryggvason, Computations of film boiling. Part II: multi-mode film boiling, Int. J. Heat Mass Transfer 47 (2004) 5463–5476.

[164] A. Esmaeeli, G. Tryggvason, A front tracking method for computations of boiling in complex geometries, Int. J. Multiph. Flow 30 (2004) 1037–1050.

[165] N. Al-Rawahi, G. Tryggvason, Numerical simulation of dendritic solidification with convection: two–dimensional geometry, J. Comput. Phys. 180 (2002) 471–496.

[166] M. Reimann, U. Grigull, Wärmeubergang bei freier konvektion und filmsieden im kritischen gebiet von wasser und kohlendioxid, Warme- und Stoffübertragung 8 (1975) 229–239.

[167] P.J. Berenson, Film-boiling heat transfer from a horizontal surface, J. Heat Transfer – Trans ASME 83 (1961) 351–356.

[168] V.V. Klimenko, Film boiling on a horizontal plate—new correlation, Int. J. Heat Mass Transfer 24 (1981) 69–79.

[169] F. Bazdidi-Tehrani, S. Zaman, Two-phase heat transfer on an isothermal vertical surface: a numerical simulation, Int. J. Heat Fluid Flow 23 (2002) 308–316.

[170] G. Son, V.K. Dhir, A level set method for analysis of film boiling on an immersed solid surface, Numer. Heat Transfer B 52 (2007) 153–177.

[171] G. Son, V.K. Dhir, Three-dimensional simulation of saturated film boiling on a horizontal cylinder, Int. J. Heat Mass Transfer 51 (2008) 1156–1167.

[172] K. Kim, G. Son, Numerical analysis of film boiling in liquid jet impingement, Numer. Heat Transfer A 64 (2013) 695–709.

[173] S.W.J. Welch, T. Rachidi, Numerical computation of film boiling including conjugate heat transfer, Numer. Heat Transfer B 42 (2002) 35–53.

[174] D.K. Agarwal, S.W.J. Welch, G. Biswas, F. Durst, Planar simulation of bubble growth in film boiling in near-critical water using a variant of the VOF method, J. Heat Transfer – Trans. ASME 126 (2004) 329–338.

[175] M.H. Yuan, Y.H. Yang, T.S. Li, Z.H. Hu, Numerical simulation of film boiling on a sphere with a volume of fluid interface method, Int. J. Heat Mass Transfer 51 (2008) 1646–1657.

[176] R. Arevalo, D. Antunez, L. Rebollo, A. Abanades, Estimation of radiation coupling factors in film boiling around spheres by mean of Computational Fluid Dynamics (CFD) tools, Int. J. Heat Mass Transfer 78 (2014) 84–89.

[177] S.W. Welch, G. Biswas, Direct simulation of film boiling including electrohydrodynamic forces, Phys. Fluids 19 (2007) 012106.

[178] G. Tomar, G. Bisawas, A. Sharma, S.W.J. Welch, Influence of electric field on saturated film boiling, Phys. Fluids 21 (2009) 032107.

[179] D.Z. Guo, D.L. Sun, Z.Y. Li, W.Q. Tao, Phase change heat transfer simulation for boiling bubbles arising from a vapor film by the VOSET method, Numer. Heat Transfer A 59 (2011) 857–881.

[180] Y.-Y. Tsui, S.-W. Lin, Y.-N. Lai, F.-C. Wu, Phase change calculations for film boiling flows, Int. J. Heat Mass Transfer 70 (2014) 745–757.

[181] Q. Li, Q.J. Kang, M.M. Francois, Y.L. He, K.H. Luo, Lattice Boltzmann modeling of boiling heat transfer: the boiling curve and the effects of wettability, Int. J. Heat Mass Transfer 85 (2015) 787–796.

[182] A. Mukherjee, S.G. Kandlikar, Numerical simulation of growth of a vapor bubble during flow boiling of water in a microchannel, J. Microfluid. Nanofluid. 1 (2005) 137–145.

[183] A. Mukherjee, Contribution of thin-film evaporation during flow boiling inside microchannels, Int. J. Therm. Sci. 48 (2009) 2025–2035.

[184] A. Mukherjee, S.G. Kandlikar, The effect of inlet constriction on bubble growth during flow boiling in microchannels, Int. J. Heat Mass Transfer 52 (2009) 5204–5212.

[185] A. Mukherjee, S.G. Kandlikar, Z.J. Edel, Numerical study of bubble growth and wall heat transfer during flow boiling in a microchannel, Int. J. Heat Mass Transfer 54 (2011) 3702–3718.

[186] M. Magnini, B. Pulvirenti, J.R. Thome, Numerical investigation of the influence of leading and sequential bubbles on slug flow boiling within a microchannel, Int. J. Therm. Sci. 71 (2013) 36–52.

[187] M. Magnini, J.R. Thome, Computational study of saturated flow boiling within a microchannel in the slug flow regime, J. Heat Transfer – Trans. ASME 138 (2016) 021502.

[188] W. Lee, G. Son, Bubble dynamics and heat transfer during nucleate boiling in a microchannel, Numer. Heat Transfer A 53 (2008) 1074–1090.

[189] Y. Suh, W. Lee, G. Son, Bubble dynamics, flow, and heat transfer during flow boiling in parallel microchannels, Numer. Heat Transfer A 54 (2008) 390–405.

[190] R. Zhuan, W. Wang, Flow pattern of boiling in microchannel by numerical simulation, Int. J. Heat Mass Transfer 55 (2012) 1741–1753.

[191] R. Zhuan, W. Wang, Simulation of subcooled flow boiling in a micro-channel, Int. J. Refrig. 34 (2011) 781–795.

[192] G.R. Warrier, N. Basu, V.K. Dhir, Interfacial heat transfer during subcooled flow boiling, Int. J. Heat Mass Transfer 45 (2002) 3947–3959.

[193] L. Pan, Z. Tan, D. Chen, L. Xue, Numerical investigation of vapor bubble condensation characteristics of subcooled flow boiling in vertical rectangular channel, Nucl. Eng. Des. 248 (2012) 126–136.

[194] H.L. Wu, X.F. Peng, P. Ye, Y. Gong, Simulation of refrigerant flow boiling in serpentine tubes, Int. J. Heat Mass Transfer 50 (2007) 1186–1195.

[195] Z. Yang, X.F. Peng, P. Ye, Numerical and experimental investigation of two phase flow during boiling in a coiled tube, Int. J. Heat Mass Transfer 51 (2008) 1003–1016.

[196] C. Fang, M. David, A. Rogacs, K. Goodson, Volume of fluid simulation of boiling two-phase flow in a vapor venting microchannel, Front. Heat Mass Transfer 1 (2010) 013002.

[197] J. Wei, L. Pan, D. Chen, H. Zhang, J. Xu, Y. Huang, Numerical simulation of bubble behaviors in subcooled flow boiling under swing motion, Nucl. Eng. Des. 241 (2011) 2898–2908.

[198] H. Lee, D.D. Agonafer, Y. Won, F. Houshmand, C. Gorle, M. Asheghi, K.E. Goodson, Thermal modeling of extreme heat flux microchannel coolers for GaN-on-SiC semiconductor devices, J. Electron. Pack. – Trans. ASME 138 (2016) 010907.

[199] D. Lorenzini, Y.K. Joshi, CFD analysis of flow boiling in a silicon microchannel with non-uniform heat flux, in: Proceedings of the ASME 2015 13th International Conference on Nanochannels, Microchannels, and Minichannels, San Francisco, California, USA, 2015.

[200] S. Zhou, X. Xu, B.G. Sammakia, Modeling of boiling flow in microchannels for nucleation characteristics and performance optimization, Int. J. Heat Mass Transfer 64 (2013) 706–718.

[201] Z. Pan, J.A. Weibel, S.V. Garimella, A saturated-interface-volume phase change model for simulating flow boiling, Int. J. Heat Mass Transfer 93 (2016) 945–956.

[202] N. Kurul, M.Z. Podowski, Multidimensional effects in forced convection subcooled boiling, Proceedings of the 9th International Heat Transfer Conference, Jerusalem, Israel, vol. 2, 1990, pp. 21–26.

[203] G.G. Bartolomej, V.M. Chanturiya, Experimental study of true void fraction when boiling subcooled water in vertical tubes, Therm. Eng. 14 (1967) 123–128.

[204] G.G. Bartolomej, V.G. Brantov, Y.S. Molochnikov, An experimental investigation of true volumetric vapour content with subcooled boiling in tubes, Therm. Eng. 29 (1982) 132–135.

[205] E. Krepper, R. Rzehak, CFD for subcooled flow boiling: simulation of DEBORA experiments, Nucl. Eng. Des. 241 (2011) 3851–3866.

[206] E. Krepper, R. Rzehak, C. Lifante, T. Frank, CFD for subcooled flow boiling: coupling wall boiling and population balance models, Nucl. Eng. Des. 255 (2013) 330–346.

[207] S.M. Kim, J. Kim, I. Mudawar, Flow condensation in parallel micro-channels – Part 1: experimental results and assessment of pressure drop correlations, Int. J. Heat Mass Transfer 55 (2012) 971–983.

[208] J. Yuan, C. Wilhelmsson, B. Sunden, Analysis of water condensation and two-phase flow in a channel relevant for plate heat exchangers, in: B. Sunden, C. Brebbia (Eds.), Advanced Computational Methods in Heat Transfer IX, WIT Press, 2006, pp. 351–360.

[209] E. Da Riva, D. Del Col, Effect of gravity during condensation of R134a in a circular minichannel, Microg. Sci. Technol. 23 (2011) 87–97.

[210] Z. Yin, Y. Guo, B. Sunden, Q. Wang, M. Zeng, Numerical simulation of laminar film condensation in a horizontal minitube with and without non-condensable gas by the VOF method, Numer. Heat Transfer A 68 (2015) 958–977.

[211] J. Zhang, W. Li, W.J. Minkowycz, Numerical simulation of condensation for R410A at varying saturation temperatures in mini/micro tubes, Numer. Heat Transfer A 69 (2015) 464–478.

[212] H. Lee, C.R. Kharangate, N. Mascharehnas, I. Park, I. Mudawar, Experimental and computational investigation of vertical downflow condensation, Int. J. Heat Mass Transfer 85 (2015) 865–879.

[213] G.-D. Qiu, W.-H. Cai, S.-L. Li, Z.-Y. Wu, Y.-Q. Jiang, Y. Yao, Numerical simulation on forced convective condensation of steam upward flow in a vertical pipe, Adv. Mech. Eng. 2014 (2014) 589250.

[214] C.R. Kharangate, H. Lee, N. Mascarehnas, I. Park, I. Mudawar, Experimental and computational investigation of vertical upflow condensation in a circular tube, Int. J. Heat Mass Transfer 95 (2016) 249–263.

[215] ANSYS Fluent Theory Guide, ANSYS, Inc., Canonsburg, PA, 2013.

[216] G.D. Qiu, W.H. Cai, Z.Y. Wu, Y. Yao, Y.Q. Jiang, Numerical simulation of forced convective condensation of propane in a spiral tube, J. Heat Transfer – Trans. ASME 137 (2015) 041502.

[217] A. Alizadehdakhel, M. Rahimi, A.A. Alsairafi, CFD modeling of flow and heat transfer in a thermosyphon, Int. Commun. Heat Mass Transfer 37 (2010) 312–318.

[218] X.L. Liu, P. Cheng, Lattice Boltzmann simulation of steady laminar film condensation on a vertical hydrophilic subcooled flat plate, Int. J. Heat Mass Transfer 62 (2013) 507–514.

[219] X.L. Liu, P. Cheng, Lattice Boltzmann simulation for dropwise condensation of vapor along vertical hydrophobic flat plates, Int. J. Heat Mass Transfer 64 (2013) 1041–1052.

[220] C.R. Kharangate, Experimental, Theoretical and Computational Modeling of Flow Boiling, Flow Condensation and Evaporating Falling Films (Ph.D. thesis), Purdue University, IN, 2016.

[221] H.J. Chung, H.C. No, Simultaneous visualization of dry spots and bubbles for pool boiling of R-113 on a horizontal heater, Int. J. Heat Mass Transfer 46 (2003) 2239–2251.

[222] I.-C. Chu, H.C. No, C.-H. Song, Observation of high heat flux boiling structures in a horizontal pool by a total refection technique, in: 14th International Topical Meeting on Nuclear Reactor Thermal Hydraulics (NURETH-14), Toronto, Canada, Paper 401, 2011.

[223] Y. Heng, A. Mhamdi, S. Gross, A. Reusken, M. Buchholz, H. Auracher, W. Marquardt, Reconstruction of local heat fluxes in pool boiling experiments along the entire boiling curve from high resolution transient temperature measurements, Int. J. Heat Mass Transfer 51 (2008) 5072–5087.

[224] S. Moghaddam, K. Kiger, Physical mechanisms of heat transfer during single bubble nucleate boiling of FC-72 under saturation conditions—I. experimental investigation, Int. J. Heat Mass Transfer 52 (2009) 1284–1294.

[225] E. Barrau, N. Rivière, Ch. Poupot, A. Cartellier, Single and double optical probes in air-water two-phase flows: real time signal processing and sensor performance, Int. J. Multiph. Flow 25 (1999) 229–256.

[226] S. Kim, X.Y. Fu, X. Wang, M. Ishii, Development of the miniaturized four-sensor conductivity probe and the signal processing scheme, Int. J. Heat Mass Transfer 43 (2000) 4101–4118.

[227] H.M. Prasser, A. Bottger, J. Zschau, A new electrode-mesh tomography for gas–liquid flows, Flow Measur. Instrument. 9 (1998) 111–119.

[228] T.H. Lyu, I. Mudawar, Statistical investigation of the relationship between interfacial waviness and sensible heat transfer to a falling liquid film, Int. J. Heat Mass Transfer 34 (1991) 1451–1464.

[229] T.H. Lyu, I. Mudawar, Determination of wave-induced fluctuations of wall temperature and convective heat transfer coefficient in the heating of a turbulent falling liquid film, Int. J. Heat Mass Transfer 34 (1991) 2521–2534.

[230] T.H. Lyu, I. Mudawar, Simultaneous measurements of thickness and temperature profile in a wavy liquid film falling freely on a heating wall, Exp. Heat Transfer 4 (1991) 217–233.

[231] I. Mudawar, R.A. Houpt, Mass and momentum transport in smooth falling liquid films laminarized at relatively high Reynolds numbers, Int. J. Heat Mass Transfer 36 (1993) 3437–3448.

[232] I. Mudawar, R.A. Houpt, Measurement of mass and momentum transport in wavy-laminar falling liquid films, Int. J. Heat Mass Transfer 36 (1993) 4151–4162.

[233] W. Qu, I. Mudawar, S.-Y. Lee, S.T. Wereley, Experimental and computational investigation of flow development and pressure drop in a rectangular micro-channel, J. Electron. Pack. – Trans. ASME 128 (2006) 1–9.

[234] T.G. Theofanous, J.P. Tu, A.T. Dinh, T.N. Dinh, The boiling crisis phenomenon: part I: nucleation and nucleate boiling phenomenon, Exp. Therm. Fluid Sci. 26 (2002) 775–792.

[235] T.G. Theofanous, J.P. Tu, A.T. Dinh, T.N. Dinh, The boiling crisis phenomenon: part II: dryout dynamics and burnout, Exp. Therm. Fluid Sci. 26 (2002) 793–810.

[236] S. Khodaparast, N. Borhani, G. Tagliabue, J. Thome, A micro particle shadow velocimetry (μPSV) technique to measure flows in microchannels, Exp. Fluids 54 (2013) 1474.

[237] M. Abe, E. Longmire, K. Hishida, M. Maeda, A comparison of 2D and 3D PIV measurements in an oblique jet, J. Visual. 3 (2000) 165–173.

[238] M.P. Arroyo, K. Hinsch, Recent developments of PIV towards 3D measurements, in: A. Schroeder, C.E. Willert (Eds.), Partcle Image Velocimetry: New Developments and Recent Applications, Topics in Applied Physics, vol. 112, Springer, Berlin, Germany, 2008, pp. 127–154.

[239] C. Gerardi, J. Buongiorno, L.W. Hu, T. McKrell, Study of bubble growth in water pool boiling through synchronized, infrared thermometry and high-speed video, Int. J. Heat Mass Transfer 53 (2010) 4185–4192.

[240] X. Duan, B. Phillips, T. McKrell, J. Buongiorno, Synchronized high-speed video, infrared thermometry, and particle image velocimetry data for validation of interface-tracking simulations of nucleate boiling phenomena, Experim. Heat Transfer 26 (2013) 169–197.

[241] S. Thomas, A. Esmaeeli, G. Tryggvason, Multiscale computations of thin films in multiphase flows, Int. J. Multiph. Flow 36 (2010) 71–77.

[242] R. Ranjan, J.Y. Murthy, S.V. Garimella, A microscale model for thin-film evaporation in capillary wick structures, Int. J. Heat Mass Transfer 54 (2011) 169–179.

[243] S. Narumanchi, A. Troshko, D. Bharathan, V. Hassani, Numerical simulations of nucleate boiling in impinging jets: applications in power electronic cooling, Int. J. Heat Mass Transfer 51 (2008) 1–12.

[244] Y. Liu, T. Olewski, L.N. Véchot, Modeling of a cryogenic liquid pool boiling by CFD simulation, J. Loss Prevent. Process Indust. 35 (2015) 125–134.

[245] S.M. Kim, I. Mudawar, Universal approach to predicting saturated flow boiling heat transfer in mini/micro-channels - part I. Dryout incipience quality, Int. J. Heat Mass Transfer 64 (2013) 1226–1238.

[246] S.M. Kim, I. Mudawar, Universal approach to predicting saturated flow boiling heat transfer in mini/micro-channels - part II. Two-phase heat transfer coefficient, Int. J. Heat Mass Transfer 64 (2013) 1239–1256.

[247] C. Konishi, I. Mudawar, Review of flow boiling and critical heat flux in microgravity, Int. J. Heat Mass Transfer 80 (2015) 469–493.

[248] Y. Katto, M. Kunihiro, Study of the mechanism of burn-out in boiling system of high burn-out heat flux, Bull. JSME 16 (1973) 1357–1366.

[249] A. Lefebvre, Atomization and Sprays, Hemisphere Publishing, New York, 1988.

[250] J.D. Bernardin, I. Mudawar, A cavity activation and bubble growth model of the Leidenfrost point, J. Heat Transfer - Trans. ASME 124 (2002) 864–874.